

A Novel Variable Geometry based Planar Inductor Design for Wireless Charging Application

Submitted by Maha Aldoumani

**to University of Exeter as a thesis for the degree of
Doctor of Philosophy in Engineering**

April 2023

This thesis is available for Library use on the understanding that it is copyright material and that no quotation from the thesis may be published without proper acknowledgement.

I certify that all material in this thesis which is not my own work has been identified and that any material that has previously been submitted and approved for the award of a degree by this or any other University has been acknowledged.



**University
of Exeter**

ABSTRACT

In this thesis, the performance, modelling and application of a planar electromagnetic coil are discussed. Due to the small size profiles and their non-contact nature, planar coils are widely used due to their simple and basic design. The uncertain parameters have been identified and simulated using ANSYS that has been run utilising a newly developed MATLAB code. This code has made it possible to run thousands of trials without the need to manually input the various parameters for each run. This has facilitated the process of obtaining all the probable solutions within the defined range of properties. The optimum and robust design properties were then determined. The thesis discusses the experimentation and the finite element modelling (FEM) performed for developing the design of planar coils and used in wireless chargers. In addition, the thesis investigates the performance of various topologies of planar coils when they are used in wireless chargers. The ANSYS Maxwell FEM package has been used to analyse the models while varying the topologies of the coils. For this purpose, different models in FEM were constructed and then tested with topologies such as circular, square and hexagon coil configurations. The described methodology is considered as an effective way for obtaining maximum Power transfer efficiency (PTE) with a certain distance on planar coils with better performance. The explored designs studies are, namely: (1) Optimization of Planar Coil Using Multi-core, (2) planar coil with an Orthogonal Flux Guide, (3) Using the Variable Geometry in a Planar coil for an Optimised Performance by using the robust design method, (4) Design and Integration of Planar coil on wireless charger. In the first design study, the aim is to present the behaviour of a newly developed planar coil, built from a Mu-metal, via simulation. The structure consists of an excitation coil, sensing coils and three ferromagnetic cores

located on the top, middle and bottom sections of the coil in order to concentrate the field using the iterative optimisation technique. Magnetic materials have characteristics which allows them to influence the magnetic field in its environment.

The second design study presents the optimal geometry and material selection for the planar with an Orthogonal Flux Guide. The study demonstrates the optimising of the materials and geometry of the coil that provides savings in terms of material usage as well as the employed electric current to produce an equivalent magnetic field.

The third design study presents the variable geometry in a planar inductor to obtain the optimised performance. The study has provided the optimum and robust design parameters in terms of different topologies such as circular, square and hexagon coil configurations and then tested, Once the best topology is chosen based on performance. The originality of the work is evident through the randomisation of the parameters using the developed MATLAB code and the optimisation of the joint performance under defined conditions.

Finally, the fourth design study presents the development of the planar coil applications. Three shapes of coils are designed and experimented to calculate the inductance and the maximum power transfer efficiency (PTW) over various spacing distances and frequency.

Acknowledgements

I would like to thank my supervisor Dr. Baris Yuce for his excellent supervision, guidance, encouragement, and support. I do appreciate the time he has devoted for me to make this project successful and the knowledge that I had obtained from him which will stay with me always, wherever and whenever I work in the future. I would also like to extend my thankfulness to prof. Mustafa Aziz, who was always there to support and guide me throughout my project, without his assistance this thesis might not have been possible to produce. Also, I would like to thank Dr Dibin Zhu support in the early stages of the project and for his successful guidance of my work. My deepest thanks go to my lovely family for always supporting, love, care, and blessings during my studying journey. With sad feelings, I present this degree to my father, whom I wish was alive to celebrate this achievement with me, for his encouragement to us always to study and succeed in life. I would also like to thank Exeter University which deserves my sincere appreciation for providing me the opportunity to pursue my study.

Table Of Contents

ABSTRACT	2
Acknowledgements	4
CHAPTER 1: INTRODUCTION	14
1.1 Introduction	14
1.2 Research Aims and Objectives	16
1.3 Motivation and Research Hypothesis	17
1.4 Outline of the thesis	24
1.5 Research Questions	25
CHAPTER 2: LITERATURE REVIEW	27
2.1 Introduction	27
2.2 Magnetic Sensors Types	28
2.3 Magnetic Sensors	31
2.4 Applications of Sensors	32
2.4.1 Smart Transport and Mobility Tracking	32
2.4.2 Smart Grid	35
2.4.3 Smart Environment	36
2.5 Measurements and Parameters in Magnetometers	39
2.6 PCP planar and its application	44
2.6.1 Classification of ferromagnetic materials (Diamagnetic, Paramagnetic, Ferromagnetic Materials)	44
2.6.2 Susceptibilities of diamagnetic and paramagnetic materials	45
2.6.3 Classification of ferromagnetic materials	46
2.7 Magnetic properties of ferromagnetic material	48
2.8 Application of PCB planar coils	54
2.8.1 The PCB Planar Fluxgate	54
2.8.2 Fluxgate sensors	55
2.9 Core shapes of fluxgate magnetometers	58
2.10 Core Materials	61
2.11 Operating principle	61
2.12 Wireless charger	66
2.12.1 Overview and major events in the wireless charging technology	66

2.12.2 Wireless Charging techniques	67
2.12.3 Typical wireless phone charger	67
2.13 Summary	69
CHAPTER 3: OPTIMISATION OF PLANAR COIL USING MULTI-CORE	71
3.1 Multi-Core Fluxgate	71
3.2 The Proposed Fluxgate Architecture	71
3.3 Instrumentation Details	73
3.4 Accuracy of Simulation	75
3.5 The External Magnetic Field	77
3.6 Exciting the Excitation Coil	78
3.7 Summary	80
CHAPTER 4: A NOVEL PLANAR DESIGN USING ORTHOGONAL FLUX GUIDE	82
4.1 Introduction	82
4.2 Introduction of the PCB Planar	84
4.3 The developed architecture	85
4.4 The Working Principle of the Sensing Device	88
4.5 The Sensor Development and Simulation Results	91
4.5.1 The Influence of the Induced Current on the Core Material	91
4.5.2 The Influence of the number of turns on the Coil	95
4.5.3 The Influence of the Ferromagnetic material on the Hysteresis Loop	97
4.5.4 The Influence of the Ferromagnetic Wire Width on the Hysteresis Loop	99
4.5.5 The Influence of the Ferromagnetic Core Width on the Hysteresis Loop	100
4.6 The Experimental Optimisation of the Square Coil	102
4.6.1 The Influence of the Induced Current on the Core Material	103
4.6.2 The Influence of the number of turns on the Coil	104
4.6.3 The Influence of the Ferromagnetic material on the Hysteresis Loop	105
4.6.4 The Influence of the Ferromagnetic Wire Width on the Hysteresis Loop	106
4.6.5 The Influence of the Ferromagnetic Core Width on the Hysteresis Loop	106
4.7 Summary	107
CHAPTER 5: USING THE VARIABLE GEOMETRY IN A PLANAR INDUCTOR FOR AN OPTIMISED PERFORMANCE USING A ROBUST DESIGN METHOD	109
5.1 Introduction	110
5.2 The Elements of Smart Cities	111

5.2.1 Smart Buildings	111
5.2.2 Smart mobility	112
2.2.3 Smart Energy	112
5.2.4 Smart Water	113
5.2.5 Smart waste management	114
5.2.6 Smart Health	114
5.2.7 Smart digital layers	115
5.3 Applications of Sending Techniques	116
5.4 The Scope of the chapter	118
5.5 Methodology	119
5.5.1 The Experimental Method	119
5.5.2 The Analytical Method	120
5.6 The Modelling Method	122
5.7 The Robust Design Method	124
5.8 Results and Discussion	126
5.8.1 The Experimental Results	126
5.8.2 The Modelling and Optimisation Results	127
5.8.3 The Uncertainty and Robust Design Results	131
5.9 Discussion of Results	133
5.10 Conclusion	135
5.11 Summary	135
CHAPTER 6: DESIGN INTEGRATION OF PLANAR INDUCTANCES ON WIRELESS CHARGER	137
6.1 Introduction	138
6.2 The Concept	138
6.3 The Mathematical Modelling of The Inductor	141
6.3.1 Self inductance	141
6.3.2 Mutual inductance	143
6.3.3 Practice elements	144
6.3.4 Power Transfer Efficiency	144
6.4 Design methodology	145
6.5 The Experimental Work	146
6.7 The Characteristics of the Planar Inductances	146

6.8 The Manufacturing Process of the Integrated Planar Micro Inductance on PCB- FR4	147
6.9 Circuit design and test setup	149
6.10 Measurement result	152
6.11 Conclusions	158
6.12 Summary	159
CHAPTER 7: DISCUSSION, CONCLUSIONS AND FUTURE WORK	160
7.1 Discussion	160
7.2 Conclusions	162
7.3 Further work	163

List Of Figure

Figure 2.1. Analogy between electrical and magnetic measurements	36
Figure 2.2. Typical approach for determination of the hysteresis loop	39
Figure 2.3. Typical hysteresis loop and its characteristic points B_r and H_c	48
Figure 2.4. The family of hysteresis loops obtained for various amplitudes of the magnetising fields and the magnetization curve obtained by connecting the tips of these loops (a); major and minor hysteresis loops (b)	50
Figure 2.5. Core shape of fluxgate sensor (Rod core)	54
Figure 2.6. Core shape of fluxgate sensor (Ring core)	55
Figure 2.7. Core shape of fluxgate sensor (race-track sensor)	56
Figure 2.8. Core shape of fluxgate sensor (square sensor)	57
Figure 2.9. Fluxgate principle a) core not saturated b) core saturated	58
Figure 2.10. Schematic of a double axis planar Fluxgate magnetic sensor	60
Figure 2.11. Core magnetization and external magnetic field direction: because of the excitation magnetic field each half of the core is magnetised in the opposite direction	61
Figure 2.12. Fluxgate principle explained with the waveform of the magnetic field and of the voltage induced	61
Figure 2.13. Wireless charging techniques	64
Figure 2.14. diagram of wireless charger	65
Figure 3.1. The triple planar fluxgate magnetic sensor proposed the ferromagnetic material layers are on the top, in the middle between the sensing and excitation coil and in the bottom of the fluxgate	69
Figure 3.2. specifically for a Magnetostatic setup (Parametric Adaptive Analysis) that has been used in the design	70
Figure 3.3. Illustrate the excitation circuitry and equivalent load connected to the sensor in ANSYS- Simplorer environment	71
Figure 3.4. The mesh structure of the design	72
Figure 3.5. Magnetic field vector representation for an external magnetic field applied to the sensor at $H=17A/m$	73

Figure 3.6. Vector representation of the external magnetic flux density B applied near excitation and sensor coils	74
Figure 3.7. Magnetic field on the surface of mu-metal for an excitation current of 5mA	74
Figure 3.8. The Magnetic field passing through top mu material. As shown, the excitation current of 12 mA	75
Figure 3.9. The magnitude of the magnetic field on the surface of top Mu material. As can be seen the magnetic field caused by the excitation coil is saturating the material with near 0.8 Tesla of magnetic flux density (B)	75
Figure 3.10. The magnetic vector around the excitation (and sensing coil)	76
Figure 4.1. schematic of the 3-axis planar fluxgate magnetic sensor realised	82
Figure 4.2 Top view of the 3-axis planar fluxgate magnetic sensor	82
Figure 4.3 a) The flux lines of the sensing principle of the fluxgate in X axis direction without fluxguide	84
Figure 4.3 b) The flux lines of the sensing principle of the fluxgate in Z axis direction without fluxguide	85
Figure 4.4 a) flux lines of the sensing principle of the fluxgate with the fluxguide in the X axis	86
Figure 4.4 b) flux lines of the sensing principle of the fluxgate with the flux guide Z axis	86
Figure 4.5. The effect of the induced current on the magnetic properties of the ferromagnetic core material	89
Figure 4.6. The determination of the saturation point of the ferromagnetic core material	89
Figure 4.7. The saturation process of the ferromagnetic core material at 680mA	91
Figure 4.8. The effect of the number of turns on the magnetic properties of the ferromagnetic core material	92
Figure 4.9. The change in number of turns of the excitation coil: (a) 10 turns, (b) 20 turns and, (c) 40 turns	92
Figure 4.10. The saturation of the core material when the maximum number of turns, i.e. 40 turns, is used	93
Figure 4.11. The influence of the core thickness on the output voltage of the device	95

Figure 4.12. The influence of the wire width on the flux density through the core	96
Figure 4.13. The influence of the core width on the flux density through the core	98
Figure 4.14. the measurement setup	99
Figure 4.15: The BH curves based on 680mA (experimental vs. Simulation)	100
Figure 4.16. The effect of the number of turns on the magnetic properties of the ferromagnetic core material (experimental vs. Simulation)	101
Figure 4.17. The influence of the core thickness on the output voltage of the device (experimental vs. Simulation)	102
Figure 4.18. The influence of the wire width on the flux density through the core (experimental vs. Simulation)	102
Figure 4.19. The influence of the core width on the flux density through the core (experimental vs. Simulation)	103
Figure 5.1. The fabricated coils on the PCB, for 3D printed support structures: (a) square coil topology; (b) circular coil topology; (c) hexagon topology	116
Figure 5.2. The stages involved in Finite Element Analysis (FEA) modelling of the proposed design	118
Figure 5.3. The various topologies of the modelled coils: square, circular and hexagonal, respectively	119
Figure 5.4. The experimental result between the resulting inductance and the spacing between the excitation and sensing coils	123
Figure 5.5. The modelling and simulation results of the square (a), hexagonal (b) and circular (c) coil topologies	125
Figure 5.6. The simulation results in varying the spacing distance between excitation and the sensing coils	125
Figure 5.7. The Figure-Of-Merit (FOM) value as a function of number of turns and spacing between the coils for the square (a), hexagonal (b) and circular (c) designs, respectively	127
Figure 5.8. (a) The Ordinary Kriging response surface, (b) the variance plot and, (c) the contour plot of the inductance	128
Figure 5.9. (a) The Blind Kriging response surface, (b) the variance plot and, (c) the contour plot of the inductance	129
Figure 6.1. The defined integrated coils, namely: square, circular and hexagonal, respectively	137
Figure 6.2. a. Inductor bias and b. magnetic field around	139
Figure 6.3. Mutual inductance	140

Figure 6.4.Parasitic elements	140
Figure 6.5. Equivalent circuit of a mutual inductor	141
Figure 6.6. Different steps of lithography	145
Figure 6.7. (a) Square, (b) Circular, (c) Hexagonal structure for the input and output inductor	146
Figure 6.8. Test setup a) Square, (b) Circular, (c) Hexagonal structure for the input and output inductor	147
Figure 6.9. Test circuit schematic	147
Figure 6.10. Test table including signal generator and oscilloscope to excite and measure the mutual coil	148
Figure 6.11.Voltage waveform on the inductor	149
Figure 6.12. PTE values against the spacing distance	150
Figure 6.13 PTE values against the Frequency	151
Figure 6.14. PDL values against the spacing distance	152
Figure 6.15. Frequency values against the inductance	153

List Of Tables

Table 2.1:Features of sensor types and their applications	28
Table 2.2 : A Comparison of the available technologies of magnetic sensors in terms of the detectable field	37
Table 2.3: A classification of the various magnetic materials based on the major applications	38
Table 2.4: The classification of the various materials based on the magnetic properties and the relative permeability values	45
Table 2.5: Typical Values of Maximum Relative Amplitude Permeability of Some Ferromagnetic Materials	51
Table 2.6: Main Parameters of Hysteresis Loop of Various Soft Magnetic Materials	53
Table 2.7: Typical Parameters of Hysteresis Loop for Various Hard Magnetic Materials	54
Table 4.1: The various excitation current values with sensitivity in the range	95
Table 5.1. The structural parameters of the proposed Printed Circuit Board (PCB) inductor	121
Table 5.2. The various features of the designed coils	124
Table 6.1: The geometrical characteristics of the examined inductors	148
Table 6.2. measurement results (f=10 MHz)	154

CHAPTER 1

INTRODUCTION

1.1 Introduction

Electricity has become the heart of today's modern societies, where the consumption of electricity has increased immensely [1]. It is therefore tough to survive without electrical power; many appliances and devices are dependent on this electrical power to operate. such as, kitchen appliances, ventilators, entertainment, heating systems, washing machines and others[1]. Conventionally, the use of wires for transmitting electricity has been adopted for many applications but in recent years, technological advancements have resulted in the onset of the Wireless Power Transmission (WPT)[1]. The fundamental idea that is driving WPT is to avoid the harmful use of wires while also removing the complexity of managing power cords[1-2]. For example, portable electronic gadgets such as mobile phones, tablets, computers, domestic robots, drones, and so on are typically powered by batteries[2]. With the advancement of wireless power transmission, the market is expanding beyond smartphones to include a broader range of applications in computing, wearable, hearables, small appliances, smart homes, medical, industrial, robotics, automotive, 5G telecom, and retail[2]. Because of their quick growth and numerous applications, portable electronics are increasingly becoming a part of our daily lives[2]. Furthermore, there will always be an increased demand for smart products that can charge without being plugged in, thus demonstrating the end of cable use[2]. As a result, there is a need to develop new technologies to eliminate the need for cumbersome wires or adapters [1-3]. As part of their proposed project, the research team at MIT invented the word

WiTricity, whereby WiTricity is nothing more than Wireless Electricity, which offers the transfer of electricity to a distant location without the need for cables. Essentially, WiTricity nullifies the need to have a separate charger for each electronic device we use. This is the primary benefit that can be derived from this technology. It is necessary to determine a position where portable gadgets are placed while they are automatically charged. WiTricity guarantees that all electronic gadgets may charge themselves without the need to plug into a power socket or use chargers. Safety aside since no cords are required, WiTricity has proven to be convenient because there is no prerequisite for effective manual recharge or battery replacement, and it appears to be more dependable because the devices never will run out of battery power. Furthermore, WiTricity aids in achieving sustainability goals by being environmentally friendly through the reduction of the usage of throwaway batteries. Even though WiTricity offers automatic wireless charging, it only works over limited distances. As a result, WiTricity is currently in the development phase with several research projects underway to better its potential uses, such as charging larger cars or machinery and operating over greater distances. Therefore, the goal of this study is to provide a revolutionary technique for charging mobile phones utilising WiTricity without the usage of cable chargers. The relevance of this effort is to provide an effective low voltage power transmission over a relatively short distance. The proposed work guarantees that mobile users will be able to carry their phones wherever, even if there are no charging facilities. Often when electronic gadgets are used in daily activities, regardless of the device, it is necessary to recharge the gadgets on a regular basis using wired chargers. However, there may be times when there is a power shortage due to natural disasters such as cyclones, earthquakes, and so on. In such an instance, is it possible to wirelessly transfer power from one phone to another?[1-2]

Keerthana and Pragadeshwar solved this issue in their research by eradicating the requirement for physical electrical supply to portable devices, by allowing for the simple transfer of electrical charge from one cellular telephone to another via inductive coupling[1-2]. This is incredibly handy in an emergency. There could be areas where integrated wiring systems are inaccessible or impossible to reach. Therefore, developing practical means to transfer electricity between two systems without requiring wires is the next big technological advancement. Power can be transported using one of three methods: inductive coupling (short-range), resonant induction (mid-range), or electromagnetic radiation transmission (long-range). The intention behind the efforts was to charge a low voltage gadget rapidly and effectively utilising inductive coupling. Similarly, it may not always be practical to bring Smartphone chargers with us wherever we go. It is difficult to always have mobile phone chargers on hand and in all places. In their study, Vithyaa and Marthandan aimed to address the implementation challenges of WPT usage for smart phones and cars [1-3]. Zaman et al. stressed the importance of developing a simpler model for transferring electrical energy from one mobile phone to another utilising series-series technology for inductive charging [1-2].

1.2 Research Aims and Objectives

The aims and objectives of the various design studies will investigate the current work alongside the outcomes and the originality of the work in each corresponding study. The main four common topics that will share amongst all designs studies are the involvement of composite materials, the multi-core of planar coil, the application of uncertainty models to simulate the uncertain parameters in the structure and Three shapes of coils will designed to calculate the maximum power transfer efficiency (PTW)

over various spacing distances and frequency and inductance. These four main subjects will be discussed in more detail in the following chapters. Generally, these types of applications suffer from various uncertainties that originate from the material itself alongside or from structure and low power transfer efficiency PTE. This makes the study of uncertainties in such structures very crucial from the design point of view. The study of uncertainties provides a set of optimum design parameters related to size, weight, safety and cost of such structures. The thesis will investigate four different designs study, namely: multi core planar coil (chapter 3), A Novel Planar Design Using Orthogonal Flux Guide (chapter 4), Determining the Optimal Geometry in Planar inductor Using Robust Design Method (chapter 5) and Design and Integration of Planar Inductances on wireless charger (chapter 6).

1.3 Research Questions

More research is necessary to create a low-cost, more efficient, and simple WPT that is compatible with every phone model. Because of their environmentally beneficial characteristics, electric cars are gaining traction over traditional equivalents (that rely on natural resources). On et al reported an experimental WPT technique for charging electric automobiles via inductive coupling [2]. In addition, Sultana et al. suggested designing a WPT-based system for charging electric cars by incorporating WPT circuitry within automobiles [1-3]. This circuitry was triggered when the electrical cars arrived at the charging station, mostly to address battery concerns with electrical vehicles. Mou examines the benefits and drawbacks of each WPT technology, the research aims of WPT such as enhancing transmission efficiency and distance, current state-of-the-art WPT technologies, and the open research difficulties of WPT in his

study. In addition, the prospect of charging numerous devices via WPT in the foreseeable future is highlighted in [1-4].

1.4 Motivation and Research Hypothesis

The Research Hypothesis of this study shows the investigation and the performance of various topologies of planar coils when they are used in wireless chargers. For this purpose, different models in the FEM and ANSYS Maxwell FEM package have been used to analyse the models while varying the topologies of the coils were constructed and then tested with topologies such as circular, square and hexagon coil configurations. The described methodology is considered an effective way for obtaining maximum PTE with a certain distance on planar coils with better performance. The hypothesis of this work was mainly named

- **Optimisation of Planar Coil Using Multi-core.**

This part of the work studying the schematic of the micro planar structure realised for the triple cores planar. to concentrate the field using the iterative optimisation technique. In other words, better performances can be obtained by using magnetic top and bottom shields. Magnetic shielding involves the use of high magnetic permeability material panels that provide a preferential path for the magnetic flux line materials such as the mu-metal. This material has a greater permeability to magnetic fields (H) than the air surrounding them and therefore concentrates the magnetic field lines. By a strategic placement of the ferrite materials, it was possible to concentrate this magnetic

field and therefore influence the intensity and the shape of a field. This design study has investigated the followings:

- The magnetic field will be easily passed through the material (i.e., the upper and lower cores), it will wrap around the coils instead of going further away from the coil and this will allow the magnetic field to stay altogether within the top and bottom core.
- The second benefit of having the top and bottom cores is that the magnetic flux will not be able to pollute the environment.
- The third advantage of the multiple cores is that the coils will intensify the field within the sensor which means that less current is consumed to obtain the desired results.

- **A Novel Planar Design Using Orthogonal Flux Guide**

The work presented provides a novel planar design that has the ability to concentrate and guide the field in a highly efficient manner by employing orthogonally cylindrical ferromagnetic tube and set of ferromagnetic cubes in order to deflect and emit the field in the desired path. A micro-fluxgate sensor has been developed during the current study utilising ANSYS. In other words, an optimised study of the geometry of the magnetometer provides savings in terms of material

Also, this design study examined the developed ANSYS model to test advanced materials, i.e. amorphous and metaglas, as well as to optimise the geometry of the magnetic planar. In other words, the current design study presents an optimised design of the materials and geometry of the magnetometer which provides savings in terms

of material usage as well as the employed electric current to produce an equivalent magnetic field.

Also, this design discussed the evolution and the results of the model planar that has been designed by ANSYS software, this work allows to define a design way for the development of the magnetic planar. The results of the model have been simulated using different coil characteristics that are given below.

- The excitation current value that ensures the saturation for ferromagnetic material and how the current is affecting the (BH) curve which in turn will affect the sensitivity of the sensor.
- Different number of turns and analyse the BH curves of each case.
- The output voltage with different thickness ferromagnetic materials.
- Different ferromagnetic wire width.
- Different ferromagnetic core width.

The design stages involved in the current project started with finding the amount of the excitation current value that ensures that the ferromagnetic material is saturated. This has been achieved using magnetostatic simulations to evaluate the excitation peak current necessary to saturate the ferromagnetic material.

- **Determining the Optimal Geometry in Planar inductor Using Robust Design Method**

This design study introduces a novel of using the Meta-model-based design optimisation to develop the electromagnetic sensors by analysing the behaviour of different planar coils topologies: circular, square and hexagon coils for the application

such as wireless charger, tracking and location identification, etc. for the smart cities by using Meta-model-based design optimisation. The Meta-model-based design optimisation is becoming increasingly popular in the industrial practice for the optimisation of complex engineering problems, especially to reduce the burden of computationally expensive simulations. The idea behind the Meta-model-based design optimisation is to build a surrogate model (or a meta-model) from a reduced number of simulations runs and subsequently use the model for optimisation purposes. Moreover, this design study has provided the optimum and robust design parameters in terms of coil shapes, number of turns and the spacing between the coils on the output inductance. This means that the combined effects of these variables on the output inductance was studied to obtain the optimum values for the number of turns and the spacing between the coils that provided the highest level of inductance from the coils. The originality of the work is evident through the randomisation of the parameters using the developed MATLAB code and the optimisation of the joint performance under defined conditions. The ANSYS Maxwell 3D FEM software package has been used for the evaluation of the different coil topologies: circular, square and hexagon coils. Then, an impedance analyser was used for characterising the manufactured versions. A comparison of both the measured and simulated performance of coils with different topologies (circular, square and hexagon) is presented in this case study.

The study has considered the following:

1. Study of various shapes of coils(Circular, Square and Hexagon) coils has been presented, using Meta-model-based design optimisation, Ansys Maxwell simulation

and experimentation when they are used in inductive sensing. The topology of the coil has also an effect on the performance of the sensor.

2. In total, three shapes of coils were designed, simulated and experimented to calculate the inductance and the magnetic flux density over various spacing distances. The different coil geometries generated different magnetic fluxes. The higher the magnetic flux the better the inductance.
3. Good correlation between the Finite element (FE) modelling simulation and the experimental measurements for developing the design of planar coils. The obtained results from the Ordinary and the Blind Kriging models for the optimum configuration (square) design (the best configuration). The 'Mean Squared Error' of the Leave-out cross validation was chosen to evaluate the quality of the fit as well as the predictive capability of the technique. These optimisation methods have both interpolated and extrapolated the data based on the short-term measurements from lab experiments. This is a very good way to predict the long-term behaviour based on short-term measurements. This saves time and cost associated with long experimental time and hence, it is favourable. In these plots, the response surface is constructed based on the equations of the Ordinary and Blind Kriging approaches whereas the dots are those simulated by the MATLAB code that randomly assigns the data points and runs the analysis through ANSYS. The described methodology is considered an effective way for the development of sensors based on planar coils with better performance. Moreover, it also confirms a good correlation between the experimental data and the FEM models. Once the best topology is chosen based on performance, an optimisation exercise was then carried out using uncertainty models. That is, the influence of variables such as number of turns and the spacing between the coils on the output inductance has been investigated. This means that

the combined effects of these two variables on the output inductance was studied to obtain the optimum values for the number of turns and the spacing between the coils that provided the highest level of inductance from the coils.

- **Design and Integration of Planar Inductances on Wireless Charging Systems.**

The novelty of this design study is the application of a newly developed model to constrain the uncertain parameters while simulating others to keep the original shape. Fully planar WPT of circular, square and Hexagon are made on FR4 circuit boards and experimented. The significance of these designs is to achieve maximum power transfer efficiency (PTE) with high power delivered to the load (PDL). This is fabricated to determine the accuracy of power transfer efficiency PTE, power delivered to the load (PDL) and the inductance values over various spacing distances and frequency. It is desirable to achieve the highest possible inductance and quality factor for the targeted 10 MHz application considering the level of specific absorption rate (SAR) in the human body. This design study presents a study which uses a wireless power transfer(WPT) system based on a magnetically coupled fully printed spiral. This design study introduces a novel solution of developing the efficiency and unfavourable effect of low coupling magnetically coupled fully planar coil printed spiral resonator-based wireless power-transfer systems. Three shapes of coils were designed and experimented to calculate the inductance and the power transfer efficiency (PTW) over various spacing distances and frequency; they obtained results that showed that the inductance decreases with the frequency and this was found to apply to all inductors.

The study has considered:

- PTE values against the spacing distance between the coils in circular, square and hexagon coils.
- PTE values against frequency.
- Inductance as a against the frequency for all the different realised integrated coils.

The possibility of both circular and square architecture is explored, and their performance is optimised to generate maximum efficiency at specific operating distance. The performance of these architectures is analysed based on efficiency of power-transfer and power delivered. It is found that the square coils generate high power-transfer efficiency (80%) compared to circular coils (79%) at 10 mm distance between receiver and transmitter with air medium and at a frequency of 10 MHz. Contrarily, the circular resonators can generate higher power (430 mW) than square resonators (290 mW) under the same conditions and medium. Overall, the square coil design provided the highest inductance and power transfer efficiency followed by the hexagonal and then the circular geometry. This was also the case while changing the spacing distance between the coils. as a conclusion, the experimental measurements concluded that the square mutual inductor in comparison with the circular and hexagonal can transfer the energy better. Overall, the square coil design provided the highest inductance and power transfer efficiency followed by the hexagonal and then the circular geometry. This was also the case while changing the spacing distance between the coils.

1.5 Outline of the thesis

Chapter 2: presents background that discusses the various aspects of uncertainty models related to composite structures, also discusses the magnetometers, materials of that magnetometers and its applications. This is essential in order to understand the various parameters and variables involved in the four design studies which makes it easier for the reader to make judgements and draw conclusions based on the obtained results.

Chapter 3: chapter 3 employs the built up ANSYS model to simulate the behaviour of a newly developed planar coil. This part of the work studying the schematic of the micro planar structure realised for the triple cores planar. to concentrate the field using the iterative optimisation technique. In other words, better performances can be obtained by using magnetic top and bottom shields as it is the case in the current design.

Chapter 4: was examining the developed ANSYS model as well as present a novel planar design that has the ability to concentrate and guide the field in a highly efficient manner by employing orthogonally cylindrical ferromagnetic tube and set of ferromagnetic cubes in order to deflect and emit the field in the desired path. In addition to 1) evaluate the excitation current value that ensures the saturation for ferromagnetic material and how the current is affecting the (BH) curve which in turn will affect the sensitivity of the sensor. 2) Different number of turns and analyse the BH curves of each case. 3) Compare the output voltage with different thickness ferromagnetic materials. 4) Different ferromagnetic wire width. 5) Different ferromagnetic core width.

Chapter 5 :Describes the novelty of the two methods: Ordinary and the Blind Kriging ,which was considered an effective way to develop , investigates the performance of various topologies of planar sensors when they are used in inductive sensing as well as to simplify the design diversity despite the distinct geometric designs, this includes the number of wire turns, the metal wire gap, the cross-sectional area of the metal wire, the coil resistance, the coil inductance and the dimensions of the ferromagnetic core. Moreover, three shapes of coils were designed, simulated and experimented to calculate the inductance and the magnetic flux density over various spacing distances.

Chapter 6: The novelty of this chapter was the application of a newly developed model to constrain the uncertain parameters while simulating others to keep the original shape. Fully planar WPT of circular, square and Hexagon are made. The significance of these designs is to achieve PTE values against the spacing distance between the coils in circular, square and hexagon coils as well as PTE values against frequency and Inductance as a against the frequency for all the different realised integrated coils, in addition to the maximum PTE values with high PDL. This is fabricated to determine the accuracy of power transfer efficiency PTE, PDL and the inductance values over various spacing distances and frequency. It is desirable to achieve the highest possible inductance and quality factor for the targeted 10 MHz application considering the level of specific absorption rate (SAR) in the human body.

CHAPTER 2

LITERATURE REVIEW

2.1 Introduction

This thesis investigates the various aspects related to composite structures that contain uncertain parameters. In order to provide a strong background to the current thesis, it is essential to discuss the various aspects of uncertainty models related to composite structures in an effort to provide the reader with a short summary of all the relevant models involved in such analysis. This is why a large space has been devoted to manufacturing of composites from which most uncertainties evolve in such structures. The current chapter also discusses the magnetometers, materials of that magnetometers and its applications. This is essential in order to understand the various parameters and variables involved in the four design studies which makes it easier for the reader to make judgements and draw conclusions based on the obtained results. A magnetic sensor is a device that is capable of measuring the magnetism of a magnetic material as well as the direction, strength or the change of a magnetic field at a given location. An example is the Compass which works based on the principle of measuring the direction of the ambient magnetic field. In this context, the first magnetometer was invented by Carl Friedrich Gauss in 1833 followed by many attempts to develop its working function such as the addition of the Hall Effect which is still widely used [4]. This type of magnetometers is extensively used in measuring the earth's magnetic field as well as the use for geophysical applications to detect the

magnetic anomalies of various types. Moreover, such magnetometers are widely used in military applications to detect submarines [4-5]. In the current years, significant efforts are placed towards the development of micro-sensors in terms of reducing the fabrications costs while increasing the resolution of the device as well as the dynamic range of the sensor. The integration of such applications with electronics not only improves the development of such devices but also results in more compact and portable solutions which increase the areas of applications of such inventions [6].

It is worthwhile mentioning that the current thesis attempts to develop, fabricate and characterise the fluxgate suitable for operation within a wide linear range. The fabrication process of the proposed fluxgate should be in agreement with the existing CMOS technology wherein the sensor is fabricated as a post process on CMOS wafers. The fabrication process should be of low cost with the sensor structure being operable with low power while maintaining a high resolution. The main challenge is the miniaturisation process of the sensor's dimensions where it is known that the reduction in the sensor's dimensions lead to an increase in the resulting noise which is undesirable [6-7].

2.2 Magnetic Sensor Types

Today, with the rapid advances in sensor technology, there are a handful of sensors that can be used to monitor and capture various physical aspects of the external environment, such as light, temperature, humidity, magnetic fields, and sound. Magnetic sensors can be classified into three groups as given below:

- **Ambient Fluid Properties**

The ambient fluid in both the air and water includes particulates, chemical substances, and biological molecules. The ambient air use cases are most relevant to City Scanner, as it uses land vehicles hence Table II is limited to these use cases. The most common application in this category is air quality monitoring [8].

- **Electromagnetic Properties**

Urban areas include an increasing number of electronic devices which emit an agglomeration of radio waves and electromagnetic fields. These radio waves, similar to visible light and infrared radiations, are part of the electromagnetic spectrum and have wavelengths longer than infrared light [9].

- **Magnetic sensors**

- **Light (Photonic Properties)**

Multispectral light sensors are used to capture the infrared and the visible regions of the electromagnetic spectrum. In the case of autonomous vehicles, multispectral imaging has applications in navigating through the built environment. Infrared imaging has also been helpful for some use cases beyond thermal efficiency, for instance, the detection of methane gas leak [10].

An overview of typical sensor types and their corresponding urban applications are provided per property type in Table 1. This table shows the basic sensor structure,

nature of output signal, advantages and disadvantages in addition to the applications of such sensors [6].

Table 2.1: Features of sensor types and their applications [7].

Type	Sensor	Applications
Ambient fluid	Particulate matter	1. Monitoring the distribution of fine 2. particulates (e.g. PM2.5, PM10).
	Chemical pollutants	Monitoring the distribution of various pollutants.
	Methane sensor	Detecting methane leaks.
	Nano sensors	1. Detecting explosive material. 2. Detecting chemical substances.
	Temperature, Humidity, Air pressure	Monitoring the airborne particulate radioactivity.
	Particle radiation	Monitoring the airborne particulate radioactivity
Electromagnetic	WiFi, Bluetooth	Crowd and station mapping by scanning WiFi
	GPS	1. Localization and annotating sensor data. 2. Inferring mobility aspect of vehicles (mobility mode of people or traffic status).

	RFID scanner	1. Tracking and managing assets in urban areas. 2. Sensing of spatial information by implanted beacons.
	Isotropic sensors, magnetometers	Monitoring the electromagnetic field level
Photonic	visual camera	1. real time imaging of urban areas 2.monitoring of crowd and vehicles for event managements and security purpose 3.Monitoring of traffic
	Thermal camera	1.Monitoring energy efficiency of built environment 2.Monitoring crowd 3.detecting natural gas and CO2 emission 4.Monitoring infrastructure(power lines, stress surface)
	photo sensor	monitoring stress lightning infrastructure quality

2.3 Magnetic Sensors

In literature, most of the magnetic sensors are utilised to measure different properties in different applications hence they have been implemented as either direct or indirect measurement techniques. These types of magnetic measurement sensors are called magnetometers. In “direct measurement techniques”, two essential parameters are the most important elements to be considered as tuning parameters which are the strength

and the direction of the magnetic field. Examples of direct measurement techniques include [11-15]:

- Earth's magnetic field measurement for navigation purposes;
- Controlling the magnetic apparatus ;
- Magnetic field measurements to be used in medical area, i.e. mapping the heart or brain's function.
- It could be used to measure displacement and velocity, or linear and angular positions of moving parts which are considered as a mechanical quantity. This can be achieved by monitoring the change of magnetic that is obtained by a permanent magnet;
- Monitoring of the electrical current carried in a conductor, by measuring the generated magnetic field around the conductor [15-16].

Certain performance requirements are required in order to fulfil the above applications, and this includes, but not limited to, the linearity, magnetic field resolution, offset, sensitivity, power consumption, spatial resolution, size, temperature coefficients and noise. Generally speaking, there are two distinct application areas for magnetic sensors; first area requires high resolution and accurate sensing techniques, where cost is not weighed, whilst the second area involves huge scale applications, where batch-fabricated and inexpensive magnetic field sensors are desired. Of the virtues of modern and advanced magnetic sensors, one can mention sensitivity, low noise, stability and small footprint, where new trends in customer products drive the demand for operation from low-voltage batteries, as well as lower power consumption [16].

2.4 Applications of Sensors

2.4.1 Smart Transport and Mobility Tracking

With the rapid growth in the number of cars over recent years, there is an increasing need for efficient transport management, in order to avoid traffic jams and optimise traffic flows, especially at intersections. As smart cities prevail with an increasing capability to be instrumented with a diverse range of mobile and fixed sensors, connected via wireless and wired networks, these in turn enable a richer set of smart city Intelligent Transport System (ITS) services. Such services include adaptive personalised maps, adaptive vehicle navigation, smart fleet management and traffic monitoring, road incident detection, congestion avoidance, speed control via smart interaction with roadside controls, context based vehicle maintenance, car parking aids, human driver monitoring and better driving safety [11-16]. A conventional way to regulate traffic flow is by the use of traffic lights. These typically have fixed switch interval times, which are not adjustable to traffic conditions. Traffic jams have significant impacts on fuel consumption due to the frequent starts and stops, as well as increased carbon emissions. An adaptive scheme, dependent on traffic conditions, is more desirable. In this context, a method to estimate the number of cars approaching an intersection could generate information for switch interval times to be dynamically adjusted based on traffic conditions. For such an intelligent system to be realised, efficient methods to detect traffic (i.e., count the number of cars) are required. There have also been proposed smart intersections without traffic lights and stop signs. In that approach, wirelessly interconnected vehicles can communicate with each other and use decision-making for collision avoidance. Cheap methods of sensing cars involve induction loop detectors which are buried in roads. Loops detectors can be

used to detect the presence of metals, which is interpreted as a vehicle. Moreover, they can enable an estimate of the kind of vehicle which has been sensed, its speed or other parameters, which can be useful for traffic flow management. To estimate a vehicle's weight, other methods such as weight in motion (WIM) can be used, whose sensors (e.g. piezoelectric systems, capacitive mats, bending plates, load cells, and optical WIM) are mounted on road surfaces. These highlighted methods usually carry high installation and maintenance costs. Less intrusive (but not as accurate) and more sophisticated methods involve video cameras [11]. These approaches are more attractive mainly because cameras can be easily installed and the level of required maintenance is low, compared to previously described approaches. Furthermore, in the instances where surveillance cameras are already installed, these can be used for intelligent transportation applications. The system which consists of multiple standard CCTV cameras and personal computers (PCs) was tested in different environments (e.g. airports and tunnels). The main drawback of computer vision-based methods is their performance dependency on environment conditions, such as lighting, occlusions and weather. For night-time scenarios, street lamps and traffic lights can be used for vehicle sensing, as vehicles can be detected by considering the distance between vehicle's headlights [11][12]. Apart from vehicle detection, smart cities use mobility data recorded by integrated sensor systems. A system using such data is M-Atlas, which is focused on the concept of a trajectory, i.e., a sequence of time stamped locations, sampled from the itinerary of a moving object. Trajectories pertaining to human travel or movement can be reconstructed from the data sensed in various contexts, including Global Navigation Satellite System (GNSS) tracks from vehicular or hand-held navigation devices, call detail records from mobile phone (GSM) carriers and providers, time-stamped location records from online services or social networks,

and so on. GNSS technologies allow us to record individual mobility data across the entire urban network. In Italy, a sample of 3% of the whole vehicle population is monitored for insurance purposes, providing information on single trajectories with a spatial scale of 2 km and a time scale of 30 seconds scale 30 seconds. Moreover, one datum is always recorded when the vehicle engine starts or stops. Each datum includes position, speed, motion direction, and GNSS quality. Despite the relatively poor spatial resolution of such GNSS data, it is possible to perform a real time reconstruction of the individual trajectory dynamics on the road network. Analytical detection of patterns in spatiotemporal mobility can support planning and regulation of traffic flows [12].

2.4.2 Smart Grid

The electricity demand is expected to increase globally for more than two-thirds by the year 2035 according to the International Energy Agency. Such increase in electricity demand will put a higher burden on the current outdated and overstressed power infrastructure. The existing power grid suffers from unreliability due to the lack of efficient monitoring, fault diagnostic, and automation techniques. These problems are not related only to electrical power infrastructure but to water, gas, heat and other city infrastructures as well. Yet, the solutions for electrical power infrastructure are leading in this field. Some of the specific electrical power infrastructure related problems are unidirectional flow from the generating stations to the customers, estimation and prediction of supply based on previous available data, mechanical switches causing slow response times, and centralised generation schemes. Smart grid has emerged to tackle these challenges, where the name suggests an intelligent power infrastructure. Smart grid technology promises to make the world power systems more secure, reliable, efficient, flexible, and sustainable. It can be defined as a modern infrastructure

with efficiency and reliability enhanced through automated control, modern communication infrastructure, monitoring and measuring technologies, and advanced energy management based on demand optimization, energy and grid availability etc. Some of the solutions to mentioned problems propose bi-directional flow and decentralised generation schemes. A bi-directional system is an improvement to the conventional distribution scheme in the sense that electricity flows from the utility to the client's premises and vice versa. A more efficient use of energy is then possible, whereby electricity can flow back to the utility (to be stored for later use) in cases of low demand. The concept of distributed generation enables a scenario where, instead of having a centralised generation scheme, additional electricity generation points can be located closer to customers, reducing thus the impact of losses on electricity transportation over long distances. Additionally, this enables more innovative demand response programs to be put into action. Preferably, these distributed generation points could be ecological and use renewable sources like wind, sun and water energy. In a smart grid, reliable and real-time monitoring is highly required to provide solutions quickly when natural accidents or catastrophes occur to prevent power disturbance and outage. Hence, intelligent monitoring and sensing capabilities to ensure real-time response from the power grid are necessary. Wireless sensor networks can be used as compared to traditional communication technologies because of its low-cost, rapid deployment, flexibility, and aggregated intelligence via parallel processing. Data acquired by these networks can then be used as feedback information about performances and reliability of the grid for the authorised institutions. An important sensing application in smart grid, amongst others, is the monitoring of overhead transmission lines. By monitoring the lines, utilities ensure that power delivery occurs within safe limits. For instance, systems like STAMP sense the

temperature, sag and tension values of an overhead line in real time and determine the state, or health, of the line from these measurements. Apart from monitoring and controlling the grid, sensors can also be used for active monitoring of a household power consumption and thus provide savings and a more and more dynamic billing system [12].

2.4.3 Smart Environment

If the city is not well organised and equipped to face the stress of rapidly growing urbanisation, chaos quickly takes place. The quality of life, the security, the effectiveness of citizens' services, the economic development and attractiveness, and the quality of the environment may decrease quickly affecting the life of the community [13]. As a solution for preserving a smart city environment, a concept of smart environment is proposed, where air and water quality, temperature, humidity and other parameters would be continuously measured. In that way, the changes of environment could be tracked, and pollution could be kept at a reasonable level. Special attention is paid to the mitigation of emission which is a serious threat to our planet, and this is one of the main goals of smart cities. Monitoring of the environment requires a large number of various sensors to be placed, mostly outdoors at locations such as parks, rivers etc. In this regard, the placement of wireless sensors on vehicles or buildings is proposed, so that air pollution in a smart city can be monitored. With the development of the technology, the numbers of electromagnetic fields and the mechanisms, devices and systems working in the wave base, hence the intensity of the electromagnetic field that these systems spread as well, show a rapid increase. The use of 3G and 4G systems being the new-age communication and transmission systems have caused these changes to be increased rapidly in the recent years. The physical and biological

impacts of these fields on the plants and the living beings that have frequency spectrum varying generally from Hz to increments of GHz become frequently a current issue. Some other problems related to fast-growing cities are lighting systems that cause light pollution in the areas around big cities and big energy consumption, noise pollution that has negative effects on people living and working in cities, and waste management that will represent ever growing problems for cities in the future. In order to solve these problems, today's technology should be used and smart solutions found [11][12]. Listed below is an overall comparison between the various types of magnetometers in terms of the detectable field as well as the various applications. It can be seen that some of these magnetometers are suitable solutions developed for the measurement of low range (i.e. micro Tesla and tens of micro Tesla) of magnetic flux densities with high accuracy and sensitivity for low magnetic fields, such as the magnetic field of Earth with a maximum intensity of about 50 μ T [13].

Table 2.2 : A Comparison of the available technologies of magnetic sensors in terms of the detectable field [14].

Magnetic Sensor's Technology	Detectable Field (Tesla)				
	10^{-14}	10^{-10}	10^{-6}	10^{-2}	10^2
Search coil magnetometer					
Fluxgate magnetometer					
Optically pumped magnetometer					
Nuclear precession magnetometer					
SQUID magnetometer					
Hall magnetometer					
Magneto Diode					
Magnetotransistor					
Fibre optic magnetometer					
magneto optical sensor					
magnetoimpedance magnetometer					

Table 2.3: A classification of the various magnetic materials based on the major applications [13-14].

	Definition:	Major application:	Most common sensor:
High Sensitivity	Field gradient or differences measurement because of triggered (in the magnetic field of Earth) or dipole moments which are constant.	1. Magnetic anomaly detection. 2. Mapping of brain function	1. Optically pumped magnetometer 2. SQUID
Medium Sensitivity	Disruption measurement in direction and/or magnitudes of magnetic field of earth because of induced or permanent dipole moments	1. Mineral prospecting 2. Magnetic compass	1. Fluxgate 2. Magnetoresistance Search coil.
Low Sensitivity	Measurement of stronger fields than the magnetic field of Earth.	1. Current measurement 2. Noncontact switching	1. Hall sensor 2. Search coil

2.5 Measurements and Parameters in Magnetometers

Magnetic measurements find applications over a wide range of disciplines. The direct and indirect measurements of magnetic parameters such as the magnetic field strength H , flux density B , permeability μ , susceptibility χ , or magnetostriction λ are commonly applied in science and technology works carried out in paleomagnetism, magneto archeology, mines detection, displacement or proximity testing, current measurement, non-destructive testing of materials, medicine diagnostics, and in many other applications. As a practical example, magnetostriction sensors are often used for measurement of exotic quantities such as acidity pH, blood coagulation, concentration of castor oil (ricin), or even presence of Salmonella bacteria [17].

Although the basic operation of magnetometers is based on measurements of voltage and current signals, accurate measurements of magnetic fields are complex and often ambiguous. For a long, it was assumed by scientists that the magnetisation of magnetic materials could be reliably achieved through two main characteristic parameters; one being the magnetic field H , and the other being flux density B . Later on, following the emergence of international standards, it was concluded that the less-popular polarisation term J (where $J=B-\mu_0 H$) provided a better definition for a materials magnetisation state than flux density did. Nowadays, it is suggested by specialists that adopting the parameter magnetisation, M , would provide an even better description of the magnetisation state. [18]. In literature, research on the direct measurement of magnetic field strength in magnetic materials divides between two main techniques; first adopting Ampere's law by measuring the magnetising current, and second adopting Faraday's law by using search coils. Even today, it is still debated whether certain magnetic field sensors measure the magnetic field strength H or magnetic flux density B . As opposed to electrical measurements, where fundamental parameters are well-established, magnetic measurements are still being studied today [18]. Electrical measurements are founded on a linear relationship between current and voltage known as Ohm's law. As depicted in figure 2.1, due to the potential difference, V , across the sample, a current, I , will flow through it. The magnitude of the current flowing through the material depends on the resistivity of the material, known as ρ , which is directly related to the electrical resistance R , such that, $R=\rho l/A$, where l is the length and A is the cross-sectional area of the sample. Subsequently, the current, I , flowing through the material can be calculated according to Ohm's law which is given by [19]:

$$I = \frac{V}{R} \quad (2.1)$$

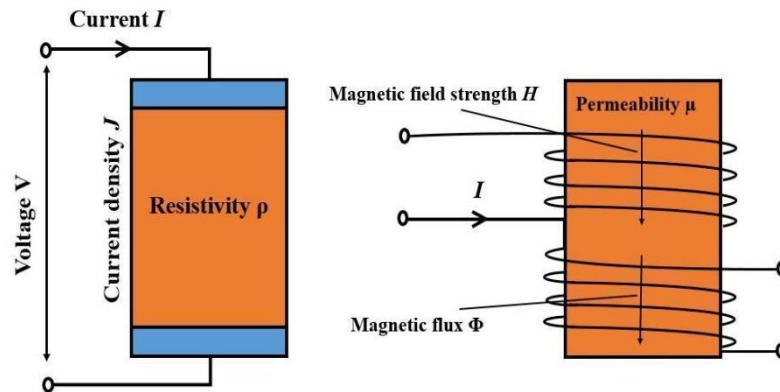


Figure 2.1. Analogy between electrical and magnetic measurements [20].

In magnetism, the term current density (J) is used to provide a more precise description of the response of a particular material with resistivity ρ , when subjected to an electric field, E [20]. It can also be seen in Figure 2.1 that the response of the magnetic material can also be represented by its permeability μ , under influence of the magnetic field strength H , which is generated by the current I flowing in the coil. The H -field, subsequently, gives rise to the magnetic flux Φ . Thus, the response of the material with permeability μ under the magnetic field strength H can be characterised by its flux density as $B = \Phi / A$.

The flux density, B , is often detected by the electric voltage induced in the secondary coil, which is composed of n turns. The magnitude of the induced voltage is highly dependent on the time derivative of B . Although the relationship between magnetic field strength H and flux density B can be described by a relatively simple equation given by [20]:

$$B = \mu H \quad (2.2)$$

Where μ is the permeability of the employed material. The tests involved in characterisation of magnetic materials are usually far more complex than those required for electrical measurements. This is due to the followings:

- Usually in a typical sample of current conducting material, e.g. cuboid or cylinder, the current distribution is uniform with some exceptions, i.e. due to skin effects for high-frequency currents). In the case of magnetic materials, this condition is almost completely opposite, where due to demagnetising fields, the sample under test is usually magnetised non-uniformly with few exceptions, e.g., in ellipsoidal-shaped samples.
- The relationship between the current and voltage is normally linear for most conducting materials with some exceptions. In other words, this allows the description of such materials using a single scalar value that is its resistance R . On the contrary, a non-linear relationship exists between the magnetic field strength H and the flux density B in most typical magnetic materials. This means that it is required to use the whole relation of $B = f(H)$, also known as the magnetisation curve.
- The currently used current-conducting materials are homogeneous which means that the distribution of the current along the material is uniform. However, due to the grain and domain structure of most magnetic materials, the samples are often magnetised non-uniformly.
- Additionally, most of the current-conducting materials are isotropic, with a few exceptions, where the tensor of resistivity is a necessity; oppositely, most magnetic materials exhibit anisotropy of their properties [20-21].

When testing a sample of a particular magnetic material, it is difficult to on the hypothesis about the flux density of the sample, as this parameter largely depends shape of the sample under test, unless the sample shape is pre-selected to be, for example, a ring core, Epstein frame, or sheet/strips. Generally, closed magnetic circuits are recommended; thus, open samples need to be closed by use of an external yoke. The strength and the flux density are highly nonlinear. Therefore, generally it is necessary to use the whole relation $B = f(H)$ known as the magnetisation curve. In the case of DC (static) magnetisation, as according to Faraday's law, to induce voltage, the magnetic flux must be changed. As a result of these technical difficulties that accompany the testing of magnetic materials, almost all the tests are conducted in professional laboratory settings. The hysteresis loop is commonly recognised as a symbol of magnetism, which can be considered the most-frequently tested characteristic of magnetic materials. A typical method of testing the hysteresis loop is presented in figure 2.2. As can be noted, the flux density is represented by its time derivative, which often requires an integrating amplifier; though, modern oscilloscopes are capable of performing this operation. Now, according to Ampere's law, and considering the voltage drop V_H in figure 2.2, the exciting magnetic field strength can be determined as $H = I_1 n_1 / l$, where l is the length of magnetic path and n_1 is the number of turns of magnetising winding. In case of a ring sample, the value of l is close to the mean circumference of the ring. The flux density is usually derived from Faraday's law, such that, $dB/dt = -V_2/n_2A$ [20].

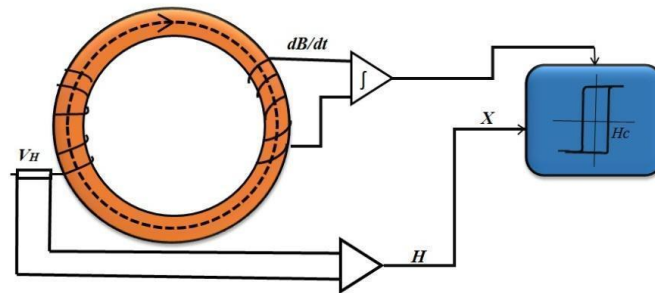


Figure 2.2. Typical approach for determination of the hysteresis loop [20].

2.6 PCP planar and its application

2.6.1 Classification of ferromagnetic materials (Diamagnetic, Paramagnetic, Ferromagnetic Materials)

Some common materials, based on their magnetic properties, are listed in Table 2.4 [21]. The magnetic behaviour of different materials can be classified into several groups; the main three groups include ferromagnetic materials, diamagnetic materials, and paramagnetic materials. Paramagnetic materials produce a small magnetisation in the same direction as the applied field, with a positive susceptibility value of around 10^{-5} to 10^{-3} . On the contrary, diamagnetic materials have negative susceptibility values in the range of -10^{-5} . On the other hand, ferromagnetic materials have susceptibility values well above one [21].

Table 2.4: The classification of the various materials based on the magnetic properties and the relative permeability values [21].

Material	Magnetic Classification	Relative Permeability μ_r
Copper	Diamagnetic	0.999991
Water	Diamagnetic	0.999991
Vacuum	Nonmagnetic	1
Air	Paramagnetic	1.0000004
Aluminium	Paramagnetic	1.00002
Cobalt	Ferromagnetic	250
Nickel	Ferromagnetic	600
Iron	Ferromagnetic	5000
78 Permalloy (78.5Ni)	Ferromagnetic	100000
Mumetal (75Ni, 5Cu,2Cr)	Ferromagnetic	100000

In addition to the three of mentioned magnetic materials, there are some other types of magnetic materials, which are all very closely related to ferromagnets. These materials include ferrimagnets, antiferromagnets, helimagnets and superparamagnetism, all of which were discovered many years after the emergence of the three classical groups of magnetic materials above. From a magnetic measurement perspective, the ferrimagnets are almost indistinguishable from ferromagnets, while the antiferromagnets and helimagnets were for many years mistaken for paramagnets [22].

2.6.2 Susceptibilities of diamagnetic and paramagnetic materials

The magnetic susceptibility of diamagnetic and paramagnets is considered to be constant at constant temperature and relatively low magnetic field H . Linear relationship between M and H could be observed. Hence magnetisation can be defined as [23] from equation (2.3)

$$M = \chi H \quad (2.3)$$

$$B = \mu_0(1 + \chi)H \quad (2.4)$$

$$B = H\mu_0\mu_r \quad (2.5)$$

$$B = H\mu \quad (2.6)$$

In paramagnets, μ_r is slightly greater than that in the diamagnets, whilst χ is slightly greater than zero in paramagnets and slightly less than zero in diamagnets. While the susceptibilities for various materials in ferromagnets, neither susceptibility χ nor permeability μ_r has a constant value, instead, both parameters are functions of the prevailing magnetic field H and the previous history of the material [23-24].

2.6.3 Classification of ferromagnetic materials

Ferromagnetic materials can be easily classified to soft and hard magnetic material according to their coercivity, which is a structure-sensitive magnetic property. This implies that in such materials, the sample is subject to change characteristics under different thermal and mechanical treatments [25]. It has been found in the past that, mechanically hard samples of iron and steel had a high coercivity, whilst soft materials

had a low coercivity. Therefore, the term 'soft' was used to distinguish ferromagnets on the basis of the coercivity[26].

Soft Magnetic Materials:

In various crystalline, amorphous and nanocrystalline elements, and alloys and compounds, low coercivity and high permeability can be realised. General requirements for magnetic material design include low magnetocrystalline and strain anisotropy, or a number of easy directions and negligible inner stress [27]. Amorphous materials with zero magnetocrystalline anisotropy ($K_i = 0$), and nanocrystalline materials, in which the small grain size averages out the anisotropy, are usually desired. Anisotropic materials are often adopted for their parallel design of flux path that allows for easy directions, however, in fluxgate sensors, the easy direction is perpendicular in order to achieve low noise. In most cases, to preserve the intrinsic material parameters after mechanical deformation, stress-relief annealing is a necessity [27-28].

Crystalline Materials:

Metallic crystals without imperfections, such as pure iron and nickel, are the classic types of soft magnetic materials. Some examples of widely used alloys include nickel-iron (e.g. permalloy, supermalloy and mu-metal with very high permeability), cobalt-iron (with highest saturation), silicon-iron (cheap material with increased resistivity for reduction of eddy currents), and silicon-aluminium iron (e.g. sendust, which is mechanically hard) [29].

Amorphous metals:

Amorphous metals are alloys mainly based on iron and cobalt, with additions of boron and silicon. Usually, they are produced by the rapid solidification from melt spinning of thin wires and ribbons. The main advantages include high permeability and low losses, while drawbacks include relatively lower saturation magnetisation (0.75 to 1.6 T) when compared to crystalline iron alloy and limited magnetic core design options due to the low thickness of the tape [29][30].

Hard Magnetic Materials:

Permanent magnets are used to provide a magnetic field on their surface. The same hard magnetic materials that are used to make permanent magnets benefit from high coercivity and remanence magnetisation. They usually operate in the second quadrant of the hysteresis loop (i.e. the demagnetisation curve). Given that the knee of the B - H curve sits well below the safe operation point, it is possible to achieve a high stability; otherwise, a changing air gap or a strong external field could partially demagnetise a magnet, especially at elevated temperatures [31]. The maximum energy product $(BH)_{\max}$ is an important material property; magnets made of high $(BH)_{\max}$ materials are usually small. In order to best utilise the properties of the magnetic material, the optimum operating point should be chosen as close to $(BH)_{\max}$ as possible [32].

2.7 Magnetic properties of ferromagnetic material

Ferromagnetic material is considered as the most significant magnetic material for adoption in a diverse set of engineering applications, due to their high permeability which enables for high magnetic inductions to be obtainable under modest magnetic fields and also their ability to retain magnetisation, and thus, act as a field source itself.

In addition, the torque generated by the ferromagnetic material on a magnetic dipole in a field can be used in electric motors. The ferromagnetic elements of interest in the periodic table include iron, cobalt, nickel and several of the lanthanides, which are all technologically vital. Thus far, it has been discussed that ferromagnets have, in general, a large relative permeability and susceptibility [33].

Permeability

The relationship between the flux density, B , and the magnetic field strength, H , a magnetised material is governed by the permeability of the material as shown in equation 2.7. However, this is not a practical approach for the characterisation of certain properties of a material [34]. This requires the determination of the relative permeability μ_r , which is the ratio of the permeability μ relative to the permeability of the free space μ_0 i.e. $\mu_r = \mu/\mu_0$. Subsequently, the flux density, B , can be expressed as:

$$B = \mu_r \mu_0 H \tag{2.7}$$

Theoretically, permeability μ could be employed as an ideal merit for characterisation of the properties of magnetic materials as it conveys direct information on the relationship between two main material parameters, i.e. the flux density, B , and the magnetic field strength, H . However, in practice, certain complexities must be overcome as a result of the following:

- The relationship between B and H is almost always nonlinear, and thus, the magnitude of permeability depends on the working point, i.e. the magnetic field strength;

- The shape of the material plays an important role in that the permeability of a magnetised body can be completely different to the permeability of a raw material. Moreover, the magnetisation is non-uniform along the whole body and only a mean value can be determined;
- Most magnetic materials are polycrystalline, and therefore, they have different properties (including permeability) for various directions of magnetisation, in which case the material is said to be anisotropic.
- Permeability depends on many other factors such as frequency, the presence of harmonics which cause deviation from sinusoidal shape of flux density, etc. [33][34]. Therefore, although permeability is a very useful parameter from a physical perspective, in technical applications (e.g. in the design process), the magnetisation curve would serve a better tool in describing the magnetisation process. Nevertheless, in certain applications, permeability can still be the most important measurement factor, for example, in magnetic shielding design, where the higher the value of permeability, the more effective the shielding is, or in magnetic concentrator design, where a magnetic material with highest possible permeability is mostly preferred. Presently, it is possible to procure ferromagnetic materials with relative permeability as high as one million. Table presents the typical values of maximum relative permeability for some commercial ferromagnetic materials [35].

Table 2.5: Typical Values of Maximum Relative Amplitude Permeability of Some Ferromagnetic Materials [36].

Material	μ_{max}
Iron	6,000
Pure 99.9 iron	350,000
Silicon iron (non oriented)	8,000
Silicon iron (oriented)	40,000
Silicon iron (cubic texture)	100,000
Permalloy 78Ni-22Fe	100,000
Supermalloy 79Ni-16Fe-5Mo	1,000,000
Permivar 43Ni-34Fe-23Co	400,000
Amorphous Metglas Fe40-Ni38-Mo4-B18	800,000
Amorphous Metglas Co66-Fe4-B14-Si15-Ni1	1,000,000
Nanocrystalline Nanoperm Fe86-Zr7-Cu1-B6	50,000 at 1KHz

Coercivity H_C and Remanence B_R

When the field is reduced to zero after magnetising a magnetic material the remaining magnetic induction is called the B_R . The remanence is used to describe the value of either the remaining induction or magnetisation when the field has been removed after the magnetic material has been magnetised to saturation. [37] On the other hand, the magnetic induction can be reduced to zero by applying a reverse magnetic field of strength H_C which is normally known as the ‘coercivity’. It is strongly dependent on the condition of the sample, being affected by such factors as heat treatment or deformation. As with the remanence, a distinction is drawn by some authors between the coercivity field, which is the magnetic field is needed to reduce the magnetization to zero from an arbitrary level, and the coercivity which the magnetic field needed to reduce the magnetization to zero from saturation [38].

Hysteresis and related properties

The most common way to represent the main magnetic properties of ferromagnetic materials is by plotting their magnetic induction B through various field strengths H . Alternatively, plots of magnetisation M against H can be used to characterise the magnetic properties of ferromagnetic materials, which can provide the same information as using B versus H relationship; this is true due to the fact $B = \mu_0(H + M)$. The term 'hysteresis', meaning 'to lag behind', was introduced by Ewing, who was the first to systematically define this parameter in magnetism. An illustration of a typical magnetic hysteresis loop is shown in Figure 2.3 [39].

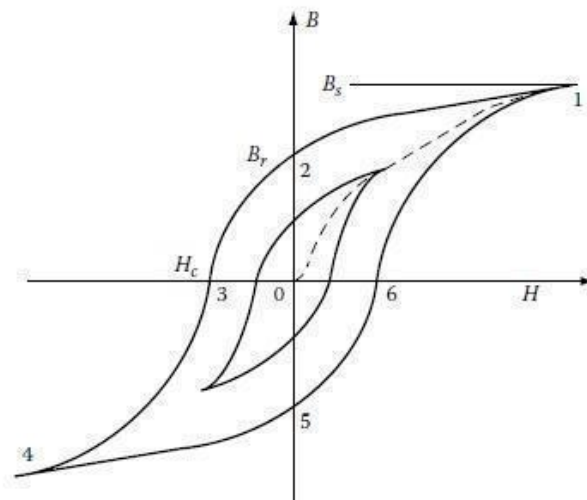


Figure 2.3. Typical hysteresis loop and its characteristic points B_r and H_c [39].

Considering the hysteresis loop shown in Figure 2.3, the start point is always from the demagnetised state. The first part of the path, between '0' and '1', poses similar behaviour to the primary magnetisation curve. However, it is clear that the return path from '1' to '2' is quite different to the ascending magnetising curve. For point '2', where magnetic field strength is zero, the material remains magnetised. This magnetisation

is called the residual or remanence flux density B_r , also known as remanence magnetisation. In order to achieve zero flux density (i.e. point '3'), it is necessary to apply a magnetic field equal in magnitude but opposite in direction. This field is called coercivity H_c [38][39]. The magnetic coercivity is a crucial parameter in characterisation of soft magnetic materials. This is due to the dependency of magnetic losses on the area of the hysteresis loop. From Figure 2.3, it is evident that the smaller the value of the coercivity, the smaller the power loss [40].

Table 2.6 provides a list of typical coercivity (H_c) and saturation flux density (B_s) values derived from hysteresis loops of various soft magnetic materials. Similarly, Table 2.7 presents the hysteresis parameters as derived for some hard magnetic materials, i.e. the permanent magnets [41].

Table 2.6: Main Parameters of Hysteresis Loop of Various Soft Magnetic Materials[41].

Material	H_c (A/m)	B_s (T)
Iron	70	2.16
Pure 99.9 iron	0.8	2.16
Silicon-iron (non oriented)	40	1.95
Silicon-iron (oriented)	12	2.01
Silicon iron (cubic)	6	2.01
Permalloy 78Ni-22Fe	4	1.05
Supermalloy 79Ni-16Fe-5Mo	0.15	0.79
Permendur 50Fe-50Co	160	2.46
Amorphous Metglas Fe40-Ni38-Mo4-B18	8	0.88
Amorphous Metglas Co66-Fe4-B14-Si15-Ni1	0.24	0.55
Nanocrystalline Nanoperm Fe86-Zr7-Cu1-B6	3	1.52

Table 2.7: Typical Parameters of Hysteresis Loop for Various Hard Magnetic Materials [41].

Material	B_H (kA/m)	B_r (T)	$(BH)_{max}$ (kJ/m ³)
Ferrite BaFe12O19	144	0.35	26
Alnico Fe—Co-Ni-Al	52	1.30	44
SmCo5	690	0.92	200
Sm(Co-Fe-Cu-Zr)	560	1.12	240
Nd-Fe-B	780	1.35	320

After arriving at point '3' on the hysteresis loop shown in Figure 2.4, the magnetic field is moved further in the negative direction until the negative flux density saturation point, shown by '4', is reached. Note that reversing the direction of magnetic flux (i.e. from negative to positive) does not close the loop at point '0' and rather closes at point '1'. If the material is magnetised by an alternating sinusoidal field, that will correspond to a full hysteresis loop at every cycle of the alternating field [40][41].

The hysteresis loops obtained at different peak values of magnetising fields often result in a family of loops, as shown by Figure 2.4 (a). Primary magnetisation curve can be obtained by connecting the tips of the resulting loops. Suppose the magnetising field reverses at an arbitrary point, in which case, the loop will no longer follow the original contour but branches out to form a minor hysteresis loop, similar to that shown in Figure 2.4 (b)[42-44].

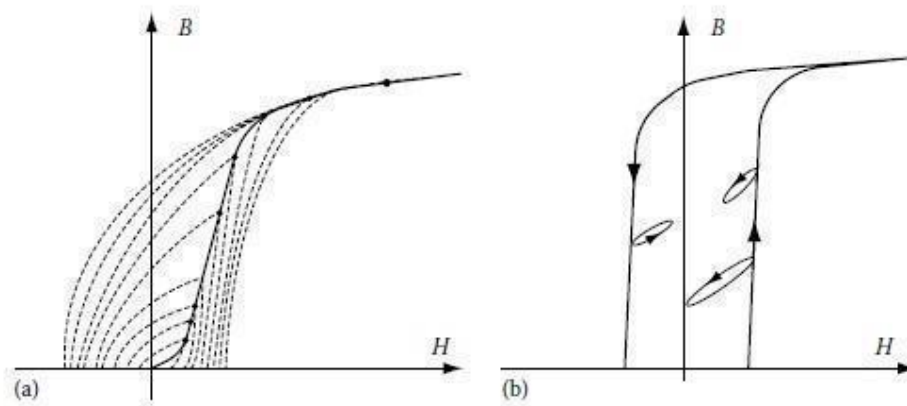


Figure 2.4. The family of hysteresis loops obtained for various amplitudes of the magnetising fields and the magnetization curve obtained by connecting the tips of these loops (a); major and minor hysteresis loops (b)[42].

2.8 Application of PCB planar coils

2.8.1 The PCB Planar Fluxgate

Several applications require small-sized magnetic sensors such as the compass and navigation systems. The fluxgate sensors are suitable candidates that fulfil such requirements as it was shown earlier. The miniaturisation of these sensors is important that can replace the wound excitation and sensing coils and this can, in turn, reduce the fabrication costs [43-44]. In this part of the thesis, the state of the art fluxgate sensors will be presented. The main focus will be on devices that were fabricated using small sized wires as this is more relevant to the scope of the work presented in the following chapters [44]. In the current section, the development and the comparison of different planar fluxgate magnetic sensor structures realised in printed circuit board (PCB) technology are presented. This work allowed us to define a design approach for the development of planar magnetic sensors and to verify the simulated performance with results in order to validate the entire procedure.

The Fluxgate structure appears to be the most feasible solution for realising precise vector magnetic field sensors to be used in Earth's magnetic field measurement; the main drawback of Fluxgate magnetic sensors is the complex construction of the core and the coils. In recent years, new topologies of planar integrated micro-fluxgate have been presented, which allow small dimensions and low power consumption to be achieved together with a simplification of the integration process. When small dimensions and low power consumption are not vital, similar topologies can be fabricated in PCB technology [45]. The choice in favour of PCB technology derives primarily from its reduced cost and efficient fabrication. On the other hand, since low power consumption and small dimensions are indeed the fundamental requirements for a magnetic field sensor to be embedded in portable devices, a micro-integrated version is mandatory for these applications [45].

2.8.2 Fluxgate sensors

A fluxgate magnetometer is a device used to measure magnetic fields, through utilisation of the non-linear magnetic characteristics of ferromagnetic core materials as the sensing element [45]. This type of magnetic sensor is a directional device, used for measuring the component of the field that is parallel to the magnetic core. Fluxgate magnetometers were first introduced in the 1930's [43][44]. Initial applications of these magnetometers were for airborne magnetic surveys and for submarine detection purposes during World War II. Later on, they were further developed for geomagnetic studies, mineral prospecting, and for magnetic measurements in outer space. They also serve both civilian and military applications, as found in various detection and surveillance devices. Despite the advent of newer technologies for magnetic field

measurement, fluxgate magnetometers still continue to be used successfully in all of the aforementioned areas, owing to their high reliability, relative simplicity and low cost [45].

With the beginning of the space age in the late 1950's, fluxgate found a new domain of application as employed in space magnetometry. The first satellite to carry a magnetometer to space was Sputnik 3 launched in 1958, which carried a servo-oriented fluxgate on-board. Later on, the USSR Venus probe launched in 1961 carried two single-axis flux gates that measure the magnetic fields around Venus[46].

In 1990, Seitz made the first attempt to fabricate an integrated fluxgate sensor, where consisted of a sputtered permalloy layer, sensing coils which were fabricated on a silicon substrate of 2 mm x 4mm area, and an excitation coil which was wound around the integrated circuit [47].

Then in 1994, Kawahito *et al.* reported a micro-machined fluxgate sensor composed of an electroplated permalloy rod, and solenoidal excitation and sensing coils [48]. Gottfried-Gottfried reported on a similar sensor structure, where metallisation lines of the CMOS process were used to fabricate the solenoidal coils, and the permalloy core was electroplated in between the metal, through the modification of the CMOS process flow [49].

The first fully integrated CMOS fluxgate sensor was reported by Schneider *et al.* in 1997 [50-52], and then by Kawahito in 1999 [50][51]. The structure was later on improved by Ripka *et al.* who added a symmetrical core layer beneath the planar coils, which formed an almost closed magnetisation path between the upper and lower cores used for the excitation [52]. More recently, Chiesi *et al.* reported on the development of a 2D micro-fluxgate compass that used the cross-shaped amorphous material

(Metglas®), patterned and glued on the sensing and excitation coils fabricated by a CMOS process [53][54].

All the sensor designs discussed above use the parallel fluxgate configuration [98]. The first attempt to miniaturise the fluxgate sensor was done on an orthogonal structure, achieved by Gise and Yarborough [56]. In their design, copper coils wound around the core were used as the sensing coils. After this approach, orthogonal configuration was almost forgotten, however, similar structures were used as GMI sensors [57].

Twenty years on from the first attempt, Chiesi et al. developed a micro-fabricated orthogonal fluxgate sensor [57][58]. In their new design, Chiesi et al. used a rectangular-shaped core of dimensions 600µm x 100 µm, made out of an amorphous ferromagnetic ribbon (Vitrovac® 6025Z), which was glued on the micro-fabricated planar sensing coils. The excitation current was provided through the wires directly bonded to the core[59]. In 2000, Kejik et al. reported on the development of a 2D PCB fluxgate sensor working in the orthogonal mode [60]. The sensor consisted of a pair of excitation and a pair of sensing coils, which were placed in a cross shape on the PCB, being orthogonal to each other [61].

Nowadays, developments of this particular magnetic sensor are expected to rely on the CMOS technology for the coils and CMOS-compatible post-process technology (i.e. sputtering) for the core deposition; all the extra effort is for the possibility to realise a micro-fluxgate sensor with a very low power consumption (few milliWatts), over the smallest spatial occupation possible[62].

2.9 Core shapes of fluxgate magnetometers

The applications of fluxgate magnetometer can be classified based on the core shapes utilised in these systems such as : the rod core, the ring core sensor and the racetrack sensor, square and hexagon core type. These will be discussed individually in this section in order to highlight the differences between those configurations. Testing of integrity of materials by using sensing coils of square type is discussed.

Rod core

In this configuration, the core is made of two ferromagnetic strips or wires. These are excited by individual excitation coils in opposite directions. In this case, the sensing coil is wound around both rods, Figure 2.5 [63].

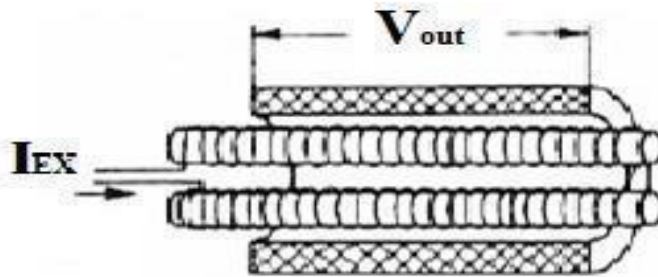


Figure 2.5. Core shape of fluxgate sensor (Rod core) [63].

Ring core sensor

In this design shape, Figure 2.6, the excitation is wound following a toroidal trend around the ring-core with the diameter of the ring-core oriented in the direction of the magnetic field that is to be measured. In one half of the ring-core, the field due to the current in the excitation coil is parallel to the external field B_0 . Whereas in the other half of the ring-core, the field is anti-parallel to the external field. In this configuration, the ring-core is constructed from a thin tape of soft magnetic material that is made into several turns. The sensing coil is a simple solenoid with its axis parallel to the field that

is to be measured. The ring-core is placed in the centre of the sensing solenoid, and this provides a design of low-noise despite the fact that ring-core sensors have low sensitivity due to large demagnetisation [64].

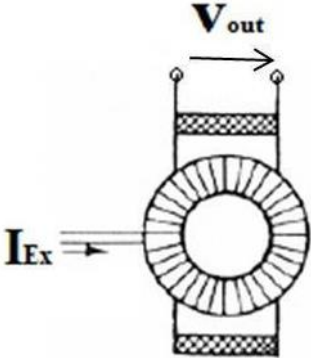


Figure 2.6. Core shape of fluxgate sensor (Ring core) [64].

Race-track sensors

In race-track configuration, Figure 2.7, the sensitivity is generally higher than that for the other types with its sensitivity being lower relative to the perpendicular field due to the lower demagnetisation factor. This means that the advantage of closed-type sensors is maintained when this configuration is employed [65].

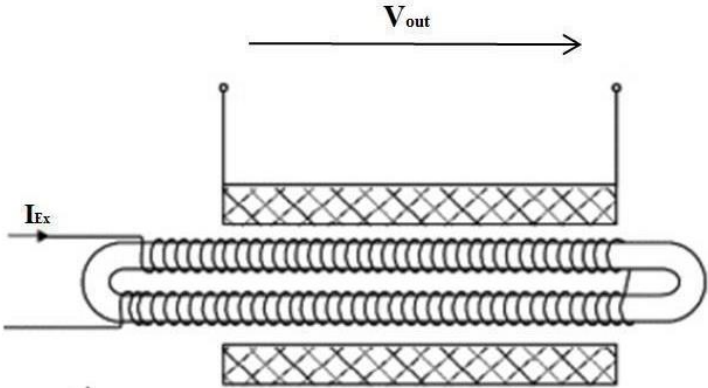


Figure 2.7. Core shape of fluxgate sensor (race-track sensor) [65]

Square core sensor

The main drawback of fluxgate magnetic sensors realised with the schematic shown in Figure 2.8 is the complex construction of the core and of the coils when they have to be realised within a planar technology (CMOS-IC or PCB), in which it would be desirable to fabricate the ferromagnetic core with a technological step on top of the planar process. new topologies of planar integrated micro-fluxgate have been recently presented. For instance, a structure for a differential single-axis planar fluxgate magnetic sensor will be discussed in the following chapters.

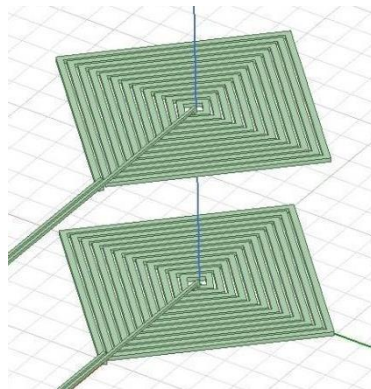


Figure 2.8. Core shape of fluxgate sensor (square sensor)

2.10 Core Materials

There are general requirements that have to be fulfilled for a material to be used as a core material and this includes:

- High permeability and low coercivity.
- Low magnetisation materials such as perm-alloys (Fe and with 78 to 81% Ni alloy) and amorphous alloys [66].
- Amorphous magnetic materials such as metallic glasses that are produced by rapid quenching. This includes Cobalt-based amorphous alloys with low

magnetostriction that are suitable for fluxgate applications. Annealing may further decrease the noise level of a tape for fluxgate core [67].

2.11 Operating principle

The basic structure of a fluxgate sensor, as depicted in Figure 2.9 [68], consists of two coils; a primary (excitation) and a secondary (sensing) coil, wrapped around a common high permeability ferromagnetic core. The excitation current, I_{exc} , flowing through the primary coil gives rise to a field that periodically saturates the soft magnetic-material core in both directions. As can be seen in Figure 2.9) b, during saturation, the permeability of the core drops and the DC flux associated with the DC magnetic field, B_0 , also decreases with it. The name of the device derives from this “gating” of the flux that occurs when the core is saturated. In the presence of the field to be measured, the second and higher-order harmonics appear in the voltage, V_{ind} , induced in the secondary coil [68][69]. These harmonic elements are in proportion to the field to be obtained and represent the coil output[70]. [70].

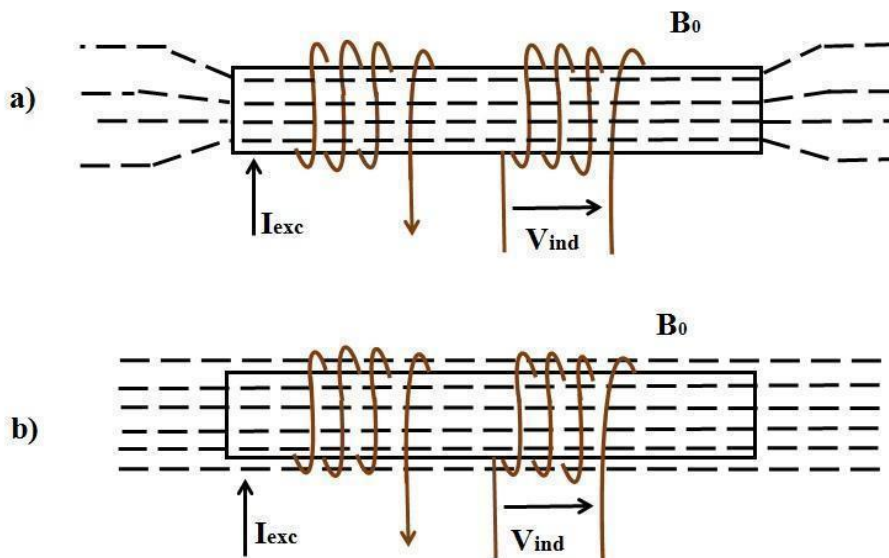


Figure 2.9. Fluxgate principle a) core not saturated b) core saturated [68].

Using Faraday's law, the amplitude of the induced voltage can be calculated as below,

$$V_{\text{ind}} = -\frac{d\Phi}{dt} \quad (2.8)$$

$$V_{\text{ind}} = -N_{\text{sens}} \cdot A \cdot \frac{dB(t)}{dt} \quad (2.9)$$

$$V_{\text{ind}} = -N_{\text{sens}} \cdot A \cdot \frac{d}{dt} \left(\frac{\mu \cdot N_{\text{exc}} \cdot I_0 \sin(2\pi f_{\text{exc}} t)}{l} \right) \quad (2.10)$$

where N_{sens} the number of is turns on the sensing coil

N_{exc} is the number of turns on the excitation coil

A is the cross-section area of the sensing coil

l is the length of the excitation coil

μ is the magnetic permeability; and $I_0 \sin(2\pi f_{\text{exc}} t)$ is the sinusoidal excitation current, injected at frequency f_{exc} [71]. It is possible to improve the sensor sensitivity by maximising the induced voltage through adoption of one of the following solutions:

- By increasing the excitation frequency f_{exc} , However, there is an upper limit given by the cut-off frequency of the relative permeability of the ferromagnetic material.
- By increasing the number of coils N_{sens} for the sensing coil.
- By increasing the cross sectional area (A) of the ferromagnetic material which, in turn, will consume more power due to the larger amount of current required to saturate the ferromagnetic material [72].

The main drawback associated with those fluxgate magnetic sensors that are constructed as shown in Figure 2.10 is the complex manufacturing processes involved in the making of the core and the coils, which have to be realised by using planar technologies (CMOS-IC or Printed Circuit Board). In these complex processes, it is desirable to fabricate the ferromagnetic core with an additional technological step, on top of the planar processes. In this situation, the solution offered in Figure 2.10 becomes more difficult to implement [73]. As a result, new topologies of planar integrated micro-fluxgate sensors were recently presented. Figure 2.10 [74][75] presents the schematic of the structure of a differential single-axis planar fluxgate magnetic sensor, where the ferromagnetic core is placed over the diagonal of the excitation coil. Supplying the excitation coil with a suitable alternating current, each half of the core saturates periodically in opposite directions, as illustrated in Figure 2.11 [74][75]. In absence of an external magnetic field, the two sensing coils connected in anti-phase exhibit an output voltage that ideally is zero [76].

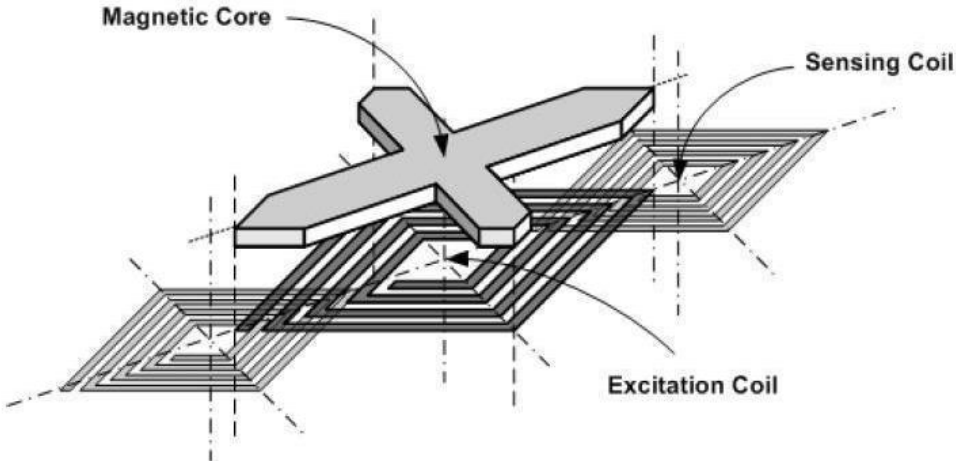


Figure 2.10. Schematic of a double axis planar Fluxgate magnetic sensor [74][75].

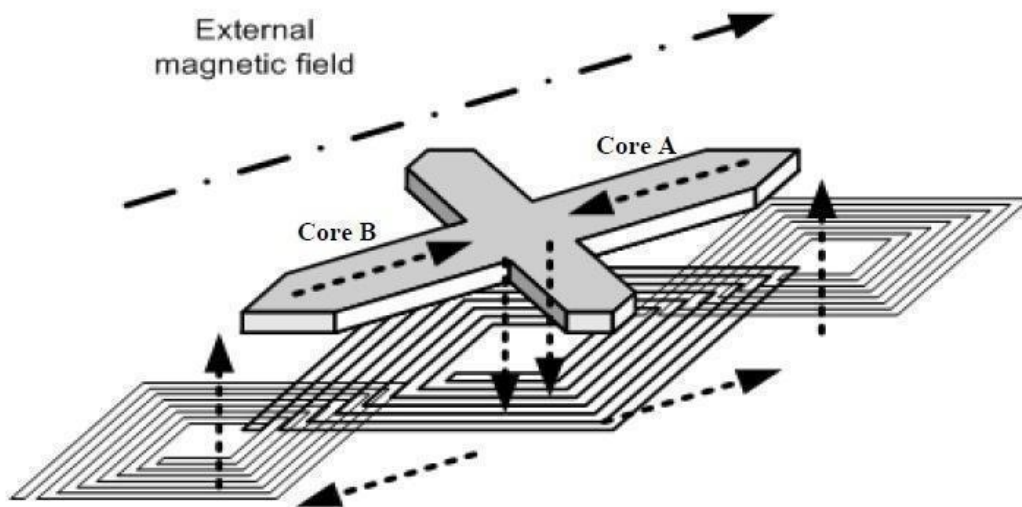


Figure 2.11. Core magnetization and external magnetic field direction: because of the excitation magnetic field each half of the core is magnetised in the opposite direction [74][75].

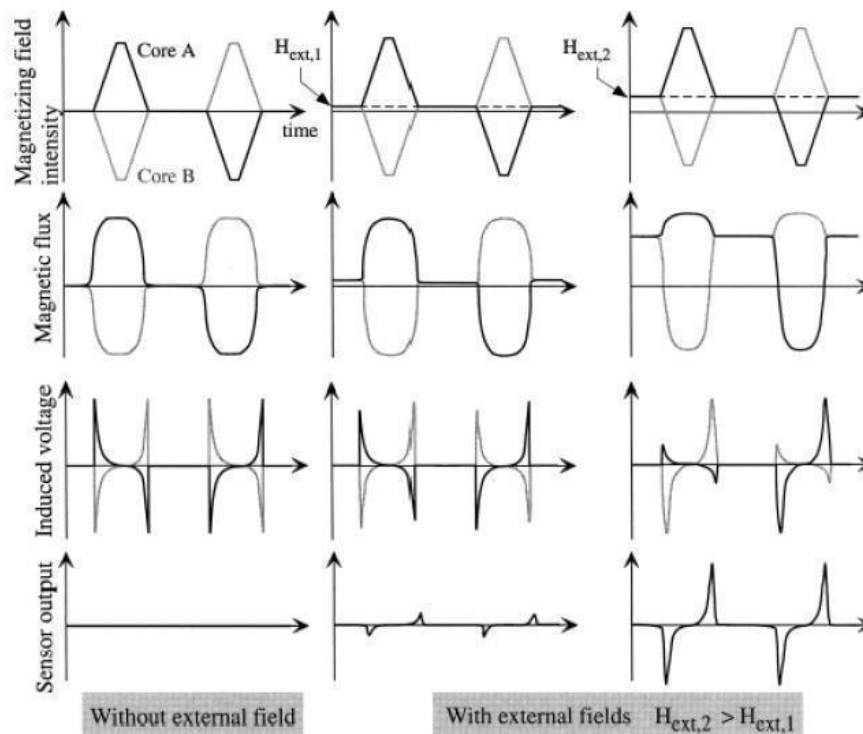


Figure 2.12. Fluxgate principle explained with the waveform of the magnetic field and of the voltage induced [74][75].

On the contrary, when an external magnetic field component is present and is parallel to the core, the magnetisation in one-half of the core is in the same direction as the external magnetic field, while the magnetisation of the other half of the core is in the opposite direction (refer to Figure 2.11) [74-76]. These results in unequal levels of voltage induced in the two sensing coils, causing an increase in the differential output voltage and modulation of its amplitude. Figure 2.12 presents the results of three different scenarios; one with no external magnetic field applied and two with different amplitudes of external magnetic fields [76][77]. With a suitable core shape, e.g. cross shape, and with four sensing coils, the structure proposed in Figure 2.11 can be implemented as a double-axis magnetic sensor [78]. Due to their small footprint, these sensors can be embedded on the top of an IC (achieving small dimensions and low power consumption), or they can be manufactured using the PCB technology [78]. The latter solution is not affected by the main disadvantages of integrated fluxgate, where the ferromagnetic material has to be deposited during the integration process, by having it as a layer of a multilayer PCB [79].

2.12 Wireless charger

2.12.1 Overview and major events in the wireless charging technology

The wireless charging technology has become a hot spot for many devices and appliances such as mobile phones, tables, and more. The first scientist to conduct experiments with wireless charging is none other than Nikola Tesla, the pioneer of alternating current electricity. In 1899, he reached a breakthrough in experiments. He transmitted a high frequency 108 volts electric power to a distance of 25 miles; enabling him to light 200 bulbs and subsequently to run an electric motor [80][81]. Tesla established the Wardencllyffe Tower to transmit electrical power globally through

the ionosphere without any cords in 1901. But this idea has not been developed further or commercialised due to the major limitations to the supporting technology (e.g. low efficiency in the system). The invention of magnetrons during the 1920s and 1930s enabled the conversion of electricity to microwaves and this helped in transferring wireless power for long distances. Until 1964, there was no technology available to convert microwaves back into electricity. W C Brown invented rectenna to enable this. Brown demonstrated this technology by powering a model helicopter using microwave power transfer. This technology further inspired numerous researches in Japan and Canada for microwave powered aeroplanes in 1980s and 1990s [81].

2.12.2 Wireless Charging techniques

Wireless charging technology's evolution is improving toward three main directions: magnetic inductive coupling, microwave radiation and magnetic resonance coupling [82]. Two of these methods, namely magnetic resonance coupling and magnetic inductive coupling work only on near-field. In the near field, the produced electromagnetic radiation covers the area close to the transmitter or the scattering objects. In this technique, the rate of absorption of radiation influences the load produced on the transmitter [82][83]. The electric power in near-field technique gradually decreases with respect to the cube of the reciprocal of distance. In contrast, microwave radiation relies on far-field techniques and is used for distance transmission. In this technique, the electric power attenuated with respect to the reciprocal of the distance. Also, in the far-field method, the absorption of radiation has minimal effect on the transmitter [83].

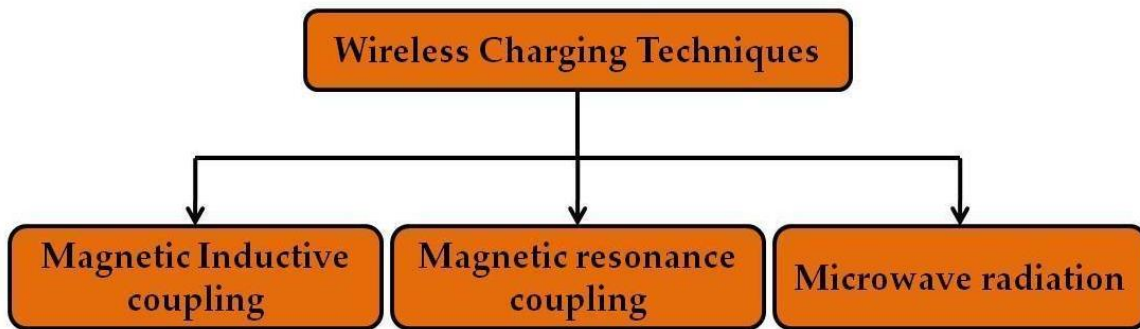


Figure 2.13. Wireless charging techniques.

2.12.3 Typical wireless phone charger

Figure 2.14 illustrates the diagram of wireless chargers. It consists of two main sides, the power transmitter on the left which is attached to the electrical grid and power receiver on the right which is incorporated into the load device is shown in figure 2.14 [84]. The key element for signal transfer for both the power transmitter and the power receiver has been defined by a resonant tank, including both coupled inductors. The primary coil is on the transmitter side and the secondary coil is on the receiver side, different topologies are proposed in (chapter 6) [84].

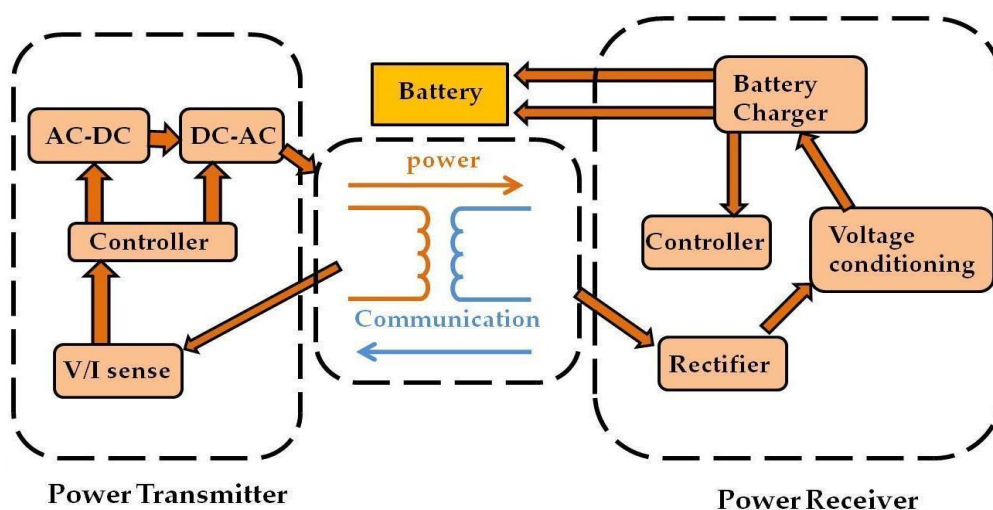


Figure 2.14. diagram of wireless charger

Figure 2.14 shows that communication data streaming in the opposite way so signal flow does not only contain of the power signal from the power transmitter to the power receiver a communication link is requested as the power transmitter needs to be constantly up to date about battery power needs and state of charge [84][85]. An amplitude modulation of the power will be drawn from the transmitter side so the communications channel is implemented through it.

In the wireless power transmitter part the transmitter coil converts the DC power AC power signal. An alternating magnetic field has been created in the coil due to induction to transmit energy by the AC current, which is linked with the wireless power transmitting coil. In the wireless power receiver the energy will be received as an induced alternating voltage (due to induction) by the receiver coils and a converter in the wireless power receiver part converts that AC voltage to a DC voltage. Lastly the load would be fed by the converted DC voltage through a voltage controller section.

So, the wireless power receiver part's main task is to charge a low power battery through inductive coupling [84].

2.13 Summary

This chapter has discussed the magnetometers, materials of that magnetometers and its applications. This is essential in order to understand the various parameters and variables involved in the four design studies. The aim of this chapter was to provide information on and background for the subsequent chapters. In chapter 3 the development of different planar Fluxgate magnetic sensor structures realised in printed circuit boards (PCB) and compares their performance based on their magnetic field parameters, the design will build up ANSYS model to simulate the behaviour of a newly developed planar coil. In chapter 4 developed ANSYS model will test the results of the

model and comparison of the output with many cases such as Evaluate the excitation current value that ensures the saturation for ferromagnetic material and how the current is affecting the BH curve which in turn will affect the sensitivity of the sensor, Different number of turns and analyse the BH curves of each case, Compare the output voltage with different thickness ferromagnetic materials, Different wire width and Different core width. In addition to the experimental optimisation and the results of the proposed planar will be compared with a Simulated optimised planar. Finally in chapter 5 and 6 the performance, modelling and application of the various shapes of coils over various spacing distances will be designed, simulated, experimented and then tested with topologies such as circular, square and hexagon coil configurations. The methodology that will be described is considered an effective way for the development of sensors based on planar coils with better performance. Moreover, it also confirms a good correlation between the experimental data and the FEM models. Once the best topology is chosen based on performance, an optimisation exercise was then carried out using uncertainty models.

CHAPTER 3

OPTIMISATION OF PLANAR COIL USING MULTI-CORE

This chapter employs the built up ANSYS model to simulate the behaviour of a newly developed planar coil which is built from a Mu-metal. In this respect, the model will examine the material as well as the developed design of the magnetometer. The current work has been published elsewhere showing the novelty of the employed design and model.

3.1 Multi-Core Fluxgate

This section presents the development of different planar Fluxgate magnetic sensor structures realised in printed circuit boards (PCB) and compares their performance based on their magnetic field parameters. This work provides a design approach for the development of planar magnetic sensors and to verify the simulated performance with results in order to validate the entire procedure.

3.2 The Proposed Fluxgate Architecture

The schematic of the micro fluxgate structure realised for the triple cores Fluxgate is shown in Figure 3.1 This structure consists of an excitation coil, sensing coils and three ferromagnetic cores located on the top, middle and bottom sections of the fluxgate in order to concentrate the field using the iterative optimisation technique. Generally speaking, magnetic materials have a property which allows them to influence the magnetic field in its environment. In other words, better performances can be obtained by using magnetic top and bottom shields as it is the case in the current design.

Magnetic shielding involves the use of high magnetic permeability material panels that provide a preferential path for the magnetic flux line materials such as the mu-metal. This material has a greater permeability to magnetic fields (H) than the air surrounding them and therefore concentrates the magnetic field lines. By a strategic placement of the ferrite materials it was possible to concentrate this magnetic field and therefore influence the intensity and the shape of a field. In this case, the magnetic field will be easily passed through the material (i.e. the upper and lower cores), it will wrap around the coils instead of going further away from the coil and this will allow the magnetic field to stay altogether within the top and bottom core. The second benefit of having the top and bottom cores is that the magnetic flux will not be able to pollute the environment. The third advantage of the multiple cores is that the coils will intensify the field within the sensor which means that less current is consumed to obtain the desired results. The planar excitation coil is characterised by 30 μm thickness, 20 turns and 400 μm pitch. The current in the excitation coil should be enough to saturate the ferromagnetic material glued over the PCB. This material is shaped similar to the shape of the coil to make the device sensitive to the two components of a magnetic field coplanar with the fluxgate. For each component of the magnetic field, the output voltage is obtained from the sensing coils placed in between the two layers of the material, having 30 μm thickness, 20 turns and 400 μm pitch. The excitation and sensing coils are realised at a distance of 50 μm from each other. The dimensions of the device are 57.3 mm width by 58.1 mm length.

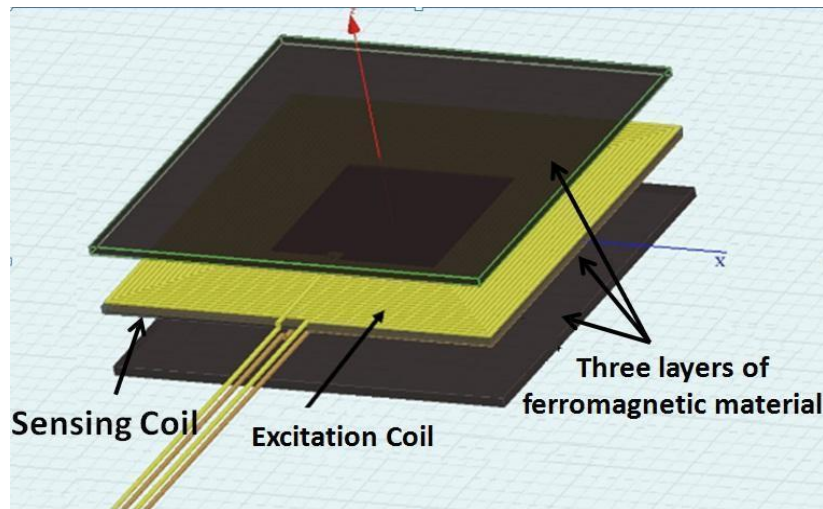


Figure 3.1. The triple planar fluxgate magnetic sensor proposed the ferromagnetic material layers are on the top, in the middle between the sensing and excitation coil and in the bottom of the fluxgate.

3.3 Instrumentation Details

The Ansys Maxwell is used for the simulations, which is based on the finite element method, the proposed micro fluxgate structure for the triple cores Fluxgate were analysed by following the Parametric Adaptive Analysis setup:

1. Parametric Model Generation – creating the geometry, Parametric Model Generation boundaries and excitations.
2. Analysis Setup – defining solution setup and frequency Analysis Setup by sweeps.
3. Results – creating 2D reports and field plots Results.
4. Solve Loop - the solution process is fully automated.

This is a virtual method which can provide important and competitive advantages with reduced time and cost to manufacture as well as improved system performance. To understand how these processes co-exist, the flow chart of the proposed micro fluxgate is shown in Figure

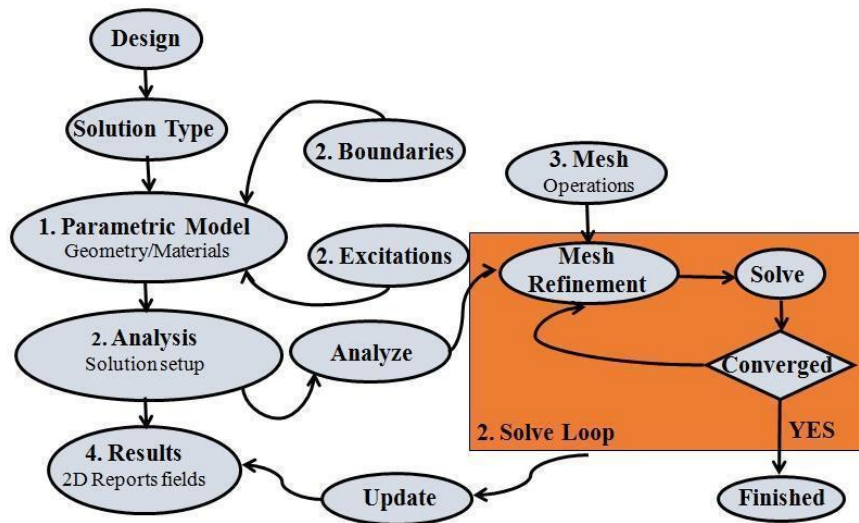


Figure 3.2. specifically for a Magnetostatic setup(Parametric Adaptive Analysis) that has been used in the design [85].

The magnetostatic model provides a range of characteristics in a very accurate way dependent on the design. The different AC characteristics of the circuit for the magnetostatic model will be investigated for the low frequency aspects of the design. For instance, if a higher frequency analysis is required, the high frequency structure simulator (HFSS) software such as the 100KHz electromagnetic simulator can be employed. In Figure 3.3, the voltage source (E1) generates a voltage that will be translated to a current. The resistance is needed in order for the circuit to become in an operational condition. When the Simplorer circuit model has been created as shown below, run the simulation and Simplorer will initiate to solve the Maxwell model. Simplorer will receive the impedance values for the core and shield once the Maxwell model is solved. Frequency Response and Transient Analysis results can be plotted when the simulation is completed.

The changes in the voltage source will alternate the current that will cause to re-simulate the entire model. A lower current value should be avoided as a short circuit might occur across the capacitor, which will affect the accuracy of the results. The frequency of the voltage signal was chosen as 10 kHz.

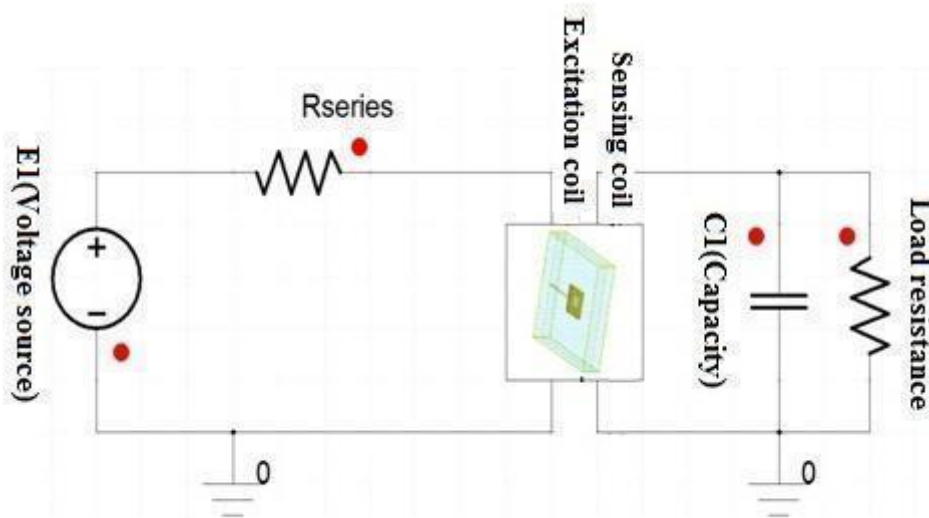


Figure 3.3. Illustrate the excitation circuitry and equivalent load connected to the sensor in ANSYS- Simplorer environment.

3.4 Accuracy of Simulation

The things that always need to be taken into consideration in this kind of simulation is the convergence as this kind of simulation is not as simple as putting the input at one end and expecting the output on the other end. In fact, this kind of simulation is handled. While the simulation is taking place, it is essential to ensure that the energy level (through the convergence feature in Maxwell) of the entire system should be less than 1%. Once this is achieved, it can be said that the simulation is completed with reliable results. I.e Maxwell generates a field solution using the specified mesh. It then

analyses the accuracy of the solution by calculating an energy value based on the error in the solution. The exact mechanism for evaluating the error varies by solution type. For a perfect solution the result would be zero, for a real, finite mesh the result is some amount of residual current density. An energy value calculated from this residual current density is called the error energy. The “Energy Error %” is the error energy as a percentage of the total energy. If more than 1 pass has been completed, the software also calculates the change in total energy from the previous pass. The Ansys Maxwell software is used for the simulations, which is based on the finite element method. Several simulations were performed to find the best geometrical configuration of the ferromagnetic material on top of the device. The accuracy of simulation is related to the number of the tetrahedral shapes that will be created after the meshing is complete. It is important to define an initial meshing setting prior to starting the iterations for refining the mesh to achieve a better accuracy. The initial mesh of the design is shown in Figure 3.4 wherein it can be seen that the mesh has fine grids next to terminals and the faces.

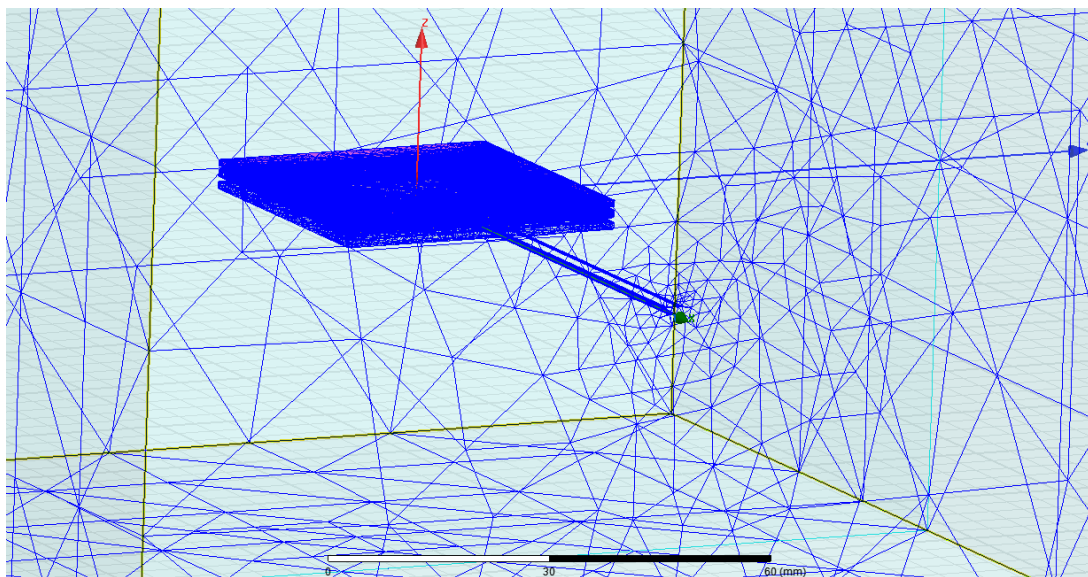


Figure 3.4. The mesh structure of the design.

The design optimization process in the current work is of an iterative nature whereby the ferromagnetic material shape was chosen as a rectangular sheet with dimensions of 57.3 mm x 58.1 mm for the mu-metal material. However, the main issue encountered in the current procedure is the creation of a good quality meshes. In other words, this had led to a large number of elements in the mesh of this particular section with 256756 volume elements.

3.5 The External Magnetic Field

The external magnetic field is the uniform magnetic field that has to be created to play the role of the magnetic field that is going to be measured by the proposed sensor. In this example, the external magnetic field is created by boundary conditions (i.e. Tangential H Field and Zero Tangential H Field) and is assumed to be constant. The value of the field is set by H (Magnetic field) and is set to be 17 A/m. The magnetic field near excitation and sensor coils is shown in Figure 3.5.

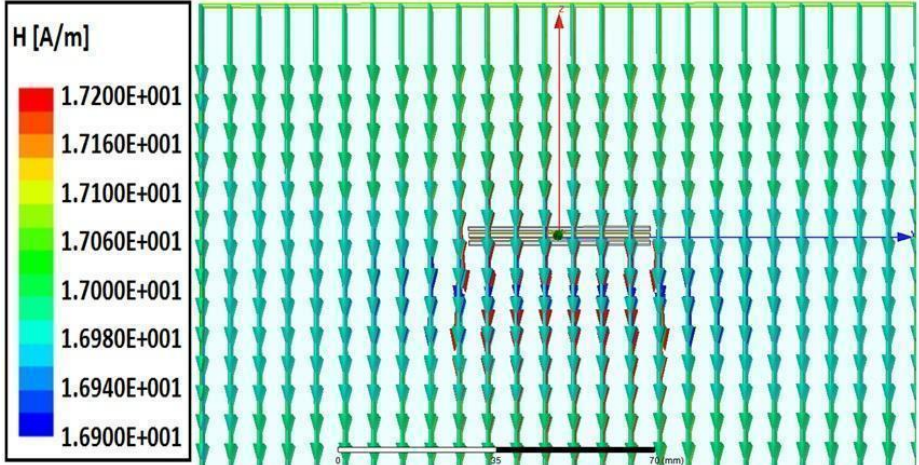


Figure 3.5. Magnetic field vector representation for an external magnetic field applied to the sensor at H=17A/m.

Figure 3.6 presents the vector of the magnetic flux density B around the excitation and sensing coils. Note that in this scenario the excitation current is kept on 0A.

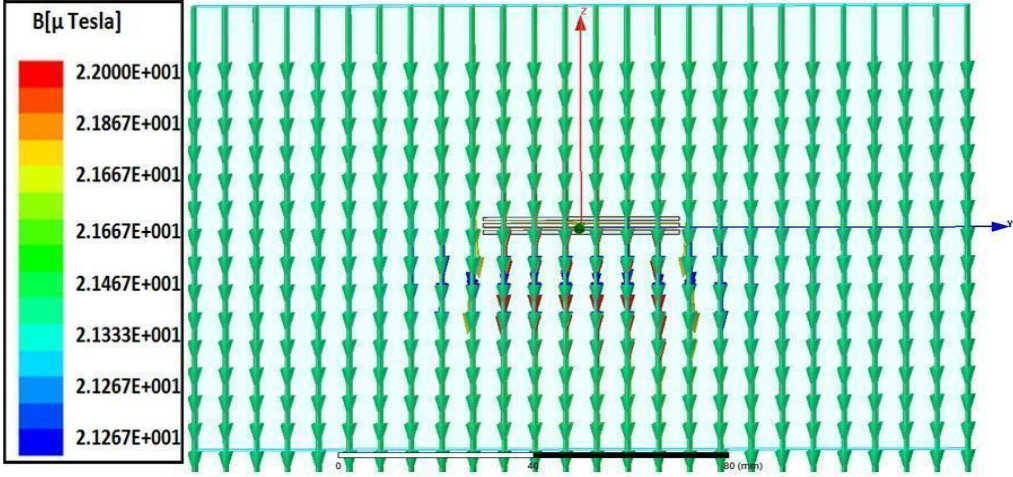


Figure 3.6. Vector representation of the external magnetic flux density B applied near excitation and sensor coils.

3.6 Exciting the Excitation Coil

In order to determine the current value that saturates the core, various values of the current have been applied where the initial value has been arbitrarily chosen as 5mA. However, as it is evident in the top view of the Mu-metal in Figure 3.7, this level of current was not suitable to saturate the core.

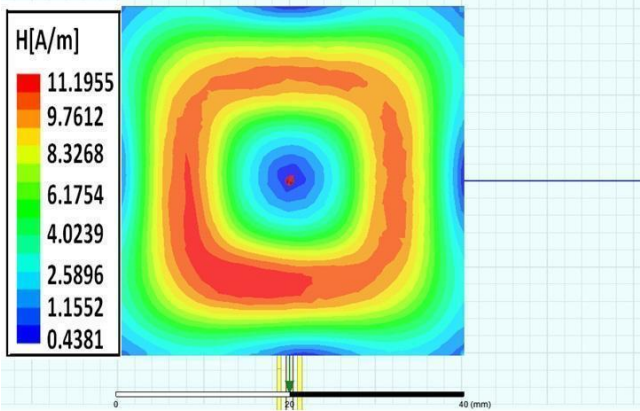


Figure 3.7. Magnetic field on the surface of mu-metal for an excitation current of 5mA.

On the other hand, when the current was increased to 12mA, it can be seen that the Mu-metal has been saturated as demonstrated in Figure 3.8. For this chosen level of current, the magnetic field distribution has been modelled and shown in Figure 3.9.

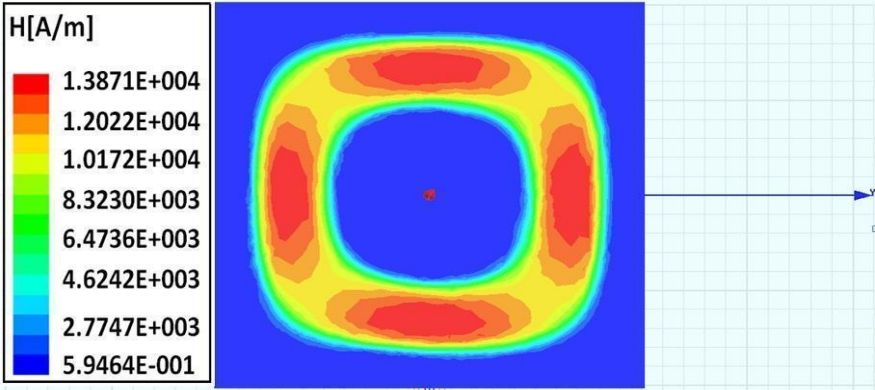


Figure 3.8. The Magnetic field passing through top mu material. As shown, the excitation current of 12 mA.

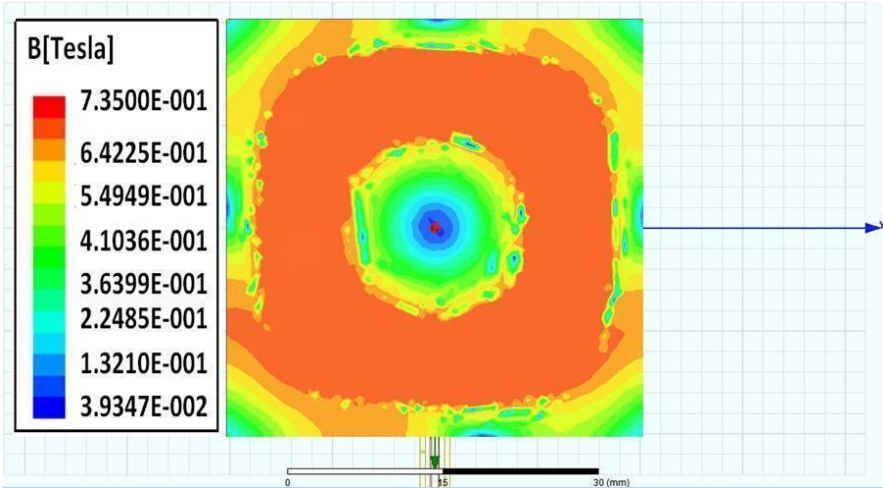


Figure 3.9. The magnitude of the magnetic field on the surface of top Mu material. As can be seen the magnetic field caused by the excitation coil is saturating the material with near 0.8 Tesla of magnetic flux density (B).

Figure 3.10 presents the magnetic field distribution inside the computational region (chosen to be air). As can be seen, by exciting the excitation coil (TX coil) with 12mA of current, the magnetic field of the excitation coil (TX coil) will override the constant magnetic field that has been applied and will start saturating the Mu-metal. The

magnetic field on the surface of mu material is presented in Figure 3.7. The magnetic flux density B is concentrated in a circular mode as shown in Figure 3.10. As can be seen, due to the saturation of the Mu-metal, the value of B does not exceed the saturation value of 0.8 Tesla.

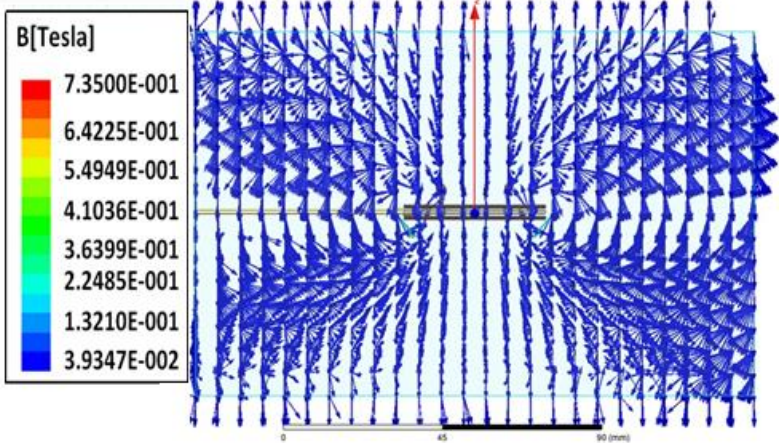


Figure 3.10. The magnetic vector around the excitation (and sensing coil).

3.7 Summary

This section presents the development of different planar Fluxgate magnetic sensor structures realised in printed circuit boards (PCB) and compares their performance based on their magnetic field parameters. This work provides a design approach for the development of planar magnetic sensors and to verify the simulated performance with results in order to validate the entire procedure. The schematic of the micro fluxgate structure realised for the triple cores Fluxgate, This structure consists of an excitation coil, sensing coils and three ferromagnetic cores located on the top, middle and bottom sections of the fluxgate in order to concentrate the field using the iterative optimisation technique. Figure 3.1 shows an exploded view of the multi core planar coil structure. The originality of the configuration lies in the geometrical design which

allows a single excitation coil to be used and optimises the three ferromagnetic cores for a given excitation coil area. This design consists in placing three ferromagnetic cores located on the top, middle and bottom sections of the coil in order to concentrate the field. Furthermore, one of the three ferromagnetic cores is placed above the excitation square coil, as illustrated in Figure 3.10, a parallel fluxgate configuration for each measurement axis is obtained. Along the excitation coil, each half of the ferromagnetic cross is subjected to the opposite direction of the excitation field H and to the same external field H_{exc} . It means that the excitation and the external magnetic fields see a core length equivalent to half the branch length and to the total branch length, respectively. Consequently the external field sees a ferromagnetic core with an equivalent apparent permeability higher than for the excitation field. The sensor sensitivity is then improved compared to a configuration with two discontinuous cores along the measurement axis. In addition to concentrating this magnetic field and therefore influence the intensity and the shape of a field. In this case, the magnetic field will be easily passed through the material (i.e. the upper and lower cores), it will wrap around the coils instead of going further away from the coil and this will allow the magnetic field to stay altogether within the top and bottom core. To obtain the optimal gain from the coil, different variables have been determined using an optimisation solution as shown in figure 3.11. This figure demonstrates an iterative Optimisation approach that explain how the simulation model works with optimisation systems. For example: The first step is to initialise the optimisation parameters such as number of turns, material type, spacing between the coils and the current in the excitation coil that saturate the ferromagnetic material to identify the search boundary for each parameter. In step 2, the aim is to generate random values for each parameter, step

3 focuses on the evaluation of results, if the gain is 0 then the optimisation process will terminate

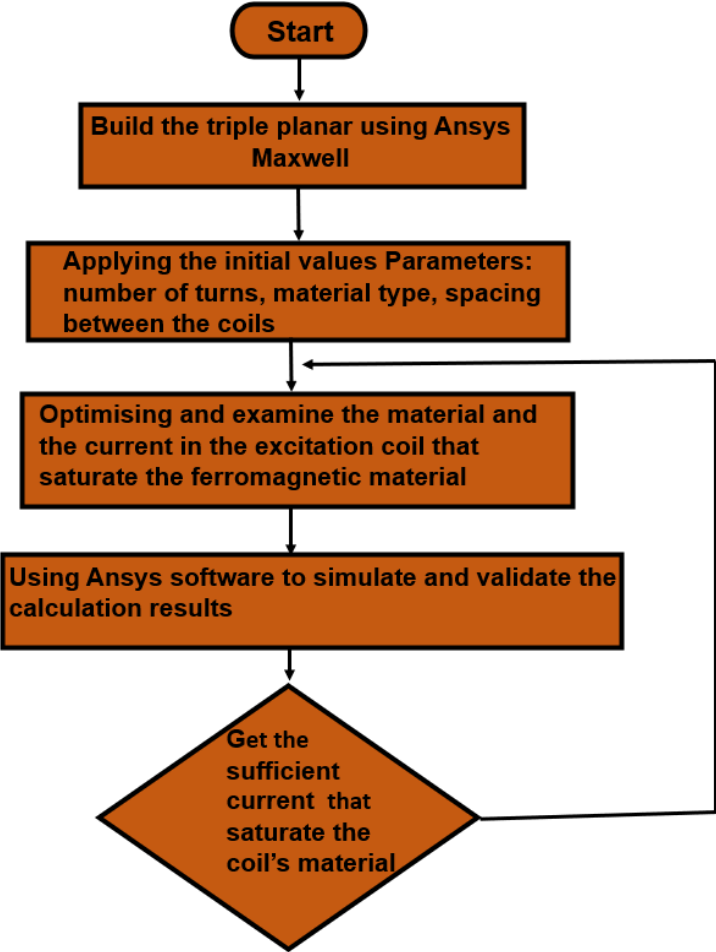


Figure 3.11. Optimisation technique

CHAPTER 4

A NOVEL PLANAR DESIGN USING ORTHOGONAL FLUX GUIDE

This chapter presents the developed ANSYS model to test different type of materials, i.e., amorphous and metaglas, as well as discusses the evolution and the results of the model sensor that has been designed by ANSYS software, this work allows to define a design way for the development of the magnetic fluxgate sensor. In the section 4.4 will illustrate the results of the model and compare the output with many cases that has been made such as Evaluate the excitation current value that ensures the saturation for ferromagnetic material and how the current is affecting the BH curve which in turn will affect the sensitivity of the sensor, Different number of turns and analyse the BH curves of each case, Compare the output voltage with different thickness ferromagnetic materials, Different wire width and Different core width. In addition to optimising the geometry of the fluxgate magnetometer. In other words, the current chapter presents an optimised study of the materials and geometry of the magnetometer which provides savings in terms of material usage as well as the employed electric current to produce an equivalent magnetic field.

4.1 Introduction

Traditional fluxgate magnetic sensors typically possess high device sensitivity, low noise density and excellent sensing accuracy. In order to determine the sensitivity of the developed sensors, the measured maximum output voltage of the sensor is divided by the maximum magnetic field strength as shown in equation

$$S = \frac{dV_{out}}{dH_{ext}} \quad (4.1)$$

The amplitude of the equivalent magnetic field noise, H_n is found

$$H_n = \frac{\sqrt{V_{total}}}{S_{total}} \quad (4.2)$$

Where H_n is the equivalent magnetic field noise in T/ $\sqrt{\text{Hz}}$, V_{total} is the total voltage noise of the sensor in V/ $\sqrt{\text{Hz}}$, and S_{total} is the total sensor sensitivity in V/T sensors accuracy depending on its feature however the equation 4.3 can be used to identify error rate of a sensor.

$$\text{Sensor error rate} = \frac{(\text{Expected sensor value} - \text{Measured sensor value})}{\text{Expected sensor value}} \quad (4.3)$$

However, they are still inferior to other magnetic sensors in the aspects of bulky coil volume of coils, higher power consumption and lower integration capability [86]. Other competitive magnetometers such as anisotropic-magnetoresistance (AMR), tunnelling magnetoresistance (TMR), giant-magnetoresistance (GMR), magneto impedance (MI) and magneto transistor (MT) devices have been extensively studied and reported [87]. Nonetheless, with the progress of system miniaturisation, the recent advance of miniature fluxgate sensors using CMOS technologies has been promising. Fluxgate magnetometers are typically applied in craft navigation, military detection and medical recognition [88]. So far prospective applications of micro-fluxgates have been considerably developed for modern digital navigation, thoracoscopic surgery, and non-destructive inspection [89]. More importantly, recent development of fluxgate vector magnetometers has been brought to simultaneous 3-axis field detection methodology though such research cases are still relatively rare when compared with general uni- and bi-axis fluxgate magnetometers [89]. An interpretation method with the use of 3-

axis fluxgate magnetometer array had improved and compensated permanent and induced magnetic fields generated by magnetised objects and sensors [90]. Later a series of efforts for the development of 3-axis ring cores and sensor design, tests and calibration procedures were implemented for spacecraft missions, however, the 3-D ring core assembly rather than a planar structure may limit its wide applications in microelectronics or mobile systems [89][90]. A typical procedure for building a 3-axis vector magnetometer is to align three uni-axis sensors along the three orthogonal sensing axes [91].

On device characterization of fluxgate magnetometers, several earlier works concluded that the sensing methodology and sensitivity enhancement by adopting the multiple harmonic frequency analysis techniques are practicable [90]. In addition to magnetic core materials, design of excitation and pick-up coils is also critical to determine the functioning of a fluxgate device. Designs for planar excitation and pick-up coils or three-dimensional (3-D) coils were previously investigated [91][92]. The traditional coils of fluxgate sensors, commonly wire-wound, are usually characterised as high sensitivity and low noise; but, they are still too bulky and system-incompatible to meet the dimensional requirements of a miniature product [93][94]. To circumvent the drawbacks, micro-fluxgate sensors feature planar CMOS pick-up coils and 3-D excitation coils with wire-bonded and flip-chip [95].

4.2 Introduction of the PCB Planar

This chapter will discuss the evolution and the results of the model sensor that has been designed by ANSYS software, this work allows to define a design way for the development of the magnetic fluxgate sensor, illustrate the results of the model and compare the output with many cases that has been made such as

- ✓ Evaluate the excitation current value that ensures the saturation for ferromagnetic material and how the current is affecting the BH curve which in turn will affect the sensitivity of the sensor.
- ✓ Different number of turns and analyse the BH curves of each case.
- ✓ Compare the output voltage with different thickness ferromagnetic materials.
- ✓ Different wire width
- ✓ Different core width.

The advantage of using the PCB technology is to reduce the cost and the simplicity of prototyping. The magnetic fluxgate sensor that has been modelled is an amorphous metal that is commercially available and which is neither electroplated nor sputter produced as it is the case with most ferromagnetic materials. The materials involved in the sensor include 25 μm for Vitrovac 6025-X, the 20 μm for Vitrovac 6025-Z and the 16 μm for Metglas 2714-A). In this way it will be easy to optimise, build and analyse the design then get the results. The first step in the work is to find a suitable geometry for the model which will be optimised utilising ANSYS software to develop and analyse the sensor.

However, the ideal formulation cannot be used when the coils are not wrapped around the core of the fluxgate sensor, that's why the finite element method (FEM) by ANSYS software has been used to analyse the magnetic characteristics of the different PCB structures and their cases. The design was developed by using different shapes and new design parameters.

4.3 The developed architecture

The architecture of the design has been developed using the PCB and a comparison between the various cases has been carried out in the current work. The first stage that has been taken into consideration is the field distribution within the core by looking at the flux line diagram through the core. This structure consists of a cross shaped ferromagnetic core, a planar excitation coil and four sensing coils. The four sensing coils and the excitation coil are placed on two different metal layers in a multilayer PCB structure. The ferromagnetic cores are placed on the excitation coils diagonally, Figure 4.1 and Figure 4.2. Then the excited field will be in opposite directions in pairs, so they will cancel each other in the sensing coils. The sensing coils are placed which are underneath the excitation coil and centred on the four endpoints of the cross shape core. A cylindrical ferromagnetic tube (magnetic fluxguide) which was placed at the top of the core and set of ferromagnetic cubes (which was placed underneath the core) are acting as a flux guide in order to concentrate and guide magnetic fields. So the tube will deflect the field to be passed through the core, then the ferromagnetic cubes will emit the field into the sensing coils.

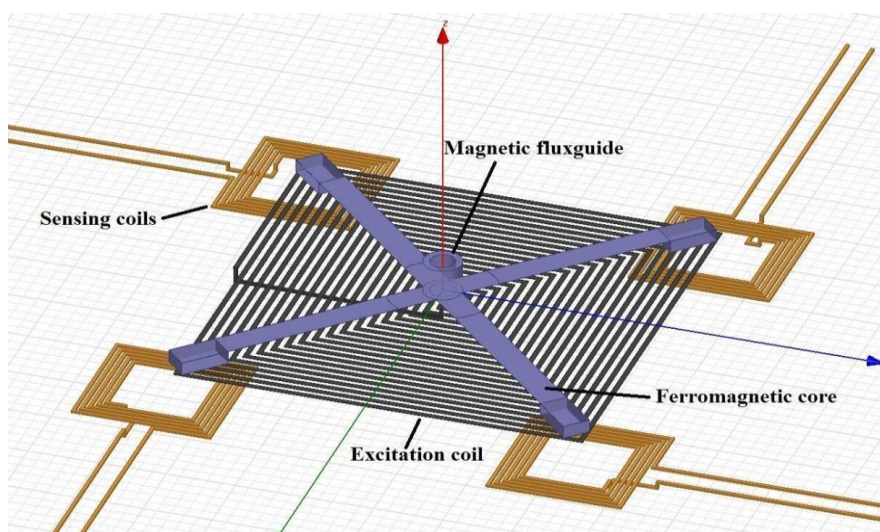


Figure 4.1. schematic of the 3-axis planar fluxgate magnetic sensor realised.

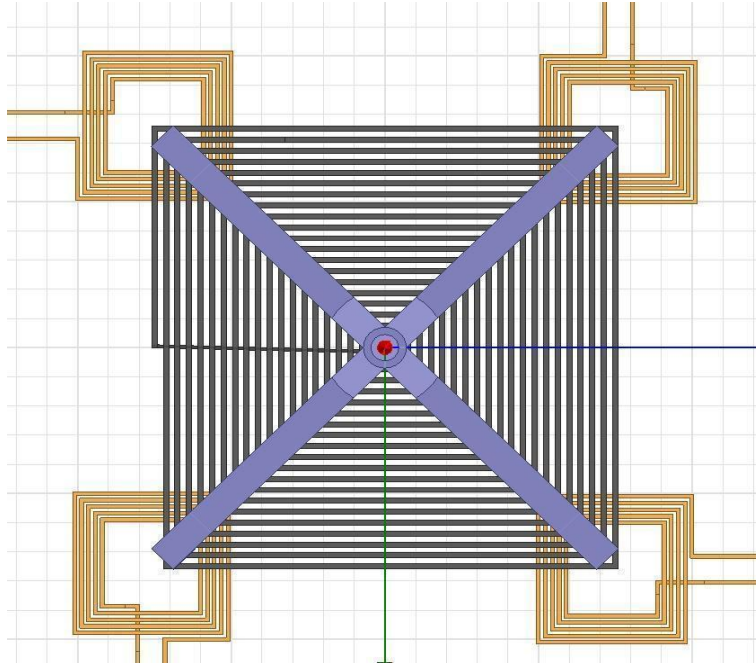


Figure 4.2. Top view of the 3-axis planar fluxgate magnetic sensor.

The ferromagnetic material that has been used for the core is an amorphous alloy known under the name of Vitrovac 6025 (6025-Z with a thickness of $20 \mu\text{m}$ and 6025-X, with a thickness of $25 \mu\text{m}$) of a high relative permeability ($\mu_r \cong 10^5$). Also, the value of B_s of this material is 0.55 T. The Vitrovac alloys (6025-Z and 6025-X) can be recognised from the shape of their hysteresis loop; this property affects the excitation current that is needed to ensure the saturation of the ferromagnetic material.

In the fluxgate sensor that has been modelled, the following parameters are modelled by simulation:

- ✓ Excitation metal layers thickness: $25 \mu\text{m}$;
- ✓ Sensing metal layer thickness: $20 \mu\text{m}$;
- ✓ Metal lines pitch: $400 \mu\text{m}$;

✓ Vitrovac thickness: 25 μm (6025 X) and 20 μm (6025 Z).

In addition to the fixed basic parameters of the design and the size of the sensor, there are some parameters that have to be optimised such as the number of turns of the excitation coil and the number of turns of the sensing coils. The four sensing coils are placed in separate layers of the excitation coil. In order to achieve a better sensitivity, a large ferromagnetic material which requires a larger current is required. The dimensions were finally set to be 40.0 x 3.5 x 0.025 mm (for the Vitrovac 6025-X). A cylindrical ferromagnetic tube was placed on the top of the centre of the crossed-core fluxgate and these acts as the fluxguide in order to concentrate the magnetic fields then emit the fields into the planar cruciform core.

4.4 The Working Principle of the Sensing Device

The system has been investigated while studying the effect of the fluxguide on the performance of the device. In general, the working principle of the planar fluxgate including the cruciform core alongside a vertically mounted fluxguide has been studied. In such a system, the magnetic field in the X-axis or Y-axis detections is distributed as flux lines which are comparable with those of the planar device in particular near the ends of the core as shown in Figure 4.3 Figure 4.4 .However, the interior part of the fluxguide system is different and this results in a trivial effect on both ends of the core as illustrated in Figure 4.3. Through the simulation of flux line distribution, it is confirmed that the tri-axis sensor with a fluxguide does not generate significant interference for X-axis (or Y-axis) detection and surely obtain the vector component of

magnetic fields in X-axis (or Y-axis) as the planar one. On the other hand, the measurement of the field in the Z-direction will involve that the magnetic field lines will be parallel to the longitudinal orientation of the fluxguide. This is evidently demonstrated in Figure 4.5 which reveals that the flux lines near the top of the fluxguide are slightly bent and hence guided into its interior and then transferred along the X-direction or Y-direction and eventually diverged into air (or vacuum).

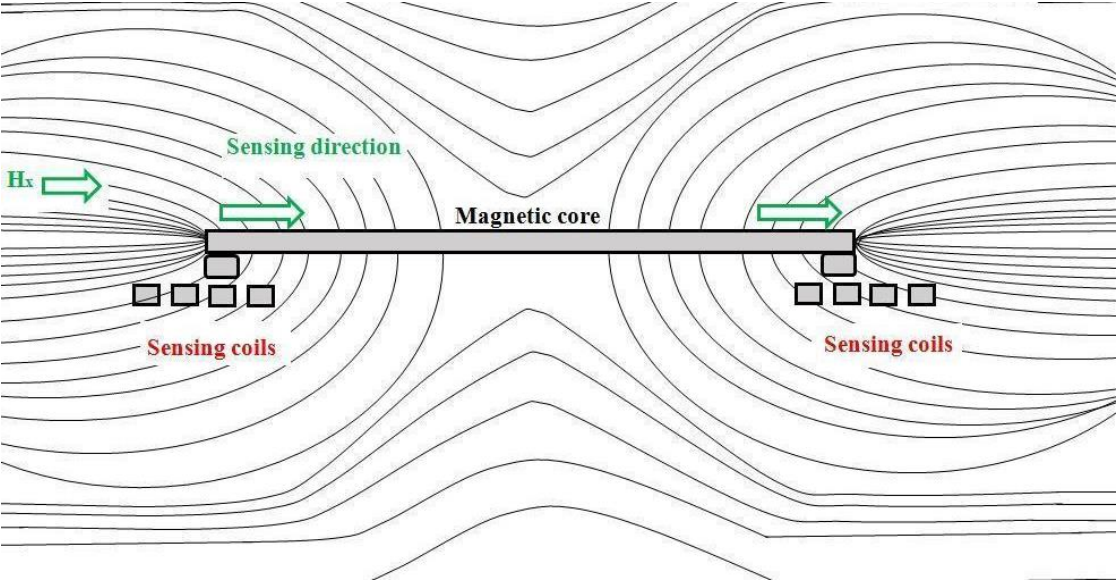


Figure 4.3. The flux lines of the sensing principle of the fluxgate in X axis direction without fluxguide.

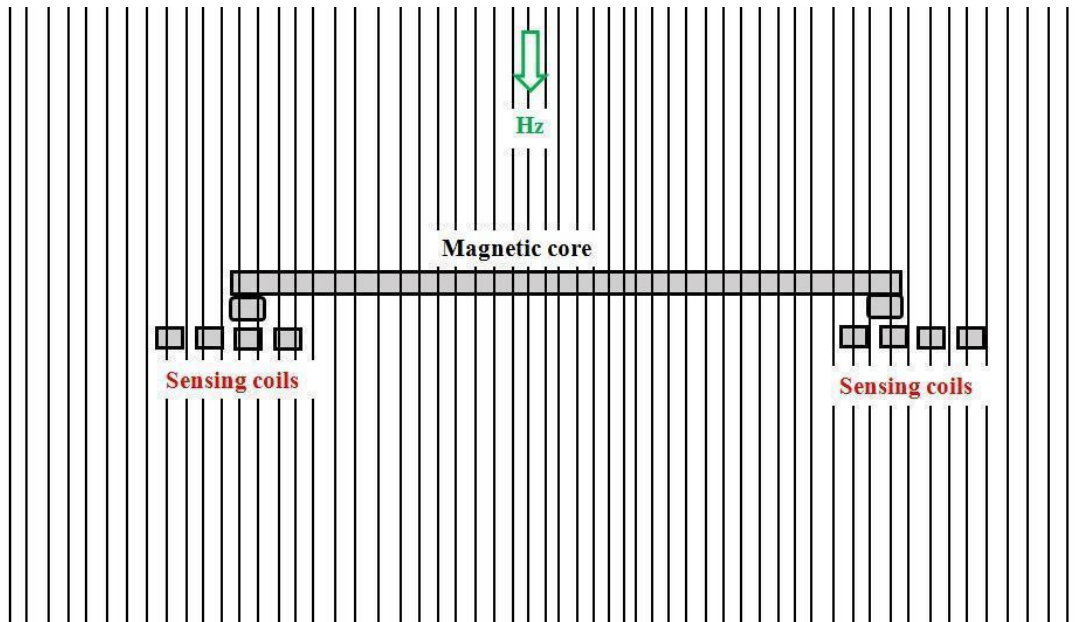


Figure 4.4. The flux lines of the sensing principle of the fluxgate in Z axis direction without fluxguide.

It can be clearly seen that the magnetic flux lines gather at the ends of the core, in addition to that these flux lines are compressed into the core until they spread out to the air again at the other end of the core. This phenomenon creates a flux density around the endpoints of the core in the sensor. In this case, the flux density that has been generated will be converted to voltage induced through the two pick-up coils. It can be concluded that an orthogonally cylindrical ferromagnetic tube and set of ferromagnetic tubes are acting as a flux guide in order to concentrate and guide magnetic fields. So the tube will deflect the field to be passed through the core, then the ferromagnetic cubes will emit the field into the sensing coils.

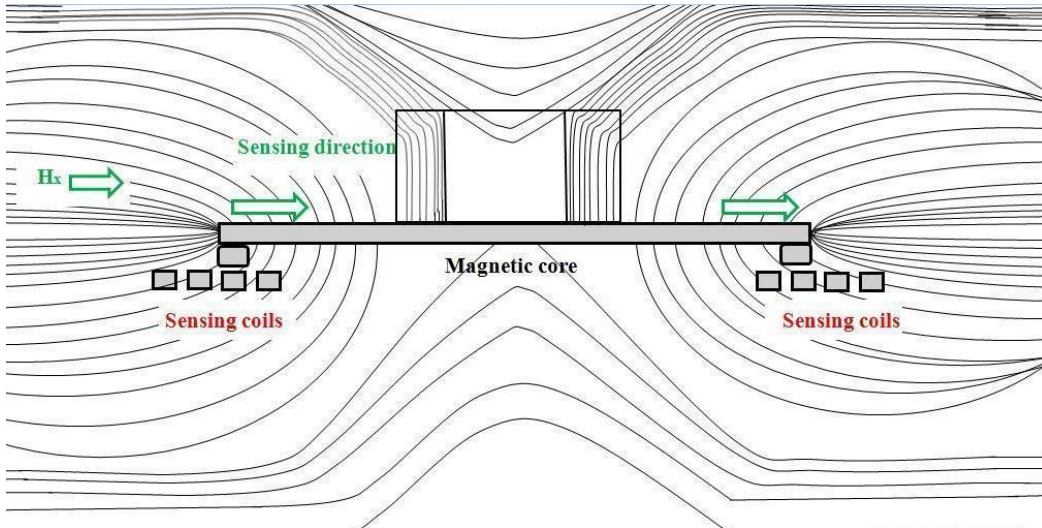


Figure 4.4. flux lines of the sensing principle of the fluxgate with the fluxguide in the X axis.

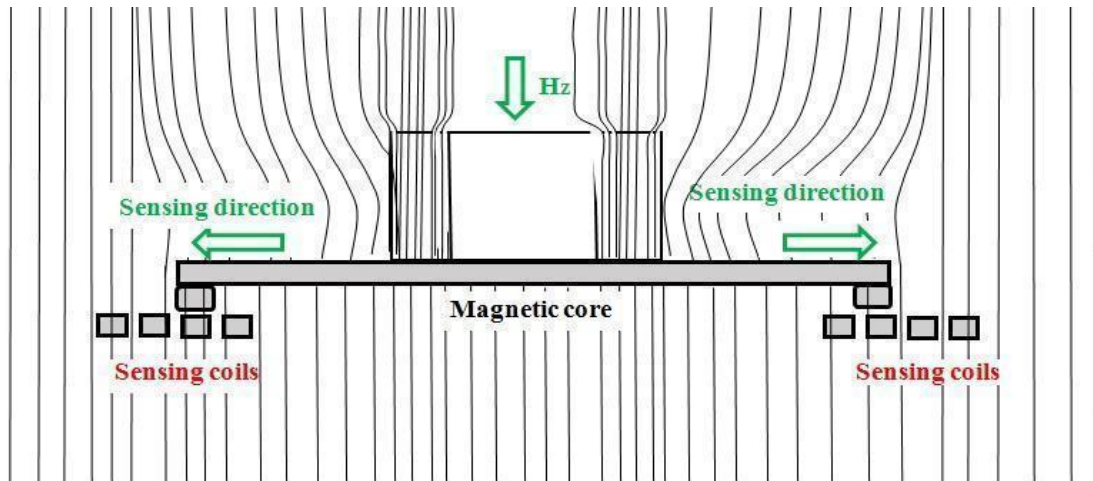


Figure 4.5 flux lines of the sensing principle of the fluxgate with the flux guide Z axis.

4.5 The Sensor Development and Simulation Results

It is important to find the optimal dimensions of the proposed fluxgate in terms of the geometry of the core, geometry of the excitation and sensing coils in addition to the number of turns alongside the width of the wire of the excitation coil. The simulation of the fluxgate sensor has taken place using the Maxwell Ansys based on finite element analysis. Several simulations were performed to find the best geometrical

configuration of the ferromagnetic core, the ferromagnetic material shape selected was a pair of rectangular sheets with dimensions of 40.0 x 3.5 x 0.025 mm (for Vitrovac 6025-X). The main issue encountered in this iterative optimisation process is the creation of a good mesh for the model of the structure. The design stages involved in the current project started with finding the amount of the excitation current value that ensures that the ferromagnetic material is saturated. This has been achieved using magnetostatic simulations to evaluate the excitation peak current necessary to saturate the ferromagnetic material.

4.5.1 The Influence of the Induced Current on the Core Material

The first step in the analysis is to determine the value of the excitation current that saturates the ferromagnetic material. This has been done using current values between 450mA and 750mA. The effect of the induced current on the magnetic properties of the ferromagnetic core material has been analysed. By looking at figure 4.5 it can be determined that all curves have different output voltages and hence are not all of them are suitable to saturate the core that will be used for a fluxgate magnetometer. Furthermore, the different shapes of the curves that have been obtained from the different amount of currents values indicate that the amount of 680mA was sufficient to cause saturation of the core of the fluxgate and perform as a good fluxgate sensor. However, it has been found that some of these amounts of the currents that have been applied do not saturate the core to make a good fluxgate at all. It is possible to grade all the amount of the currents that has been applied among themselves and conclude that the amount of (680mA) is the most suitable value to saturate the ferromagnetic material that has been used for the core, the amount of (750mA) is an average to saturate the material and the amount of (550mA) and

(450mA) are the least suitable amount of currents to saturate the ferromagnetic material to be used as cores in magnetometers. It has been observed that when the current was either high (750mA) or low (450mA), the material has not been saturated. However, at a value in-between those, i.e. 680mA, the material has reached the saturation point which is desirable. It has also been observed that for the geometrical configuration utilised in the current study, the optimum amount of 680mA was sufficient to cause saturation and get the highest sensitivity. This is in contrast to the case with the low and high currents which caused the sensitivity of the core to be dramatically dropped. In the case of Vitrovac 6025-X, a current of 680 mA has been observed to cause saturation of the ferromagnetic material, Figure 4.6, with B_{\max} around 0.54 T. The distribution of the magnetic flux density (B) along the core while the core excitation is realised has been simulated and evaluated by ANSYS Maxwell.

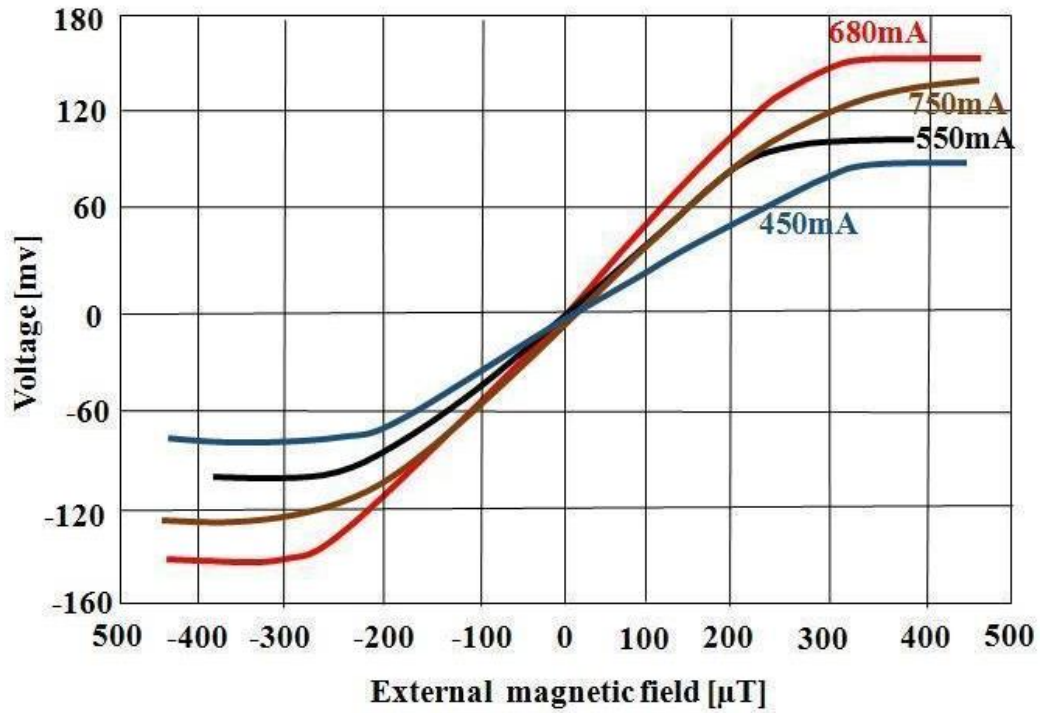


Figure 4.5. The effect of the induced current on the magnetic properties of the ferromagnetic core material.

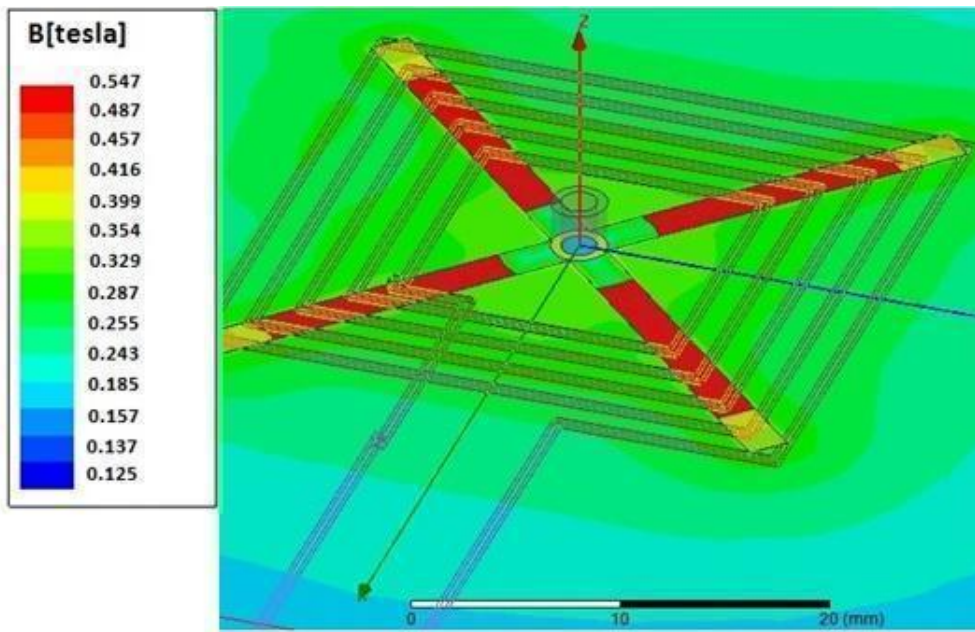


Figure 4.6. The determination of the saturation point of the ferromagnetic core material.

In order to select the suitable current to saturate the ferromagnetic material to be used as a core in magnetometers, we propose a selective parameter approach which shows

the sensitivity of the sensor. The sensitivity of the planar coil does not increase monotonically with the excitation current, but using the current values as given in Figure 4.5 causes initially a voltage levels, then gradually it starts to increase decrease, for more clear explanations this, a comparison between the sensor outputs The peak of the voltage induced in each sensing coil is proportional to the derivative of the corresponding flux linkage and, therefore, the differential output voltage exhibits in the case a different peak value and a different area. Due to the output voltage that has been produced which is proportional to the average value of the differential voltage, the sensor output is larger when the excitation current value is lower. This means that for a given geometrical configuration of the magnetic core, there is a value of the excitation current that maximises the sensitivity of the coil. The analysis is carried out for excitation currents with peak values between 450mA and 750mA. A lower current would not saturate the material, while for larger current levels the sensitivity is already decreasing. Different sensitivity values have been obtained for the various excitation currents that have been applied, and these are summarised in Table 4.1 it can be evidently seen that the highest sensitivity is observed at a current of 680mA. Table 4.1 clearly differentiates between a high sensitivity of the sensor and a low sensitivity of the sensor. Furthermore, it is possible to classify values of the sensitivity of the different currents values that has been applied among themselves and conclude that in the amount of (680mA) can get the highest sensitivity, in the amount of (550mA) can get an average sensitivity and the amount of (450mA and 750mA) can get the least sensitivity of the sensor.

Table 4.1: The various excitation current values with sensitivity in the range.

The various excitation current values [mA]	Sensitivity of the sensor[mV/ μ T]
450	0.35
550	0.41
680	0.48
750	0.38

From the simulation exercises, it has been observed that the middle section of the core has been saturated with significantly larger amounts when compared to the ends of the core, Figure 4.7. This is evident from the larger amount of the magnetic flux observed in the middle of the core material.

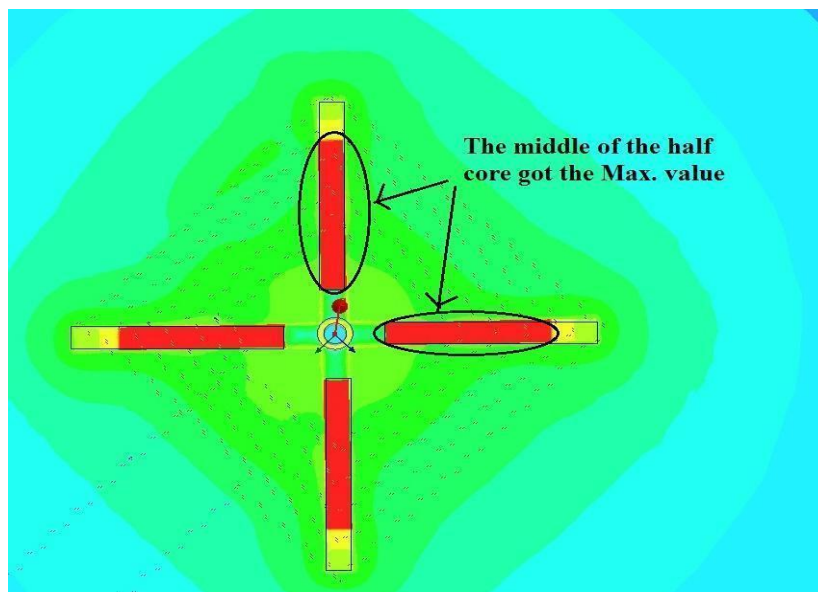


Figure 4.7. The saturation process of the ferromagnetic core material at 680mA.

4.5.2 The Influence of the number of turns on the Coil

In order to select the suitable coil to be used in magnetometers, the same model and design but with different number of turns (10, 20 and 40 turns). Looking at Figure 4.8 it can be established that each curve has a different output; voltages were obtained depending on the applied number of turns. Hence not all of them are suitable to be used as a magnetic core for a fluxgate magnetometer. Moreover, the different shapes indicate that in the case of (40 turns) should perform as a good fluxgate sensor. In addition to that, it has been found that some of these cores do not make a good fluxgate at all. It is possible to grade all the curves that has been obtained among themselves and conclude that in the case of (40 turns) is the most suitable coil for the fluxgate, in the case of (20 turns) is an average coil and the case of (10 turns) is the least suitable coil to be used in magnetometers. However, the higher the number is, the better the suitability of that coil as a fluxgate sensor. The increase in the number of turns will result in an increase in the size of the excitation coil and hence an increase in the output voltage, Figure 4.9. (turns > 40 or < 40 discussed in details in next chapter.

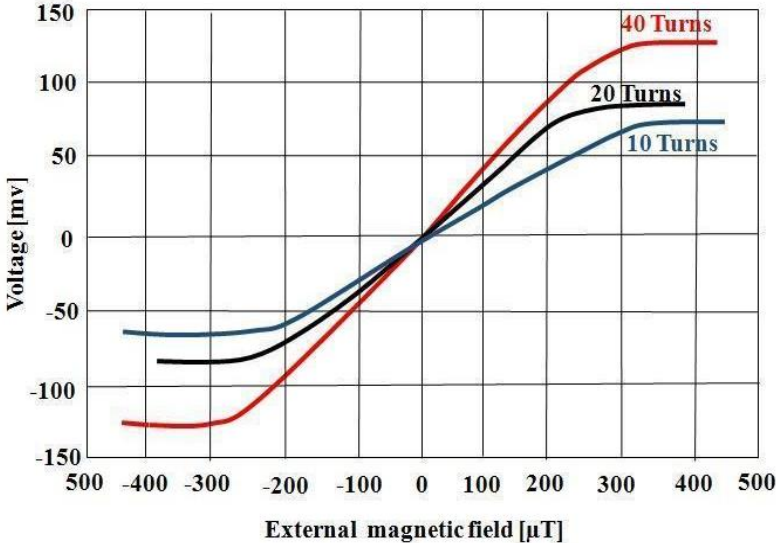


Figure 4.8. The effect of the number of turns on the magnetic properties of the ferromagnetic core material.

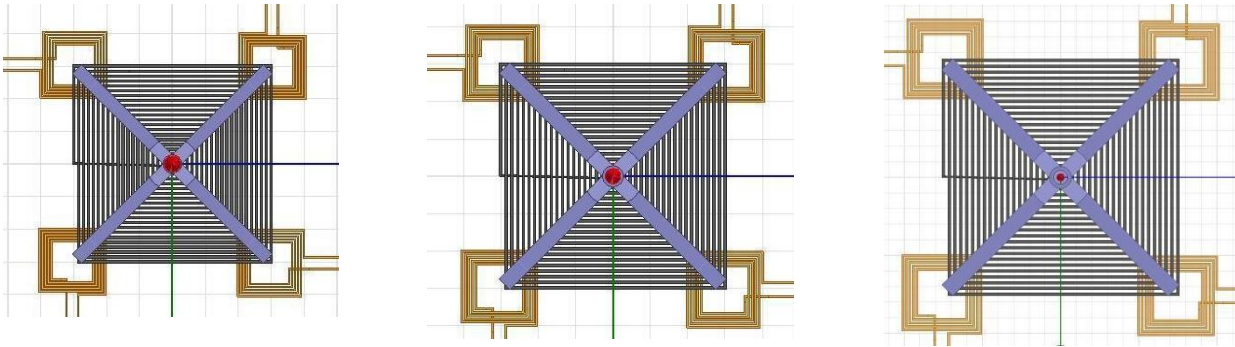


Figure 4.9. The change in number of turns of the excitation coil: (a) 10 turns, (b) 20 turns and (c) 40 turns.

The reduction in the number of turns of the excitation coil gives a lower output voltage value, therefore; the maximum voltage can be obtained with the maximum possible number of turns, i.e. in this case 40 turns of the employed model as shown in Figure 4.10. Approximate finite element method simulation of 3-dimensional as used in this study in order to show the saturation of the core material when the maximum number of turns, i.e. 40 turns, is used. Magnetic field strength's variation is colour-coded: the highest intensity being denoted by red, the lower by yellow and lowest by green. The scale of the magnetic field strength in this simulation is arbitrary.

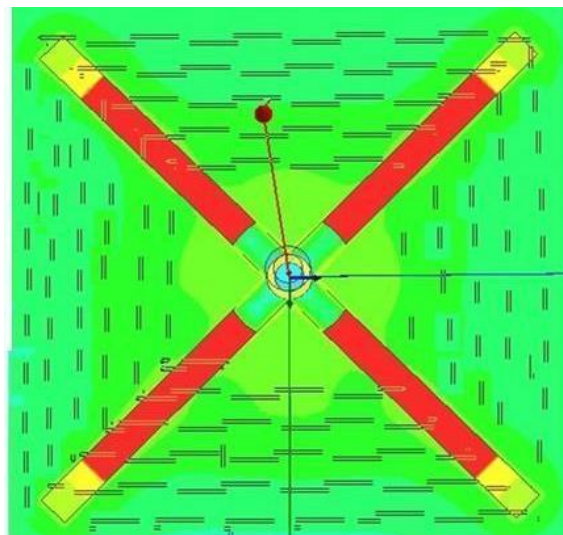


Figure 4.10. The saturation of the core material when the maximum number of turns, i.e. 40 turns, is used.

4.5.3 The Influence of the Ferromagnetic material on the Hysteresis Loop

To characterise the most suitable core for the fluxgate, the same model design has been used but with different ferromagnetic, Unlike the previous simulations of the Vitrovac 6025-X which was saturated at 680mA, a new configuration of the same material called Vitrovac 6025-Z of a smaller thickness has been employed and investigated. It is worthwhile mentioning that the thickness of the Vitrovac 6025-X is 25 μ m whereas that of the Vitrovac 6025-Z is 20 μ m. Looking at all data in this Figure 4.11 it can be established that the three different materials that have been used have different hysteresis loops due to the different thickness of those materials and hence are not all of them are suitable to be used as magnetic core for a fluxgate magnetometer. Furthermore the different shapes of the B-H loops of the materials indicating that the smaller the thickness of the core, the lower the amount of the used current, i.e. less power consumption, the lower the linearity error and the higher the sensitivity of the device which should perform as a good core for the fluxgate sensor. However, it has been found that some of these materials are not suitable for a good core fluxgate at all. It has been found from figure 4.11 that interestingly, when an additional material, i.e Metglas 2714A, has been investigated in terms of the influence of the core thickness on the output voltage. From Figure 4.11 it is possible to grade all the materials among themselves and conclude that the Metglas 2714A of thickness 16 μ m provides very close results in terms of the saturation current to those obtained by 6025-Z with the added advantage of a smaller thickness of the core. However, the sensitivity of the Metglas 2714A is significantly lower along with a higher linearity error when compared to the 6025-Z.

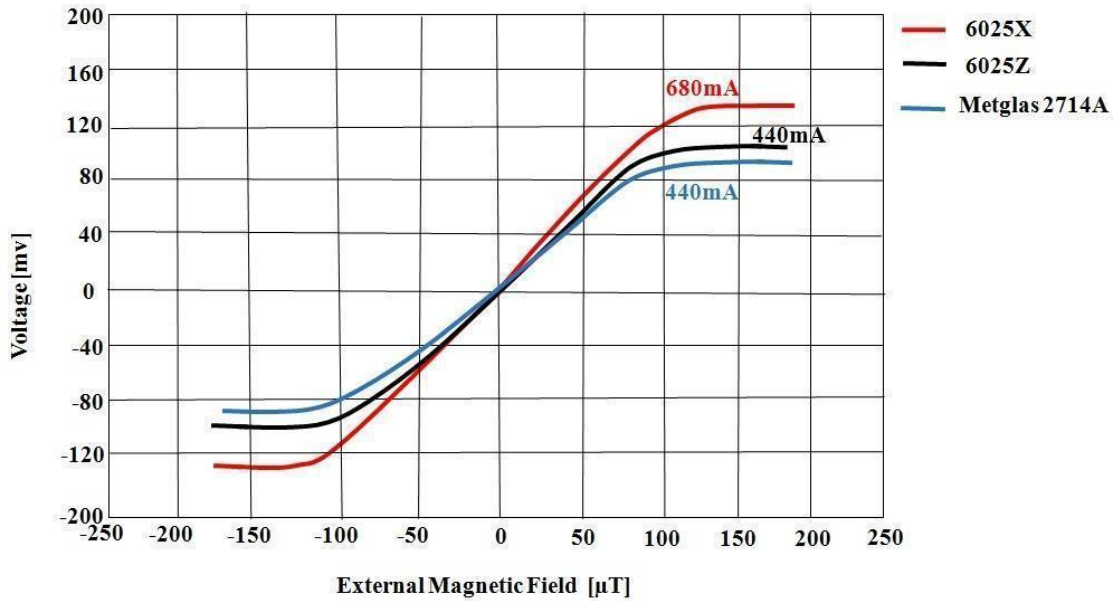


Figure 4.11. The influence of the core thickness on the output voltage of the device.

4.5.4 The Influence of the Ferromagnetic Wire Width on the Hysteresis Loop

The different magnetic flux density (B) has been measured through the core length in terms of the variation of the wire width with an excitation current of 680mA. Looking at all data in Figure 4.12 shows the different wire width from (0.1mm- 0.5mm), it can be established that all cases of different wire width have a different magnetic flux density (B) and hence are not all of them are suitable to be used as magnetic core for a fluxgate magnetometer. As shown in Figure 4.12 It can be seen that the flux density B will be the highest value in the case of (0.1mm) wire width which is suitable to be used as core for the fluxgate magnetometer. Furthermore, the different magnetic flux density (B) that has been obtained indicates that in the case of (0.1mm) wire width should perform as a good fluxgate sensor. However, it has been found that some of these cores do not make a good fluxgate at all. It is possible to grade all cases of the difference of the wire width among themselves and conclude that in the case of (0.1mm) is most suitable materials to be used as a core of the fluxgate magnetometer,

In the case of (0.2mm and 0.3mm) is an average material and the case of (0.4mm and 0.5mm) are the least suitable materials to be used as cores in magnetometers. It can be concluded that magnetic flux density (B) is inversely proportional to the wire width, i.e. the smaller the wire width the higher the flux density which is desirable.

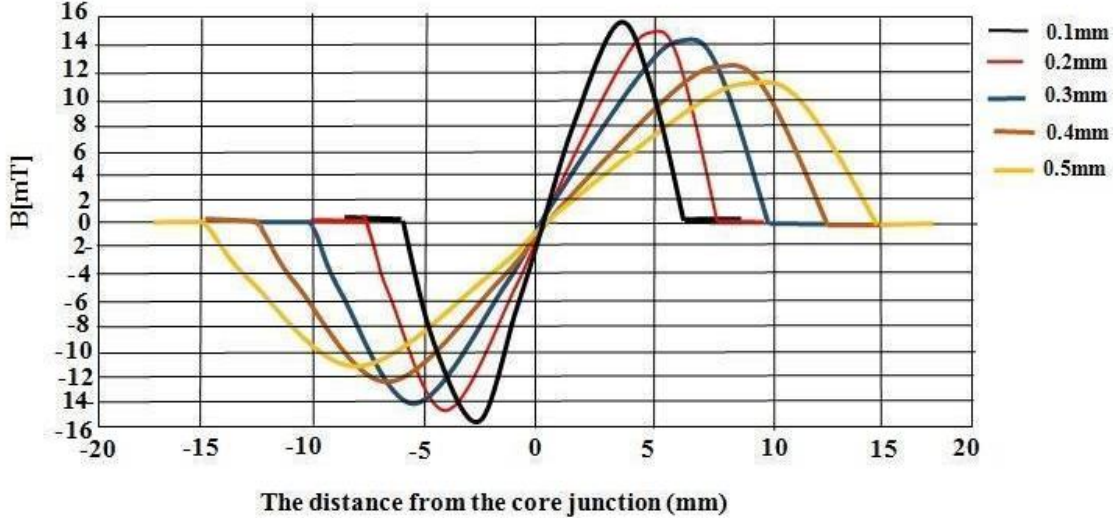


Figure 4.12. The influence of the wire width on the flux density through the core.

4.5.5 The Influence of the Ferromagnetic Core Width on the Hysteresis Loop

When the same current of 680mA was applied with the same modelled design, the core width has been investigated in terms of flux density and saturation of the core. Furthermore the different magnetic flux density (B) has been measured through the core length in terms of the variation of the core width. Looking at all curves in Figure 4.13 shows the different core width from (2mm- 5mm), it can be established that all cases of different core width have a different magnetic flux density (B) and hence are

not all of them are suitable to be used as magnetic core for a fluxgate magnetometer. As shown in Figure 4.13, it can be seen that the flux density B will be the highest value in the case of (2mm) wire width which is suitable to be used as the core for the fluxgate magnetometer. Furthermore the different magnetic flux density (B) that has been obtained indicates that in the case of (2mm) core width should perform as a good fluxgate sensor. However, it has been found that some of these cores do not make a good fluxgate at all. It is possible to grade all cases of the difference of the core width among themselves and conclude that in the case of (2mm) is most suitable materials to be used as a core of the fluxgate magnetometer, in the case of (3mm) is an average material and the case of (4mm and 5mm) are the least suitable materials to be used as cores in magnetometers. It can be concluded that magnetic flux density (B) is inversely proportional to the core width, i.e. the smaller the core width the higher the flux density which is desirable. Section 4.6.5 discussed the magnetic flux density (B) is inversely proportional to the core width theoretically.

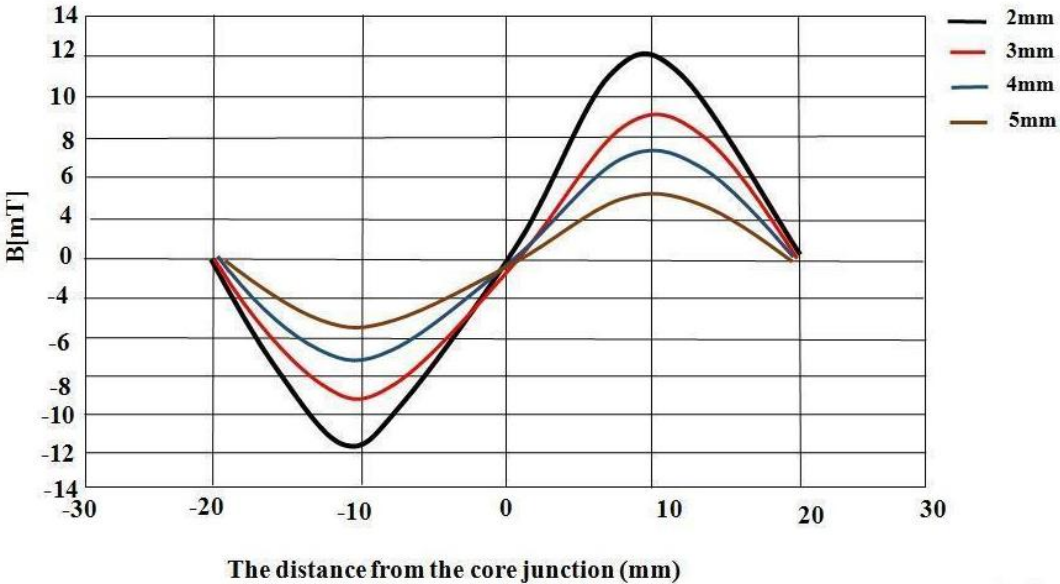


Figure 4.13. The influence of the core width on the flux density through the core.

4.6 The Experimental Optimisation of the Square Coil

The following design parameters are typically associated with a board level inductor design: 1) the excitation current value that ensures the saturation for ferromagnetic material and how the current is affecting the BH curve which in turn will affect the sensitivity of the sensor; 2) number of turns; 3) thickness of the ferromagnetic material; 4) the wire width; and 5) the core width. Simulations have been performed by varying these design parameters using Ansys software. The inductors are fabricated using a commercial PCB fabrication process.

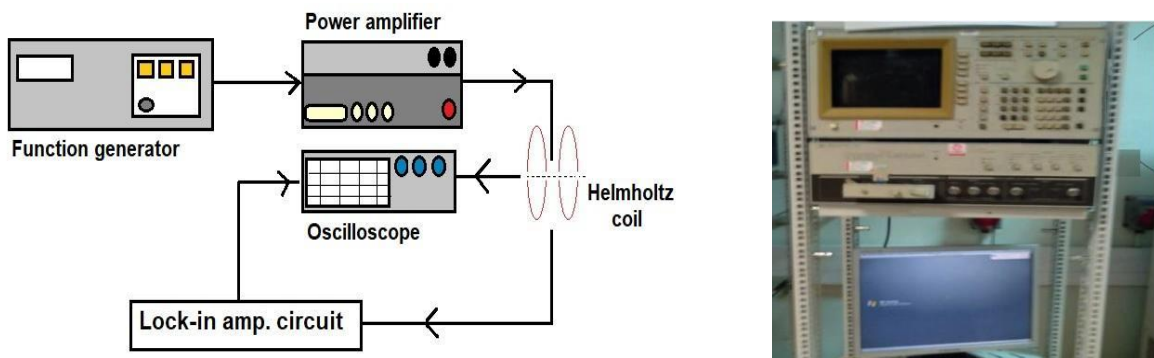


Figure 4.14. The measurement setup.

The measurement setup is shown in figure 4.14. Lab view program is written to the values of the inductances. The results of the different parameters are presented in the next sections.

- To measure the performance of square coil: The signal generator provided a sine wave signal,
- The power amplifier will magnified the sine wave signal to the excitation coil.

- Lock-in amplifiers are used to detect and measure very small AC signals all the way down to a few nanovolts, so the signal from the sensing coil has been connected to the Lock-in amplifier then the performance is monitored by an oscilloscope.

4.6.1 The Influence of the Induced Current on the Core Material

Different amounts of currents have been applied between 450mA and 750mA in the optimization and simulation part. The amount of 680mA was sufficient to cause saturation of the core of the fluxgate and perform as a good fluxgate sensor. It is possible to grade all the amount of the currents that has been applied among themselves and conclude that the amount of (680mA) is the most suitable value to saturate the ferromagnetic material that has been used for the core.

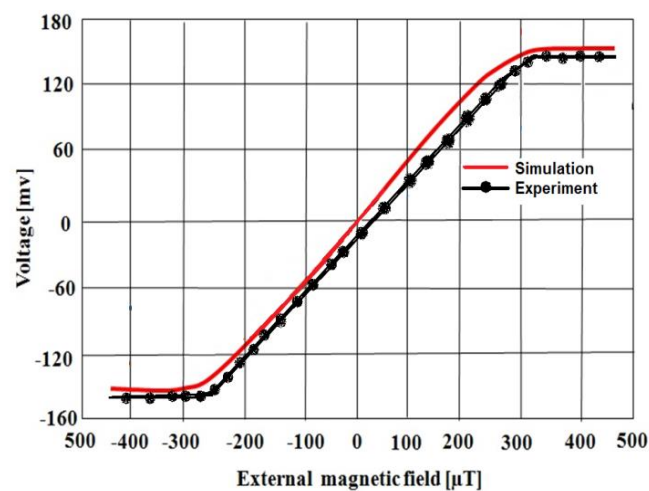


Figure 4.15. The BH curves based on 680mA (experimental vs. Simulation).

4.6.2 The Influence of the number of turns on the Coil

The maximum voltage can be obtained with the maximum possible number of turns, i.e. in this case 40 turns. The increase in the number of turns will result in an increase in the size of the excitation coil and hence an increase in the output voltage.

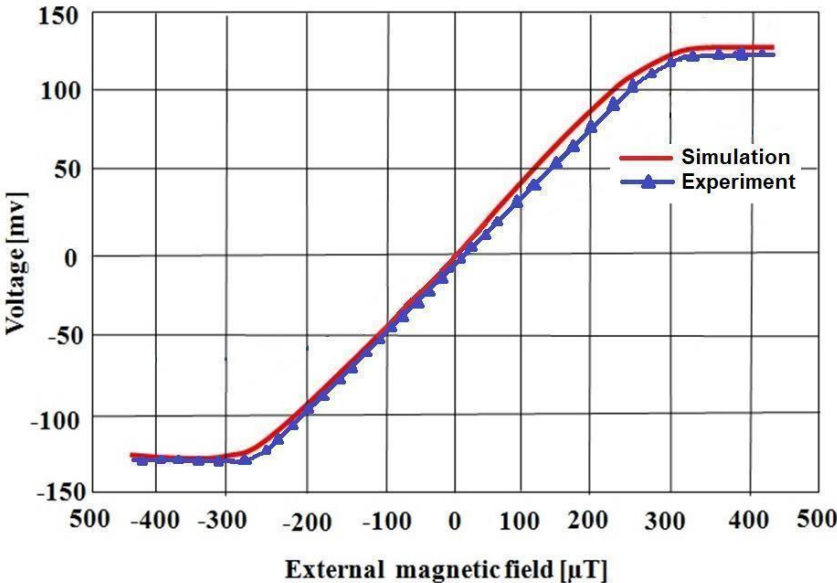


Figure 4.16. The effect of the number of turns on the magnetic properties of the ferromagnetic core material (experimental vs. Simulation model).

4.6.3 The Influence of the Ferromagnetic material on the Hysteresis Loop

To characterise the most suitable core for the fluxgate, the same model design has been used but with different ferromagnetic. A new configuration of the same material called Vitrovac 6025-Z of a smaller thickness has been employed and investigated.

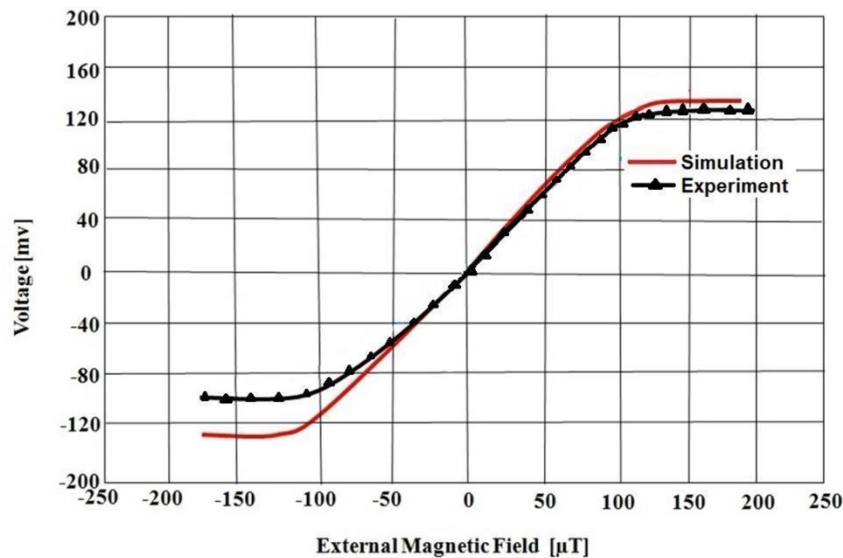


Figure 4.17. The influence of the core thickness on the output voltage of the device (experimental vs. Simulation).

4.6.4 The Influence of the Ferromagnetic Wire Width on the Hysteresis Loop

The different magnetic flux density (B) has been measured through the core length in terms of the variation of the wire width with an excitation current of 680mA in the simulation section, the flux density B will be the highest value in the case of (0.1mm) wire width which is suitable to be used as core for the fluxgate magnetometer and it has been compared experimentally as shown in the figure 4.18 bellow.

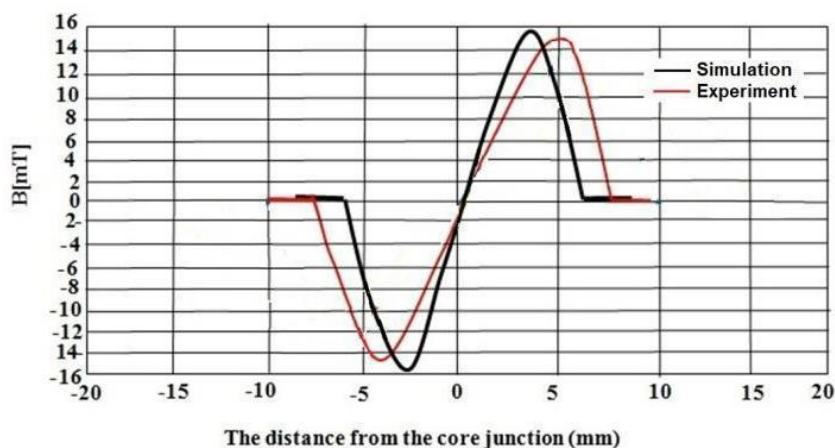


Figure 4.18. The influence of the wire width on the flux density through the core (experimental vs. Simulation).

4.6.5 The Influence of the Ferromagnetic Core Width on the Hysteresis Loop

When the same current of 680mA was applied with the same modelled design, the core width has been investigated in terms of flux density and saturation of the core. Furthermore the different magnetic flux density (B) that has been obtained indicating that in the case of (2mm) core width should perform as a good fluxgate sensor.

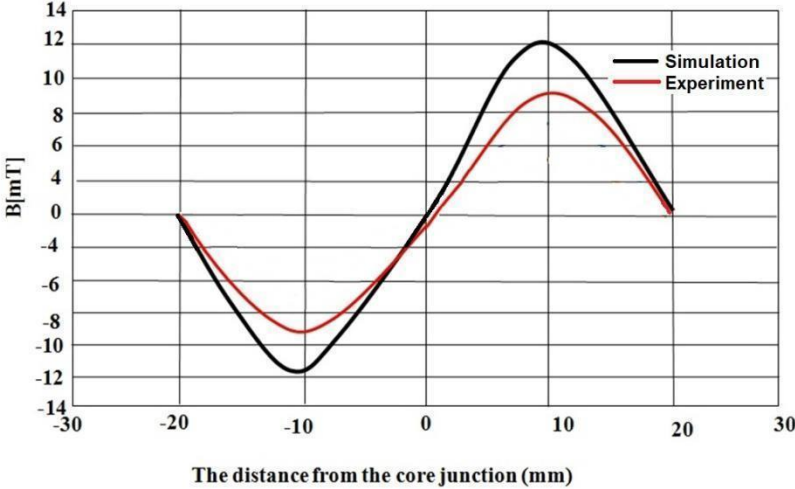


Figure 4.19. The influence of the core width on the flux density through the core (experimental vs. Simulation).

4.7 Summary

This chapter presented the developed ANSYS model to optimise the geometry of the fluxgate magnetometer and to test advanced materials, i.e., amorphous and metaglas, as well as discussed, the evolution and the results of the model sensor that has been designed by ANSYS software. In the section 4.4 the results of the model and comparison of the output with many cases has been tested such as Evaluate the excitation current value that ensures the saturation for ferromagnetic material and how the current is affecting the BH curve which in turn will affect the sensitivity of the sensor, Different number of turns and analyse the BH curves of each case, Compare the output voltage with different thickness ferromagnetic materials, Different wire width and Different core width. In section 4.6 the experimental optimisation and the results of the proposed planar were compared with a Simulated optimised planar. In chapter 5 and 6 an improvement to the proposed planar, the performance, modelling and application of a planar electromagnetic sensor will be discussed in detail. In addition to the improved Ordinary and the Blind Kriging methods will therefore be used in the next chapter as a new technique and an optimisation tool to investigate the best possible performance of various topologies of planar sensors when they are used in inductive sensing.

CHAPTER 5

USING THE VARIABLE GEOMETRY IN A PLANAR INDUCTOR FOR AN OPTIMISED PERFORMANCE USING A ROBUST DESIGN METHOD

In this chapter, the performance, modelling and application of a planar electromagnetic sensor are discussed. Due to the small size profiles and their non-contact nature, planar sensors are widely used due to their simple and basic design. The chapter discusses the experimentation and the finite element modelling (FEM) performed for developing the design of planar coils. In addition, the chapter investigates the performance of various topologies of planar sensors when they are used in inductive sensing. This technique has been applied to develop a new planar coil. The ANSYS Maxwell FEM package has been used to analyse the models while varying the topologies of the coils. For this purpose, different models in FEM were constructed and then tested with topologies such as circular, square and hexagon coil configurations. The described methodology is considered an effective way for the development of sensors based on planar coils with better performance. Moreover, it also confirms a good correlation between the experimental data and the FEM models. Once the best topology is chosen based on performance, an optimisation exercise was then carried out using uncertainty models. That is, the influence of variables such as number of turns and the spacing between the coils on the output inductance has been investigated. This means that the combined effects of these two variables on the output inductance was studied to obtain the optimum values for the number of turns and the spacing between the coils that provided the highest level of inductance from the coils.

Integrated sensor systems are a pre-requisite for developing the concept of smart cities in practice due to the fact that the individual sensors can hardly meet the demands of smart cities for complex information.

5.1 Introduction

The concept of smart growth started in the 1990s. However, the concept of smart cities manifested after the financial crisis in 2008. During this period, cities had to compete with each other across the world through global internet connectivity and networks. This led to the concept of smart cities. It is based on different areas of decision-making based on the quality of life with an inclination towards saving while deliberating on a system approach to provide a solution. Hence the smart city is a concept to manage cities using the latest technology with environmentally friendly principles in a modern way intended to save resources [96-98].

A smart city can be identified with different phrases such as a digital city, an e-city, a global community, or a cyber-city. The concept of a smart city is derived from the idea of a smart planet that is made up of specific urban areas composed of smart homes. Hence, a smart city can be defined as a safe and secure urban centre that is environmentally efficient and uses advanced infrastructures to promote sustainable economic growth that would provide a high quality of life[99]. It ensures that the needs of the current generation are catered for without compromising the needs of the future generation [99].

5.2 The Elements of Smart Cities

Different countries will benefit differently from the smart cities concept. Developing countries have an urgent need for smart cities. This is because, smart cities the concept can be used to deliver a satisfactory metropolitan infrastructure to cater to the growing need for urbanisation. Thus, smart infrastructures in cities provide the possibility of economic sustainability [100]. It is difficult to maintain infrastructure in developing countries due to cost, politics, and space. Hence, if these countries are focusing on smart cities then they will be focusing on efficient use of its current infrastructure. However, the overall purpose of smart cities in both developed and 3rd world countries is to focus on sustainable developments [100][101].

A smart city must have smart infrastructure as this is the theme in all smart cities. It includes smart mobility, governance, economy, and environment. All these components of smart infrastructure are connected and each generates its data that is used to monitor the use of various resources to ensure they are used sustainably and performance is improved. Thus, there are different elements of smart city infrastructure [101].

5.2.1 Smart Buildings

A smart building is a structure that sensibly uses different physical systems to ensure that all systems operate accordingly together to ensure optimization and efficiency. These buildings are used for energy efficiency, waste reduction, and optimum water usage and hence guarantees operational effectiveness. Smart buildings are estimated to reduce water usage by 30% and energy usage by 40%. Thus overall maintenance costs would be reduced by 10% to 30%. The first smart building is in Austria and it provides more energy than it utilises[102].

5.2.2 Smart mobility

Smart mobility is the use of alternative transport options that are cheaper, faster, and environmentally friendly while ensuring that they reduce congestion. This can be achieved by collecting data about mobility patterns and using it to optimise traffic conditions. Both mass transit systems and individual mobility structures such as vehicle and bicycle sharing and on-demand transportation. In Sao Paulo, Brazil, bicycle-sharing systems are being used and it has helped in reducing carbon dioxide emissions in the city since 2012. Similarly, uber is a smart mobility system. It ensures convenience, encourages sharing and uses technology. Uber is a common mode of a taxi in many countries across the globe [103].

There is a need for intelligent transport systems that would integrate the different transport systems in the city. It considers and collects data on various attributes such as the various network sensors, the position of public transportation across the globe, the passengers' profile, traffic lights, and navigation facilities. This data is then used to improve mobility safety, manage networks, reduce traffic congestion, improve convenience and accessibility, and reduce environmental pollution. Poznan in Poland has a modern intelligent transport system [103].

2.2.3 Smart Energy

Smart energy is the use of sensors, renewable energy sources, and digital controls to automatically distribute energy and monitor and optimise its use. Thus smart energy management systems are used to optimise grid operation by balancing the needs of the different users. Smart energy infrastructure includes renewable energy generation, automated response to demand, virtual energy plants, smart energy storage, and grid

operations, and energy-efficient innovation such as smart machines and electric automobiles. Smart energy innovations offer energy saving devices that provide energy consumption patterns and thus they can be monitored and this data used to improve energy efficiency in buildings [104].

The main component of smart energy is a smart grid. This is an electricity delivery system that transmits energy from the point of transmission to the point of consumption through the use of ICT to enhance its operations and thus customer satisfaction and environmental benefits. Japan has a smart city project called Kashiwa-no-ha. It utilises a smart grid that is made up of home energy management systems, monitoring of energy supply, and demand in real-time. The energy is generated and stored optimally to ensure that the energy management system is self-sustaining [104].

5.2.4 Smart Water

Cities across the globe are faced with the challenge of water scarcity as they lack innovative technologies that can be used for water management. Smart water is the use of innovative technologies to improve metering and movement management to ensure the water is distributed optimally [105]. Thus, with the system, more water is saved while the cost of distribution is reduced. Similarly, it ensures the water distribution system is reliable and transparent. Smart water combines physical pipe networks with data and information networks. The data is used to analyse water flow and pressure to detect any real-time anomalies, hence better water flow management . Similarly, consumers receive real-time information that they would use to conserve water and thus reduce water bills. Smart water exists in Mumbai, India. It has smart water metres in its water supply systems. The metres are managed remotely and they have helped in reducing water leakage by 50% [105].

5.2.5 Smart waste management

The total waste generated in urban cities is increasing at a faster rate than the decomposition rate. It has become difficult to collect, differentiate, and determine the types of waste that can be recycled. Waste management is a whole process that involves monitoring, collecting, transporting, handling, recycling, and disposing of the waste. The purpose of a smart waste management system is to reduce waste and separate the different types of wastes and then develop waste handling methods. Similarly, with these systems, the waste can be converted into various resources and thus develop a closed-loop economy [106].

Smart waste management is beneficial as it ensures efficiency during the process of waste collection and picks up as it can be used to predict the days of waste pick up. Sensors can be used to reduce inefficiency. With a smart waste management system, waste can be monitored, and then technology used to manage the waste as it moves from its source to the point of disposal. Smart waste management systems are currently being tested in the United Arab Emirates and Spain [106].

5.2.6 Smart Health

The current economic development practices are affecting human health especially in locations with many industrial plants. For this reason, the health and well-being of city dwellers have become a concern. Smart health-care systems are an important element of smart cities. Technologies can be used to identify epidemic hotspots. A smart-health management system can be used to provide more insight into health practitioners who can use this information to remotely diagnose, treat, and monitor patients using digital

health records. Similarly, it can be used to monitor the health of the city's residents. It focuses on prevention measures by ensuring healthy living. Smart health-care systems may help in reducing health-care inequalities by having a system that is suitable for both low and high-income societies [107].

An example of a smart health technique is crowdsourcing which is used to collect data on disease outbreaks and using it to predict potential hotspots and thus ensuring preventive measures are taken. Additionally, it is used to collect data on the patients' vital health, and this data is used to automatically alert patients about their medications and check-ups. Africa has a project called Medic Mobile project that is used by health workers in the rural areas to report any medical symptoms and then provide treatment advice using their mobile phones [107][108].

5.2.7 Smart digital layers

Smart digital is used to control operation and ensure the sustainable use of the city's limited resources. They can be used to collect and share data promptly and the city can find mitigation measures before the issues escalate to adverse levels. The digital infrastructure in smart cities can be in different layers [109].

Urban is the first layer which is the meeting point between the physical and digital infrastructure. This is made of smart buildings, smart energy, smart waste management systems, and smart mobility. The second layer is the sensors that are made up of all the smart machines that are used to manage all the parameters in the city. The third layer is connectivity to transmit data and information from the sensors to the storage and then the data aggregators. The fourth layer is data analytics in which any collected data is analysed to predict various events. Finally, the last layer is

automation. In this layer, devices are programmed and controlled across different domains [109].

5.3 Applications of Sensing Techniques

Smart cities have started to be emerging environments across the globe in which these systems have become data production centres from urban environments, buildings, vehicles, traffics, public offices, water systems [110]. Such a huge number of data helps scientists, policy and rule makers and other stakeholders to generate the most appropriate decisions. Hence, the sensory-based infrastructure has become the key concept for GPS, RFID scanners, magnetometers, Light Detection and Ranging (LIDARs), temperature and humidity air pressure measurements. Furthermore, such a concept finds applications in smart parking, structural health, smartphone detection, electromagnetic field levels, traffic congestion and smart lighting. The most widely used application of such a concept is the electromagnetic sensing system [111][112]. Sensors are important and substantial for any intelligent control system. A process is improved based on its environment and this requires a control system typically equipped with an array of sensors from which it collects the required data. One of the important applications of integrated sensor systems is the Smart Transport and Mobility Tracking system since this is needed to avoid and optimise the traffic flows on roads. As smart cities prevail with a rising ability to be instrumented, various movable and fixed sensors, connected through wired and wireless networks, are implemented. Such applications include adaptive and personalised maps, vehicle navigation, traffic monitoring and road incident detection [110–113]. A few years back, researchers have been made aware of the planar type of electromagnetic sensors and the possible defects in printed circuit boards (PCBs). The study of such planar type systems for

sensing has been extended to evaluate properties related to the near surface material such as permeability, conductivity and permittivity. The non-invasive techniques used for determining the properties of a component or structure, coherence of a material or the quantitative measure of characteristics of any object is termed as non-destructive testing (also known as NDT). Such methods can be easily used, without harming or damaging the system, for inspection and measurement. Recently, the NDT has been found in various applications and industries. The demand for the utilisation of appropriate techniques is increasing with the increase in demand of greater performance techniques for inspection. For operation in severe environments, the use of NDT approaches is considered a necessity [110–113]. Nowadays, due to the application of sensing principles in the non-destructive evaluation (NDE) and the wireless power transmission, the power coil technology has been renewed. The advantages of planar coils are more than those provided by the traditionally wound coils due to the former's wireless sensing capabilities when compared to the latter [114], small size profiles [115][116], higher levels of robustness [117][118] and the lower cost. Based on the application [119-121], these planar coils can be manufactured on hard or flexible substrates [122][123]. The inductance of a planar coil is affected by both the electromagnetic [124][125] and the physical factors and these are frequently implemented as a part of an inductance-capacitor (LC) circuit [126]. Any change in the value of the inductance affects the resonance of the circuit [127-129]. Such characteristics allow for various effective applications which include NDT and NDE [130-132], health monitoring [133][134], sensing techniques and wireless power transfer [135][136]. To monitor and capture the various physical aspects of the external environment, e.g., light, temperature, humidity, magnetic fields and sound, there exists a handful of sensor types capable of fulfilling such purposes [137]. Integrated sensor

systems involve the use of multiple complementary sensors within Micro-Electro-Mechanical Systems (MEMS) [138]. Apart from the internal connections of sensors, in the context of smart cities, it is important for them to be externally connected via wireless networks to a central unit that receives and processes the data, hence called wireless sensor networks [139][140]. That is important because cities are too complex for a single type of sensor to satisfy the demands for the analysis of information necessary for smart management.

5.4 The Scope of the chapter

In this chapter, the planar coils, being a part of a displacement sensor, will be investigated and an overview of the typical sensor types and their corresponding urban applications are discussed. This research presents a key development of the electromagnetic sensors by analysing the behaviour of different planar coils for tracking and location identification for the smart cities. The ANSYS Maxwell 3D FEM software package has been used for the evaluation of the different coil topologies: circular, square and hexagon coils. Then, an impedance analyser was used for characterising the manufactured versions. A comparison of both the measured and simulated performance of each design sensor is presented in this chapter. In order to study the interaction of magnetic, dielectric and conducting materials, sensors of a planar type such as circular, square and hexagon configurations were designed and fabricated. These sensors have a simple structure and are planar in nature. A simple fabrication technology, i.e., printed circuit boards (PCBs), is used for fabricating such sensors. The principle for operating these sensors is dependent on the interaction of the electromagnetic field, which is produced by the sensor, and the neighbouring materials to be tested. There are two coils in these sensors, namely: the sensing coil and the exciting coil. Alternating current is carried by the exciting coil which generates

an electro- magnetic field of a high frequency that penetrates in the system under investigation. In the process, eddy currents are generated on the system by the electromagnetic field induced by the system under investigation. The materials which are used for investigation are magnetic and conducting properties. The generated field in the system is modified by the field induced due to the flow of the eddy current. The resultant field is diagnosed by the coil which is placed above the exciting coil. The coil which detects the field is the sensing coil or 'pick up' coil. Amongst the utilised coil geometries, the hexagon type sensor when used for detecting cracks in metals, for instance, has a poor performance as it is affected by the non-homogeneity of the material as well as the alignment of the cracks. Hence, the square type sensors were developed to overcome such issues [139]. Furthermore, the circular pattern is less influenced by the developed eddy currents and these results in less dependence on the geometry or alignment of the sensors when compared to the other configurations.

5.5 Methodology

5.5.1 The Experimental Method

The following design parameters, Table 5.1, are typically related to the board level inductor design utilised in the experiment. The coils used for experimental measurements have the same dimensions as the ones used for simulation purposes.

Table 5.1. The structural parameters of the proposed Printed Circuit Board (PCB) inductor.

Parameters	Unit	Value
Inner radius (R)	mm	0.15
Width of the copper track (W)	mm	0.1
Gap between the copper tracks	mm	0.2
Thickness of the copper (Th)	mil	2.5
Distance between two layers (D)	mm	0.5
Turns in a single layer (N)		12

In terms of the fabrication of the three planar coils stage, each coil is constructed with copper wires. Several calibration holes are set on the board for a precise angular adjustment. By using a commercial 2-layer PCB fabrication process, different sets of inductors were fabricated. The setup of the fabricated coils is shown in Figure 5.1 a 2-port Agilent network analyser has been used to measure the excitation of the fabricated inductors. The short-open-load-through (SOLT) calibration method has been used to calibrate the network analyser by standard calibration tools. The S-parameters (S11, S12, S21, and S22) were measured for each inductor using the network analyser. The values of the inductance for each design were obtained from the Y-parameter data.



Figure 5.1. The fabricated coils on the PCB, for 3D printed support structures: (a) square coil topology; (b) circular coil topology; (c) hexagon topology.

5.5.2 The Analytical Method

A leakage inductance might develop through the transmission of electrical energy between the primary and the secondary coil. In the intervening period of time, a mutual inductance is produced due to the magnetic flux from the primary coil that cuts through the secondary coil to induce the voltage and the current in the secondary coil. Occasionally, the mutual inductance can be lower than that of the leakage inductance, which leads to minimising the magnetising flux. The relationship that is used to calculate the mutual inductance is given by Equation (5.1) [139]:

$$M = \sqrt{L_1 L_2} \quad (5.1)$$

Where L_1 is the inductance of the primary coil and L_2 is the inductance of the secondary coil. The power transferred to the sensing coil, P , can be calculated by Equation (5.2)[139-140]:

$$P = f \frac{M^2 I_p^2}{L_2} \quad (5.2)$$

Where f is the frequency and I_p is the current in the primary coil. From this relationship, it is known that the output power (P) is restricted by the mutual inductance. In this context, the mutual inductance can be calculated using many different formulae such as the Neumann's Integrals method and the Maxwell formulae as well as the use of finite element analysis (FEA). When the FEA approach is applied, the Ansys software can be utilised to simulate the output of the coils and this can provide an accurate performance using built-in advanced calculation techniques. An illustration of the stages in FEA modelling is shown in Figure 5.2.

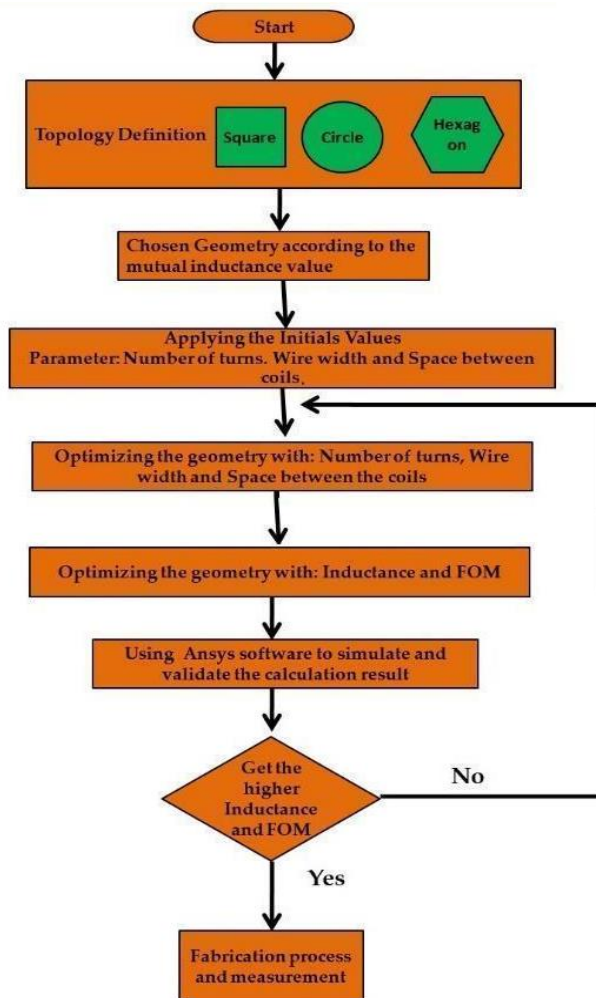


Figure 5.2. The stages involved in Finite Element Analysis (FEA) modelling of the proposed design.

5.6 The Modelling Method

The Maxwell 3d of Ansys Electronics desktop 18 Suite was utilised to simulate the different types of coils. This simulation investigates the mutual inductance or the coupling coefficient between two identical coils of which one acts as the transmitter while the other acts as the receiver. The magnetic fields generated by a defined DC current in the transmitter coil and the correspondence with the receiver coil, i.e., TX and RX, respectively, are thoroughly studied. The Ansys Maxwell software has been used to compare various coil shapes (circular, square, and hexagonal). The generated

coils using Ansys Maxwell are shown in Figure 5.3 The features of each coil design with regards to the number of turns, thickness and space between the traces are shown in Table 5.2. In this context, the space between the traces was varied according to the desired pitch value.

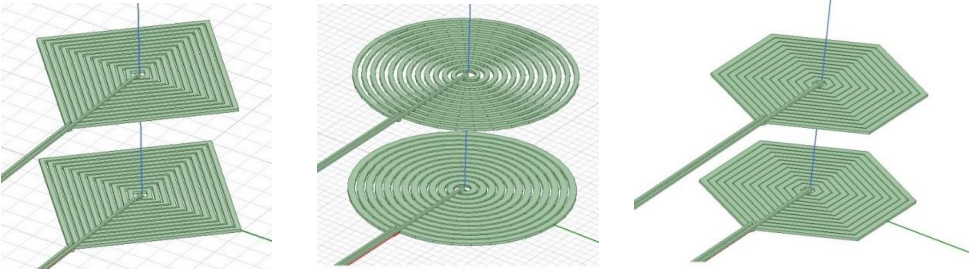
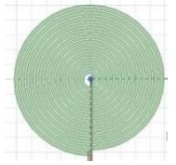
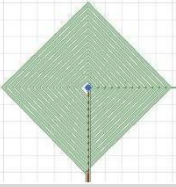
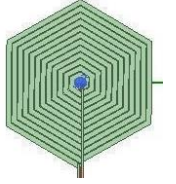


Figure 5.3. The various topologies of the modelled coils: square, circular and hexagonal, respectively.

Table 5.2. The various features of the designed coils.

Coil ID	Coil Geometry	Number of Turns	Thickness (mil)	The space between the excitation and sensing coils (mm)		
				Option 1	Option 2	Option 3
Circular		12	2.5	0.5	1	1.5
Square		12	2.5	0.5	1	1.5
Hexagonal		12	2.5	0.5	1	1.5

5.7 The Robust Design Method

The Meta-model-based design optimization is becoming increasingly popular in the industrial practice for the optimization of complex engineering problems, especially to reduce the burden of computationally expensive simulations. The idea behind the Meta-model-based design optimization is to build a surrogate model (or a meta-model) from a reduced number of simulations runs and subsequently use the model for optimization purposes [141-143]. The surrogate model, i.e., $y = f(x_1, x_2, \dots, x_n)$, approximates the relationship between the design variables, i.e. x_1, x_2, \dots, x_n , and the output variable, y [141][142]. This method can speed up the design optimization process since the function evaluations of the surrogate model are less expensive to execute when compared to deterministic simulations. The simplest type of 'Response

Surface' is a linear model in which the functional relationship $f(x_1, x_2, \dots, x_n)$ is assumed to be a linear function of the design variables [143]. Linear models can be extended to polynomial response surface models wherein the response surface is a polynomial function of the design variables. In either way, the linear or higher order response surface (polynomials) can be obtained using the 'Ordinary Least Squares' approach by minimising the sum of the squared distances of a given data points from the surface [144]. In this case, the surrogate modelling utilising the least squares approach assumes that all errors are normally distributed with given mean and variance [144]. This assumption is often too stringent in real-world problems [141-144]. The Kriging method has been pre-fixed with different names depending on the form of the regression function, $f(x)$. For instance, the simple Kriging method assumes that $f(x)$ is a known constant, i.e., $f(0)=0$. On the other hand, the ordinary Kriging approach assumes that $f(x)$ is constant but unknown, i.e., $f(x)=a_0$. For more complex processes, trend functions might be linear or quadratic polynomials. In this regard, the universal Kriging treats the trend function as a multivariate polynomial such that [141]:

$$f(x) = \sum_{i=1}^p \alpha_i b_i(x) \quad (5.3)$$

Where $b_i(x)=b_1(x), b_2(x), \dots, b_p(x)$, are the basis functions (e.g., the power base for a polynomial) and $\alpha_i = (\alpha_1, \alpha_2, \dots, \alpha_p)$ denote the coefficients. The idea is that the regression function captures the largest variance in the data (the general trend) and then the Gaussian Process interpolates the residuals [141–142]. In fact, the regression function $f(x)$ is the mean of the broader Gaussian Process Y . One of the most widely used Kriging approaches is the Blind Kriging method. In this approach, the trend function $f(x)$ is unknown and is hard to choose for a given problem [140-141]. Some feature selection methods sometimes offer the possibility to identify the most plausible interactions occurring in the data [141]. The Blind Kriging is used to efficiently

determine the base functions, or features, that capture the most variance in the sample data [142]. In this respect, a set of candidate functions is considered from which to choose for the problem. In the ideal case the sample data are almost fully represented by the chosen trend function and the stochastic process $Z(x)$ has little or no influence [141]. The idea is to select new features to be incorporated in the regression function of this Kriging model, considering features that are already a part of the regression function of the model. The whole set of candidate functions that is used to fit the data in a linear model are given by Equation 5.4 [141]:

$$g(x) = \sum_{i=1}^p \alpha_i b_i(x) + \sum_{i=1}^t \beta_i c_i(x) \quad (5.4)$$

where t is the number of candidate functions. The first part of this equation is the regression function of Kriging and, hence, the coefficients of α have already been determined independently of $\beta = (\beta_1, \dots, \beta_t)$. The estimation of β provides a relevance score of the candidate features [202][203]. A frequentist estimation of β (e.g., the least-squares solution) would be a straightforward approach to rank the features (e.g., the least-squares solution) [141–144].

5.8 Results and Discussion

5.8.1 The Experimental Results

The spacing distance between the coils changes the effective mutual inductance value as shown in figure 5.4 It is evident that the increase in the spacing distance causes a gradual decrease in the value of the generated inductance. The results were obtained

from measurements of actual displacement. It can be seen that for any given spacing value, the squared coil configuration has provided the highest level of inductance compared to the hexagonal and circular designs. Furthermore, it can be seen that the larger the spacing the lower the generated inductance and this applies to all design configurations. As the spacing value increases, the generated inductance obtained from all designs converges and this means that at larger spacing values, it becomes less dependent on the coil configuration.

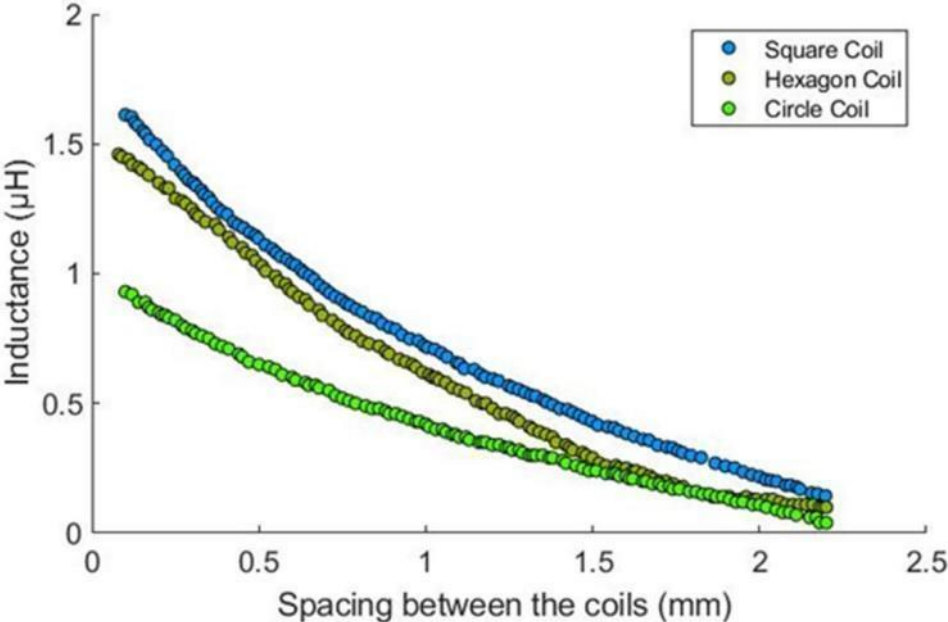


Figure 5.4.The experimental result between the resulting inductance and the spacing between the excitation and sensing coils.

5.8.2 The Modelling and Optimisation Results

To compare the effectiveness of the three proposed coil designs, the Ansys Maxwell electromagnetic software has been employed to analyse the distribution of the magnetic flux density in the magnetic cores of the excited sensors. To simplify the design diversity despite the distinct geometric designs of the excitation coils, key

design factors were maintained unchanged through the various designs to allow for comparisons. This includes the number of wire turns, the metal wire gap, the cross-sectional area of the metal wire, the coil resistance, the coil inductance and the dimensions of the ferromagnetic core. Therefore, by assuming uniform excitation currents through the coils, the simulation results, Figure 5.5, provide an approximate solution of the electromagnetic excitation condition via the excitation coils and the magnetisation of the magnetic cores. From the obtained results in Figure 5.5, it can be seen that the highest flux density recorded for the square coils was 5.55×10^{-4} T with a lowest value of 2.59×10^{-5} T. It is also evident that for this particular design, the highest flux is recorded at the centre of the coil which decreases towards the circumference of the coil, i.e., in the radial direction. On the other hand, the hexagonal coil design provided a lower maximum flux value when compared to the square coil design. The maximum value for the hexagonal design was around 4.006×10^{-4} T at the centre of the coil which, again, decreased towards the circumference of the coil, i.e., in the radial direction. The lowest value for this specific coil design was around 3.77×10^{-5} T. The flux values were lowest for the circular design with a maximum of 3.99×10^{-4} T at the centre and 6.49×10^{-5} T nearby the circumference. Overall, the square coil design provided the highest possible flux density followed by the hexagonal and then the circular geometry. This was also the case while changing the spacing distance between the coils, Figure 5.6. It can be seen that for any given spacing value, the squared coil configuration has provided the highest level of inductance compared to the hexagonal and circular designs. This is due to the size of the wire cable for each coils shows that the Hexagon coil has a lower perimeter so it requires a shorter cable however circles require second less and square shapes require higher than all others hence this increases resistance.

Furthermore, it can be seen that the larger the spacing the lower the generated inductance and this applies to all design configurations. As the spacing value increases, the generated inductance obtained from all designs converges and this means that at larger spacing values, it becomes less dependent on the coil configuration.

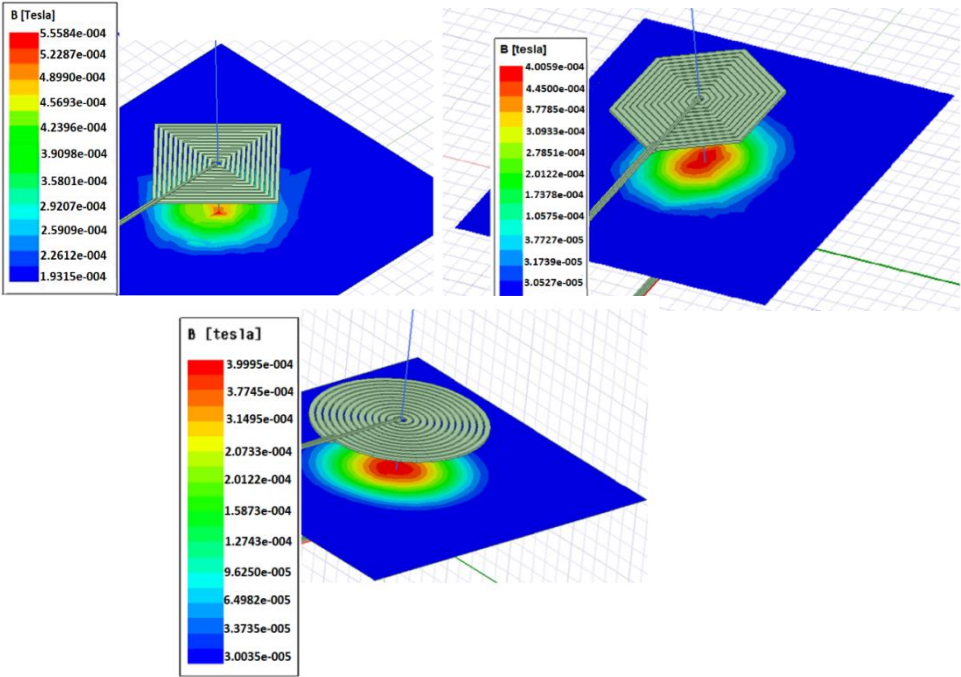


Figure 5.5.The modelling and simulation results of the square (a), hexagonal (b) and circular (c) coil topologies.

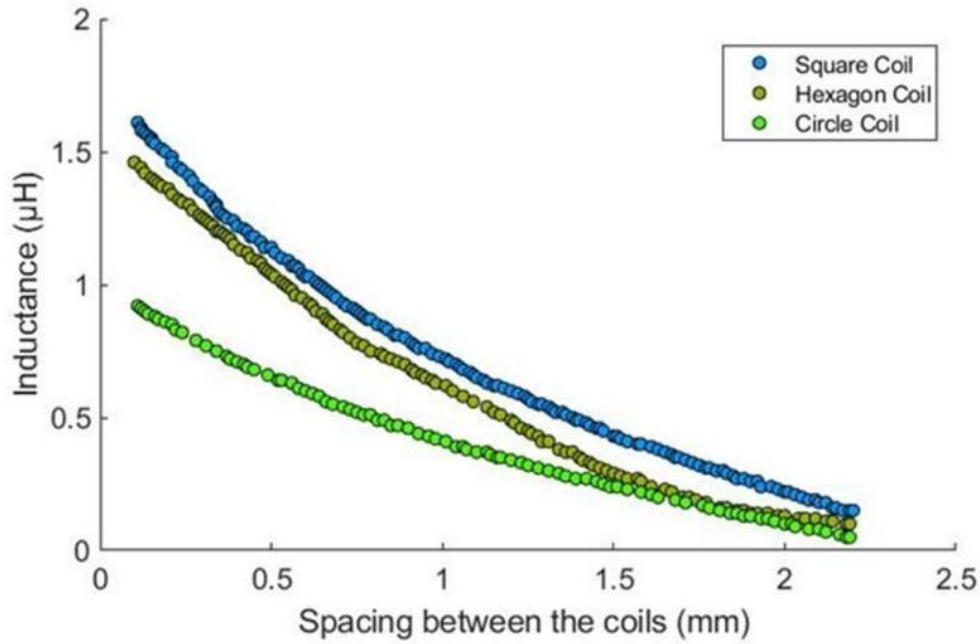


Figure 5.6. The simulation results in varying the spacing distance between excitation and the sensing coils.

The purpose of the proposed design in the current research is to optimise the design of the PCB inductor for the applications of smart cities. As such, it is desirable to achieve the highest possible inductance. The Figure-Of-Merit (FOM) of an inductor is given by equation[144].

$$FOM = \frac{L}{A} \quad (5.5)$$

where L is the inductance (μH) and A is the area of the coil (16mm for the square, 12.57mm for circle coil and 12mm for the hexagon coil) The target of optimization is to obtain the maximum possible FOM values from the given design configurations. The results in figure 5.7 show the effects of changing the number of turns and the spacing between the coils on the value of the FOM for the square, hexagonal and circular configurations, respectively. The general trend in these figures is that the higher the number of turns, the larger the value of the FOM and hence the output inductance. On the contrary, the larger the spacing between the coils the lower

the value of the FOM. Amongst all, the square coil design provides the highest FOM at any given number of turns or a spacing value.

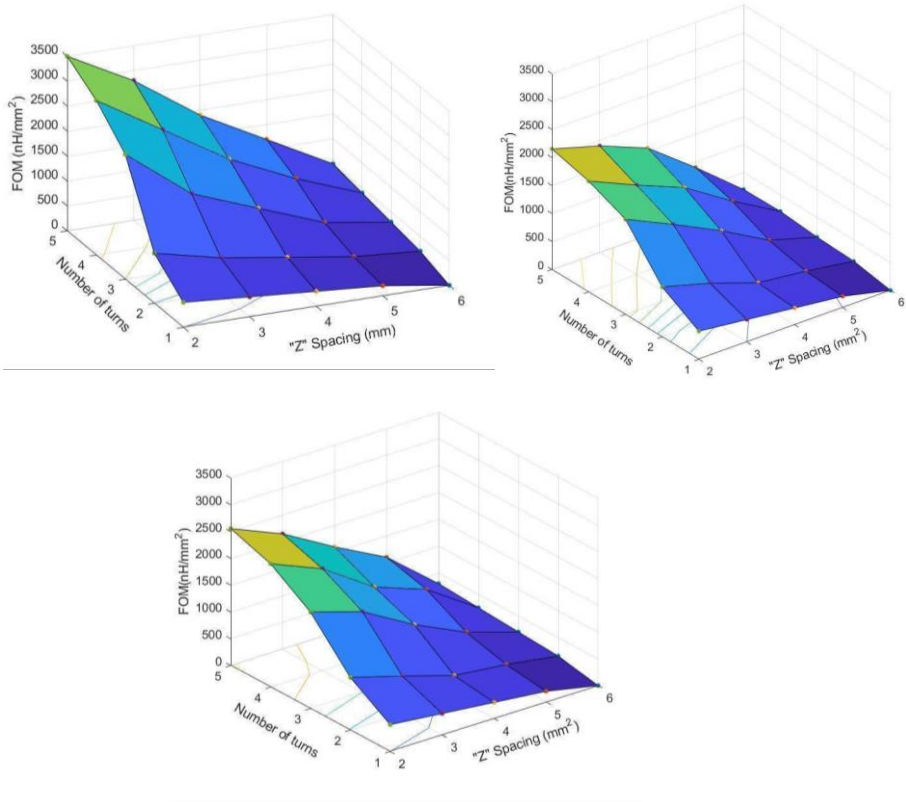


Figure 5.7. The Figure-Of-Merit (FOM) value as a function of number of turns and spacing between the coils for the square (a), hexagonal (b) and circular (c) designs, respectively.

5.8.3 The Uncertainty and Robust Design Results

The obtained results from the Ordinary and the Blind Kriging models for the optimum configuration (square) design (the best configuration) are shown in Figure 5.8 and Figure 5.9, respectively. The ‘Mean Squared Error’ of the Leave-out cross validation was chosen to evaluate the quality of the fit as well as the predictive capability of the technique. These optimisation methods have both interpolated and extrapolated the

data based on the short-term measurements which mean, creating a Kriging model can be interpreted as constructing two Kriging models in sequence: a first Kriging model of 100 samples followed by a second Kriging model constructed on the residuals of the 1000 samples. This is a very good way to predict the long-term behaviour based on short-term measurements. This saves time and cost associated with long experimental time and hence, it is favourable. In these plots, the response surface is constructed based on the equations of the Ordinary and Blind Kriging approaches whereas the dots are those simulated by the MATLAB code that randomly assigns the data points and runs the analysis through ANSYS, as can be seen in Figure 5.8a. The fit of the data is very good despite the small variances observed between the data points and the response surface as shown in Figure 5.8b. However, an optimum region characterised by the highest inductance is observed when the distance between the coils, i.e., Z spacing is between 0.5 mm to 1.5 mm while the number of turns is between 37 and 60. In this region, the highest inductance was above 20,000 μH . When looking at the results of the blind kriging optimisation approach, it becomes evident that the fits, in general, are better with a lower level of variance compared to the ordinary kriging approach, Figure 5.9a and 5.9b. Moreover, it can be seen in Figure 5.9c that an optimum region of the highest inductance is observed (yellow-coloured zone) with values exceeding 25,000 μH . It is evident that the decrease in the spacing between the coils, i.e., the Z-spacing, as well as increasing the number of coils enhances the generated inductance.

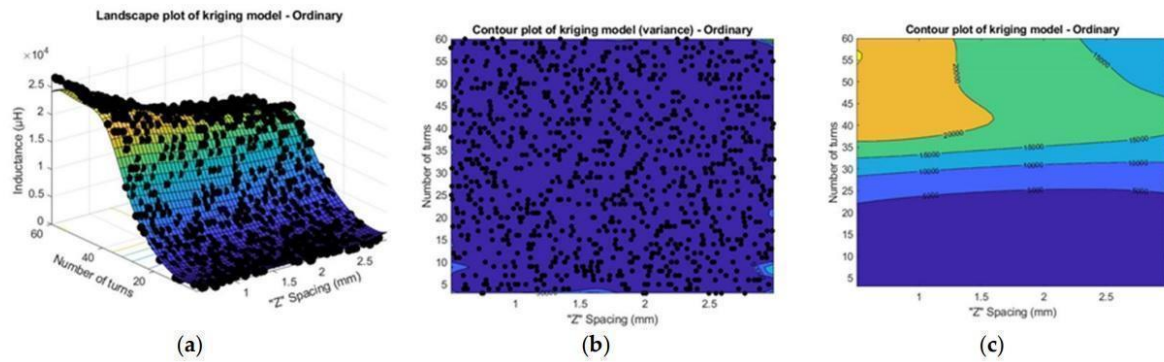


Figure 5.8. (a) The Ordinary Kriging response surface, (b) the variance plot and, (c) the contour plot of the inductance.

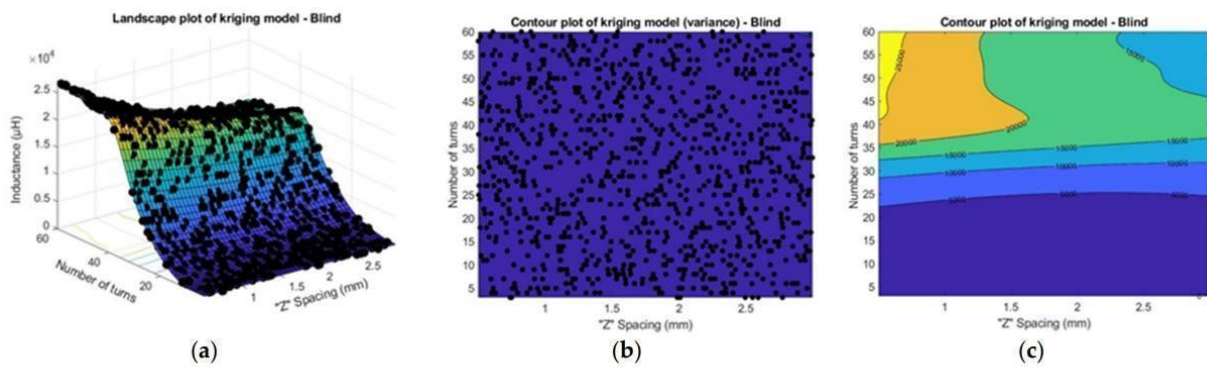


Figure 5.9. (a) The Blind Kriging response surface, (b) the variance plot and, (c) the contour plot of the inductance.

5.9 Discussion of Results

The FEM displacement results in Figure 5.4 and 5.6 show the largest inductance value for the square coil, followed by the circular and hexagon coil. There are two distinct characteristics here, one for the square and circular coils and another for the hexagon coil. Lowest measurement range is for Hexagon coil, which is approximately 0.5 mm, 1.5 mm and largest measurement range is for square and circular coils and is approximately equal to 0.2 mm. The hexagonal coil has the lowest measurement range with pitch of 1.5 mm. Contrary to this, the circular and square topologies have 1.5 mm pitch values, which is the lowest value. These are the lowest values of pitch for each

topology, respectively. The results of simulation show that alterations in topology of coil enable the sensitivity for matching the required range of displacement. The values of pitch chosen in this work to calculate the inductance and the magnetic flux density over various spacing distances. The different coil geometries generated different magnetic fluxes. The higher the magnetic flux the better the inductance. It has been observed that the inductance decreases with increasing the coils spacing distance. There is a possibility that it is due to mutual inductance because interaction between tracks of copper increases due to area which becomes densely populated. Figure 5.1 shows that fabricated coils follow the same trends for FEM counterparts. All the fabricated coils have greater values of inductance than that of simulated ones and circular and square coil topologies double the value of inductance. Square and circular coil topologies have irregularities in signal, and these are more obvious at greater pitch values but the correlation between these coils and the simulations are also good. Such type of irregularities is not visible in Hexagon topology. The data shown represent the inductance value of 80 kHz which lies in the range of 20 kHz to 100 kHz. Signal to noise ratio is small for data which are below 20 kHz. For further analysing performance of the sensor, both experimental data and FEM were fitted with an exponential line with decaying trend. There is a more rapid decrease in inductance because the decay constant is larger for hexagon topology as compared to circular and square coils. Due to the non-linear nature of the sensor, it is difficult to quantify sensitivity of the sensor. It can be seen that the spiral coil technologies have an operating range which is greater in a displacement sensing application and have greater inductance value and sensitivity as well. Due to the decrease in dimension of pitch, these parameters increase proportionally. These results show that for inductive sensing of displacement, planar coils use spiral coil topologies, ideally square, which have the highest copper

track density for the sensor to perform better. However, design considerations are dependent on the application and it is difficult for general design rules to be applied as compared to the one mentioned above.

5.10 Conclusion

This chapter presented a good correlation between the FE modelling simulation and the experimental measurements. A study of various shapes of coils has been presented, using Ansys Maxwell simulation and experimentation. The topology of the coil has also an effect on the performance of the sensor. In total, three shapes of coils were designed, simulated and experimented to calculate the inductance and the magnetic flux density over various spacing distances. The different coil geometries generated different magnetic fluxes. The higher the magnetic flux the better the inductance. It has been observed that the inductance decreases with increasing the coils spacing distance. Comparing the performance of the three shapes, the square coil geometry has shown the best performance. Generally, the experimental measurements were very comparable with the analytical and FE modelling simulations. To optimise the design of the square geometry, optimisation models have been employed and the optimum values of the spacing distance and number of coils were obtained. That is, for the best configuration, i.e., the square design, the optimum spacing distance was between 0.5 mm to 1.5 mm while the optimum number of turns was between 37 and 60.

5.11 Summary

This chapter has presented two improvements to the optimum configuration design which was Ordinary and the Blind Kriging methods, These optimisation methods is to

build a surrogate model (or a meta-model) from a reduced number of simulations runs and subsequently use the model for optimization purposes, This method can speed up the design optimization process since the function evaluations of the surrogate model are less expensive to execute when compared to deterministic simulations his is a very good way to predict the long-term behaviour based on short-term measurements. This saves time and cost associated with long experimental time. Both improvements to the various shapes of coils have been presented. Three shapes of coils were designed, simulated and experimented to calculate the inductance and the magnetic flux density over various spacing distances. Comparing the performance of the three shapes, the square coil geometry has shown the best performance.

CHAPTER 6

DESIGN INTEGRATION OF PLANAR INDUCTANCES ON WIRELESS CHARGER

Wireless charger technology has been efficiently used for high-efficiency power transfer in long distances. Conventionally, two-coil-based inductive links are adopted for this purpose. To develop the efficiency and unfavourable effect of low coupling magnetically coupled, fully planar coil printed spiral resonator-based wireless power-transfer systems has been presented. This chapter presents the PTE values against the spacing distance between the coils in circular, square and hexagon coils as well as the PTE values against frequency and the Inductance as an against the frequency for all the different realised integrated coils, which use a wireless power-transfer system based on a magnetically coupled fully printed spiral to investigate. The high quality-factor coils improve the efficiency significantly. The transmitter and receiver size are reduced by adopting a conformal architecture. The possibility of both hexagon and square architecture is explored and their performance is optimised to generate maximum efficiency at specific operating distance. The performance of these architectures is analysed on the basis of efficiency of power-transfer and power delivered. The system's efficiency can be found by using the equation

$$\eta=(P_{OUT}/P_{IN})\times 100\% \quad (6.1)$$

where P_{out} is output power and P_{in} is input power. In other words, the measured input power is equal to the output power plus the power loss of the system, so the square coils generate high power-transfer efficiency (80%) compared to hexagon coils (79%) at 0.5 mm distance between receiver and transmitter with air medium and at a

frequency of 10 MHz . Contrarily, the circle resonators generate lower power-transfer efficiency under the same conditions and medium.

6.1 Introduction

Wireless charging is a method of conducting power between an air gap to another electrical device for energy recharging. Wireless charging technology has come a long way in terms of efficiency and utility in recent years [145]. This chapter presents a comprehensive overview of wireless charging technology. First, an introduction of wireless charging technology has been presented. Then, a general review of standards, with a detailed description of their respective protocols for communication is given. In addition to presenting an innovative concept of wireless charger networking. This technique allows chargers to be interconnected to enable collection of information and its control. This technique is demonstrated via a user-charger assignment [145]. The experimental results clearly show that wireless charger networking yields low cost for the users to find the best chargers for recharging their mobile gadgets [146].

6.2 The Concept

Wireless charging techniques help to transmit power from a source (e.g., a charger) to a load (e.g., mobile devices) through an air gap. This technology is crucial for better user experience and convenience [146][147]. Wireless charging is rapidly progressing from theories to standards and being utilised for a wide range of commercial items. It is an essential feature for portable devices and mobile phones. Adopting wireless charging technology yields many benefits to the devices and users. It is a user-friendly

technology since the inconvenience of connection cables can be eliminated [148]. Same charger can be used for different brands and models of devices. Since they are waterproof and dustproof, chargers usually have better durability especially for contact-free devices [148]. Wireless technology provides increased flexibility In the case of devices with replaceable batteries or with connection cables which are infeasible (body-implanted sensors), costly and hazardous. Lastly, the major advantage of wireless charging technology is they provide on-demand power [147][148]. Through this they avoid overcharging and reduce energy costs. Many leading smartphone manufacturers such as Samsung, Huawei and Apple released their devices with built-in wireless charging capacity. This chapter begins with a quick introduction of wireless power transmission mechanisms. Then the foundations of wireless charging systems are explored [2149]. The data communication protocols followed by both standards are reviewed. From this review it is found that existing standards are only focused on simple data communication between a charging device and a charger. They completely avoid the communication among the other parts of a network and with chargers. Hence, we put forward a novel concept of wireless charger networking. This will enable data communication and other information transfer among the chargers. This technique is further demonstrated with the help of a user-charger assignment problem [149]. The results clearly indicate that wireless charger networking can reduce the cost of user-charger assignment [149]. The concept of a smart city or a city with integrated digital systems came into existence towards the end of the 1990s, however, it only became commercialised after the worldwide fiscal crisis in the year 2008. Everything inside a city is connected via a sort of digital infrastructure, where different components interact and respond to each other. Various electronic systems and techniques are utilised to obtain data as well as real-time information of

a city. The focus has shifted to develop this idea ever since, as a potential problem-solver for many countries facing obstacles. Analysts have identified two perceptions of what a smart city should look like. One perspective is that they are a product of a digital and viable innovation, drawn from the theory of 'smart growth' [149]. In this case, research is carried out over a defined period and the technologically motivated solutions are made, in which the job of managing a city is reinvented. On the other hand, the second view is that smart cities would come about as a result of urban digital evolutions, just as the development of the first notable computer [147-149]. It is only logical to assume that the same would occur to the technical aspects of a city. Some of the challenges that had risen over the years had caused people to think to try to generate ways and methods to overcome the challenges that were encountered. The rapid urbanisation was one of the causes. It is recorded that half of the Earth's population moved into cities by the year 2010[149], and if this is not alarming enough, it is predicted that 75% would have migrated into cities by the year 2050; approximately 6 billion people. Many countries were not - and are still not - equipped to handle the loads that came their way. Over-population can have very negative effects on a city [147][148]. A high level of disorganisation and confusion may arise if a city is not adequately prepared to manage the large number of people. Furthermore, over-population would lead to higher demands on energy resources. Generally, power lines are normally uninsulated; a small percentage of electricity is lost during transmission due to the heating effects of the wires. As the population number rises in a city, this may cause larger percentages of power to be consumed and also wasted. Simultaneously, electrical networks that are not closely monitored will become unreliable due to the fact that in the case of power failures, the response time may become longer, which could lead to more extreme damages. Road congestion and

traffic jams can also be major problems in many cities all over the world. This typically presents a 'knock on' effect with regards to over-population as well. Lastly, one of the negative consequences due to overpopulation is that a lot of people acquire diseases from the poor air quality, and this may be due to emissions of the gases released from industrial practices as well as vehicles. In other words, smart cities are intended to enhance the living conditions for the different communities around a city. If the population of a given city constantly increases without any counteraction, it is only a matter of time before that city becomes overpopulated whereby the living conditions become unsuitable for people[148][149].

6.3 The Mathematical Modelling of The Inductor

This section gives an idea of the proposed individual models for or both self and mutual inductance and their parasitic components. The models are designed for Circular, Square and Hexagon coils. Further Investigation on PTE values is also presented. Figure 6.1 gives the design of the proposed planar with the geometrical parameters for the three type's coils.

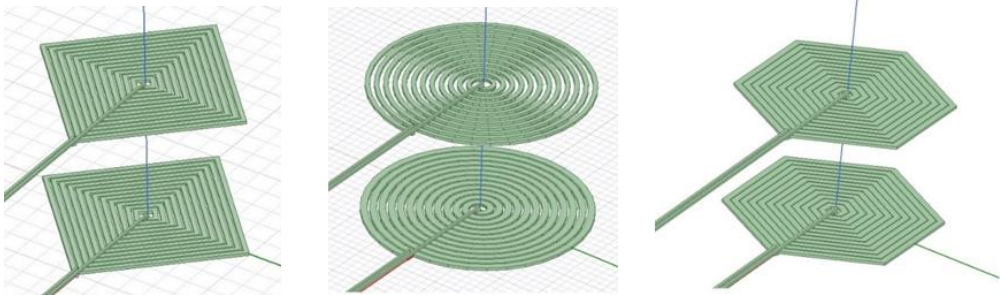


Figure 6.1. The defined integrated coils, namely: square, circular and hexagonal, respectively.

6.3.1 Self inductance

An inductor is a passive element to store magnetic energy. The energy is generated when electric current flows through an inductor as shown in equation 6.2 and figure 6.2. The self-inductance L is defined as the ratio of magnetic flux of a current carrying conductor and the amount of current conducted [150]. To measure self-inductance the sides of spirals are designed to be symmetrical current sheets. Along with this the adjacent sheets are designed to be orthogonal with zero mutual inductance.

Equation 6.2 gives all possible mutual inductance values for planar inductors by considering each turn of the coil and the total inductance can be calculated by adding all the combinations. $\rho=1$, for circular shaped TX and RX coils. In other cases such as square shaped TX and RX, ρ is approximately $(4/\pi)^2$. Therefore, the mutual inductance, M between two square shaped coils is $(4/\pi)^2$ times greater than other circular shaped ones.

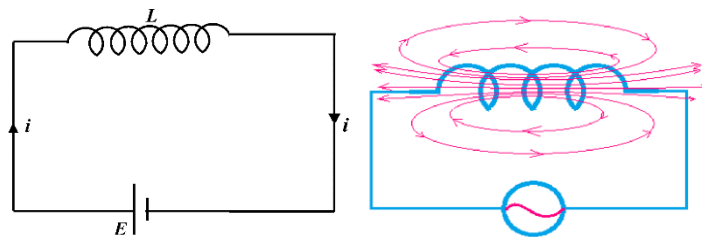


Figure 6.2. a. Inductor bias and b. magnetic field around.

$$E = \frac{1}{2} Li^2 \quad (6.2)$$

which (E) is the magnetic energy (in Joule dimension), (L) is the value of inductance (in Henry), and (i) is the value of electric current (in Ampere dimension).

6.3.2 Mutual inductance

In the previous section, a self inductor was described. When two or more coils are magnetically linked together by a common magnetic flux they are said to have the property of Mutual Inductance. Mutual Inductance is the basic operating principle of the transformer, motors, generators and any other electrical component that interacts with another magnetic field. Then we can define mutual induction as the current flowing in one coil that induces a voltage in an adjacent coil[151].

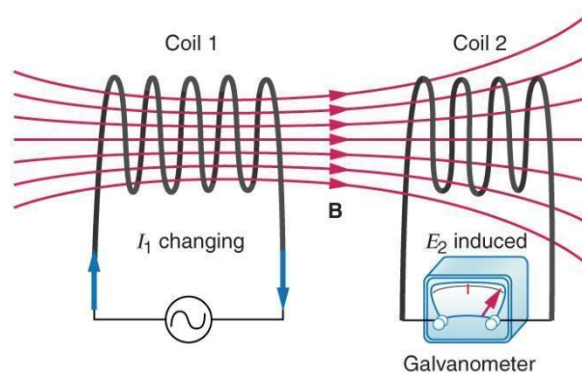


Figure 6.3. Mutual inductance.

6.3.3 Practice elements

In this chapter, will employ mutual inductance for wireless battery charger applications. Since the real mutual inductor has parasitic elements including resistance and capacitance as shown in figure 6.4, will investigate three structures including circle, square, and hexagonal structure of mutual inductor to find out which structure is more suitable when an FR4 PCB is used for substrate of inductors.

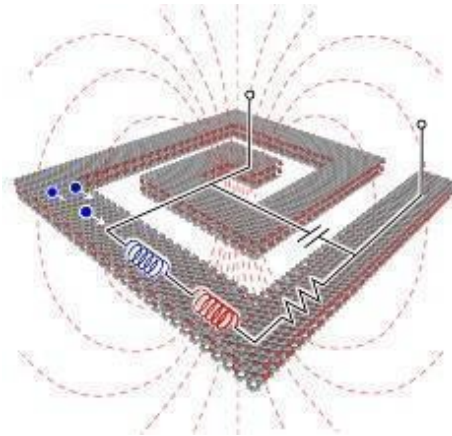


Figure 6.4. Parasitic elements.

6.3.4 Power Transfer Efficiency

The efficiency of the coils can be computed as:

PTE η can be expressed as:

$$\eta = \frac{\text{output power}}{\text{input power}} = \frac{I^2}{EI} \quad (6.3)$$

Where I is the current flow through the resistive load

6.4 Design methodology

This section presents the steps for the design of a fully planar two-coil wireless power transform system as described in the previous section. The significance of these design steps is, it will be helpful to achieving maximum PTE values with high PDL. The equivalent circuit of a mutual inductor is shown in Figure 6.5.

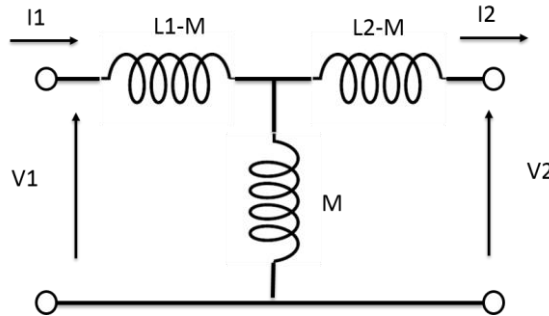


Figure 6.5. Equivalent circuit of a mutual inductor.

The value of inductance between two mutual inductor (M) is shown in equation 6.4

$$M = \frac{A \cdot \mu_0 \mu_r N_1 N_2}{l} \quad (6.4)$$

Where, μ_0 is the permeability of free space, μ_r is the relative permeability of the material which inductor is on, N_1 is in the number of turns of input inductor, N_2 is in the number of turns of output inductor, A is in the cross-sectional area in the mutual inductor, and l length of the coil. Therefore, the energy transferred from the right side to the left side is dependent to M value and thus, dependent to N_1 , N_2 , and A , and l .

6.5 The Experimental Work

Power electronics is currently evolving towards integration, as a result of the constraints related to the need to miniaturise but also to reduce the manufacturing costs. In many cases, hybrid systems offer volume reduction possibilities whereby the inductance, transformer and capacitor, represent a brake on this miniaturisation. Inductive components such as coils or transformers are key elements of power electronics. These are well-known and mastered components with regard to their discrete form, but their integration is still at the study stage and is still far from industrialisation. In this work, the focus is on the design and characterisation of spiral planar coils on a PCB-FR4 [208] the design of a PCB substrate inductor is difficult to

modify once manufactured. The current study has explored the following topologies, namely: the circular and the square topology. The parameters that have been taken into account in this study are the topology of the coil, the number of turns, width and the spacing within the coil system.

6.7 The Characteristics of the Planar Inductances

Figure 6.1 gives the design of the proposed planar and the geometrical characteristics of the coils inductors are presented in Table 6.1. For a given coil geometry, the inductance is characterised by the number of turns (n), outer coil diameter (D_{out}), inner coil diameter (D_{in}), of the conductor.

Table 6.1: The geometrical characteristics of the examined inductors.

Parameters	Symbol	Value
outer coil diameter	D_{out}	10mm
inner coil diameter	D_{in}	1mm
Number of turns	no. turns	12
Wire thickness	W_{th}	2.5mm

6.8 The Manufacturing Process of the Integrated Planar Micro Inductance on PCB-FR4

1. The fabrication process involved laying up different integrated inductor topologies on a substrate of a PCB. In this case, the mask was transferred to the copper-metallised PCB-FR4 using photolithography which aims to reproduce precise patterns over the different layers. , whether for engraving or deposition steps, the patterns of this mask will be transferred to a movie. The illustration in Figure 6.6 shows the fabrication process of the designed coils. This is summarised

as follows: The PCB-FR4 substrate was made of several layers of different thicknesses by a chainsaw, this substrate is a support of insulating material intended for receiving the impression of an electrical or electronic circuit and the various components. The copper wires were then wounded.

2. Secondly, it's important to clean the BCP plates. The copper circuits of the coils of the different topologies were realised on a flex.

3. Prior to engraving, to recreate accurate patterns on the layers for deposition and graving steps the mask was transferred to the copper-metallised PCB using photolithography

4. A lamination process was conducted whereby the topologies were printed on a glass plate containing a chromium layer in order to obtain the mask.

5. The engraving process was done by etching the metallised inorganic substrate using a photosensitive film. To eliminate the copper from the surface of the flex by wet etching the photosensitive film needs to be removed, then etched the bonding layer, that's allowed to remove the copper on the surface of the flex. In addition to that the sample has been wetting in a solution form of iron perchloride and the water which is heated to about 27 °C. The copper has been protected by dissolving the part of the unprotected copper with the cured film and show the desired pattern.

6. A rinsing process was done using water and NaOH or acetone to remove the resulting blue film and show the conductive lines.

7. To avoid oxidation the component is heated up to 70C.

8. To remove any oxides remained the inductor has been varnished

9. Finally to make sure that the central and external stud is connected to each other by bonding.

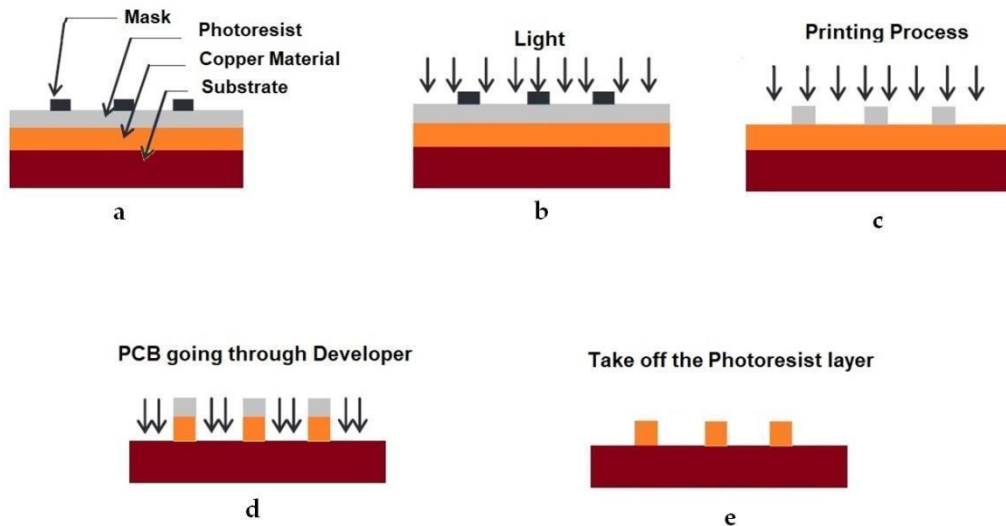


Figure 6.6. Different steps of lithography.

To produce the mask, the pattern needs to be engraved on a glass plate that is already covered with a layer of chrome. The mask needs to transfer to flex copper. Etching stage allows the erasing of the copper from the upper layer of the flex. The sample has been wetting in a solution form of iron perchloride and the water which is heated to about 27 °C. The samples washed with water then heated up them up to 70c to protect them to be oxide.

To avoid oxidising the inductors the samples were varnished. The three different coils have been created and presented as shown in Figure 6.7.

6.9 Circuit design and test setup

Fully planar WPT of circular, square and Hexagon are made on FR4 circuit boards. This is fabricated to determine the accuracy of PTE , PDL and the inductance values. Figure 6.7 a, b and c represents the fabricated circular, square and Hexagon coils. Three different structures including circular, square, hexagon used as input inductor and output inductor are shown In Figure 6.7. The parasitic elements are different in these cases and we are experimentally looking for the minimum parasitic elements (Resistance and Capacitance) and thus maximum energy transfer.



Figure 6.7. (a) Square, (b) Circular, (c) Hexagonal structure for the input and output inductor.

We keep the fixed size for the inductors. We assume one side is the exciter in the fixed location, and another is the portable receiver. We expect when the receiver is closed to the exciter, it means the “I” parameter will be reduced, then, notable electromagnetic energy is transferred to the receiver wirelessly. The measurement setup is shown in Figure 6.8 to verify the fabricated coils. Resonant circuit was built for the square, circular and Hexagon coils. For the measurement a power source was used by a signal generator, in addition to an oscilloscope and an LCR metre was used. By calculating the current and voltage the transmitted and received power can be easily obtained. To test the circuit, we connected the input inductance to a voltage source $V_{in}= 10$

$\sin(2\pi \cdot 10\text{MHz} \cdot t)$, and then measured the output voltage on the receiver. The test setup is shown in Fig. 6.8.

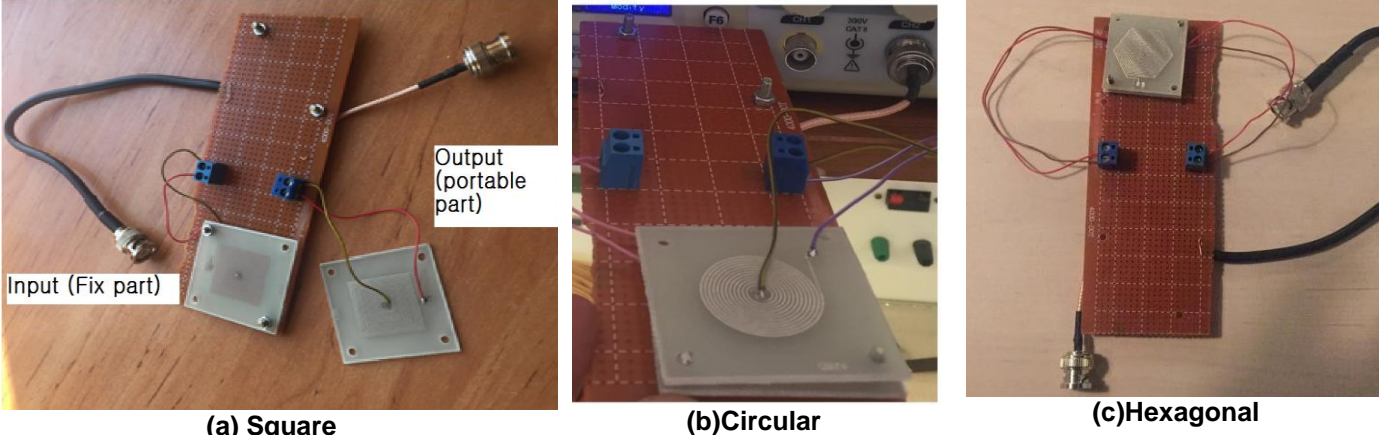


Figure 6.8. Test setup a) Square, (b) Circular, (c) Hexagonal structure for the input and output inductor.

We repeated this setup for circular and hexagonal structure too. So, the exciting (transmitter) coil keeps fixed on the veroboard and the receiver is closed and then gotten away. The schematic of the test circuit and the test table are shown in Figure 6.9 and Figure 6.10 respectively.

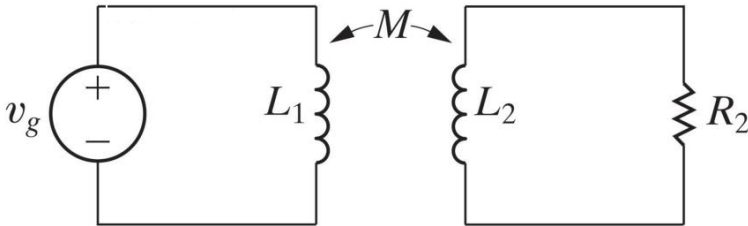


Figure 6.9. Test circuit schematic.

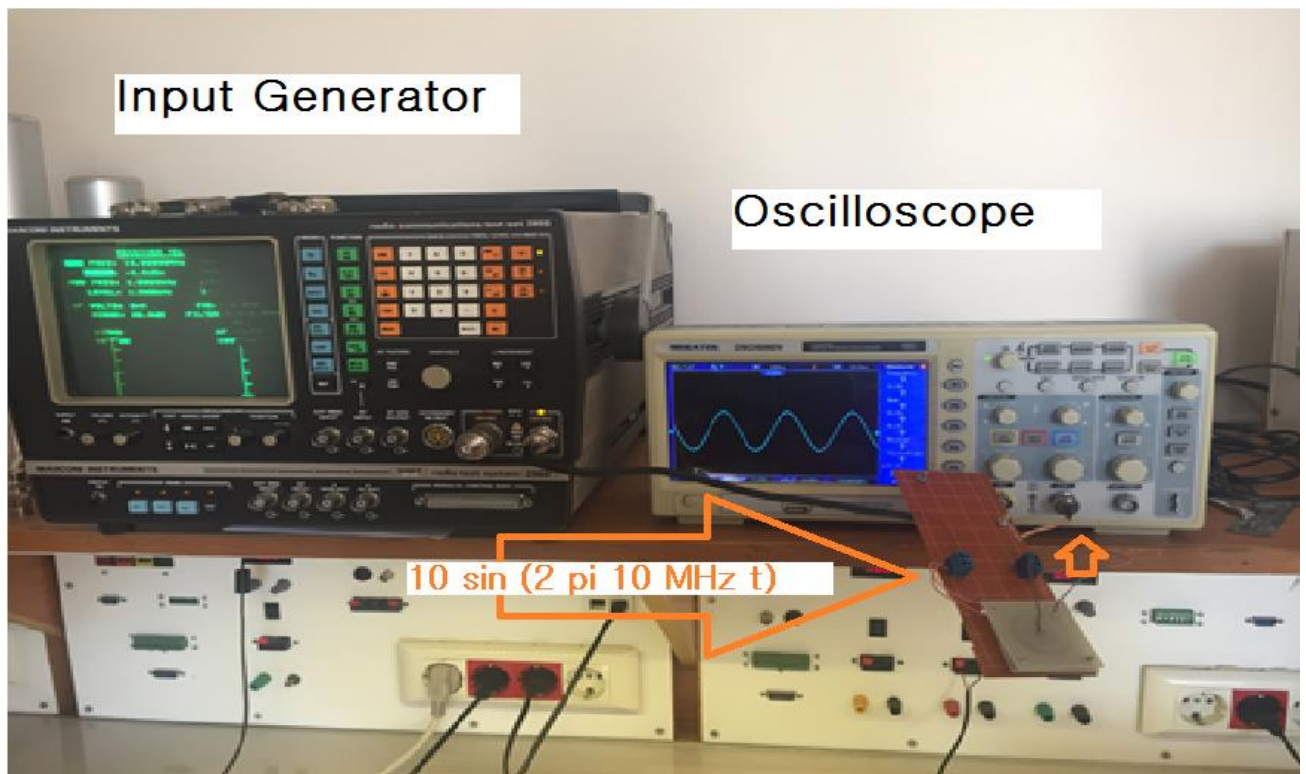


Figure 6.10. Test table including signal generator and oscilloscope to excite and measure the mutual coil.

6.10 Measurement result

Different sets of inductors were fabricated using commercial PCB fabrication methods. The fabricated inductors as explained in the previous section, the input inductor has been excited with a 10 V / 10 MHz RF signal. We follow the receiver voltage by oscilloscope to find out which structure can better transmit the energy. The measurement results are shown in Table 6.2. **the squared coil configuration has provided the highest level of output compared to the hexagonal and circular designs, this is due to the size of the wire cable and the shape for each coil.** Also ,it is desirable to achieve the highest possible inductance and quality factor for the targeted 10 MHz application considering the level of specific absorption rate (SAR) in the human body. The following design parameters are typically associated with the

board level inductor design: the number of the metal layers, the spacing between the metal traces, the width of the metal trace, and the number of turns n.

Table 6.2. measurement results (f=10 MHz).

Structure	Input signal	Distance	Output signal
Square	$10 \sin(2\pi ft)$	L=0.5 mm	$6.4 \sin(2\pi ft)$
Hexagonal	$10 \sin(2\pi ft)$	L=0.5 mm	$6.2 \sin(2\pi ft)$
Circular	$10 \sin(2\pi ft)$	L=0.5 mm	$5.4 \sin(2\pi ft)$

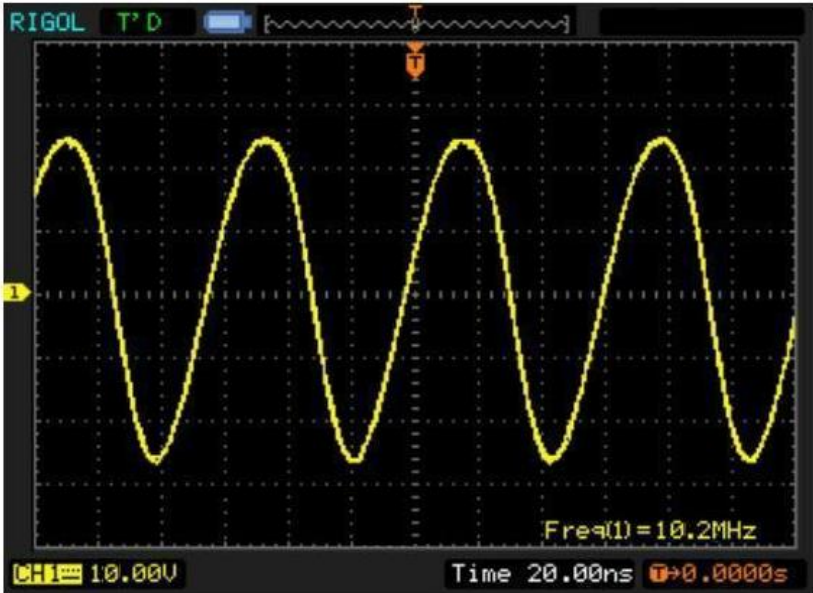


Figure 6.11. Voltage waveform on the inductor.

Figure 6.12 represents the measured PTE values against the spacing distance between the coil in circular, square and hexagon coils. The spacing distance between the coils changes the effective inductance value as shown in Figure 6.12. It is clear that the value of the Power transfer efficiency (PTE) is decreasing when the spacing distance increases. The results were achieved from measurements of actual displacement. It can be seen that the squared coil configuration has come up with the

highest level of Power transfer efficiency (PTE) compared to the hexagonal and circular designs. Furthermore, it can be seen that the lower Power transfer efficiency (PTE) generated by the larger the spacing and this applies to all design configurations.

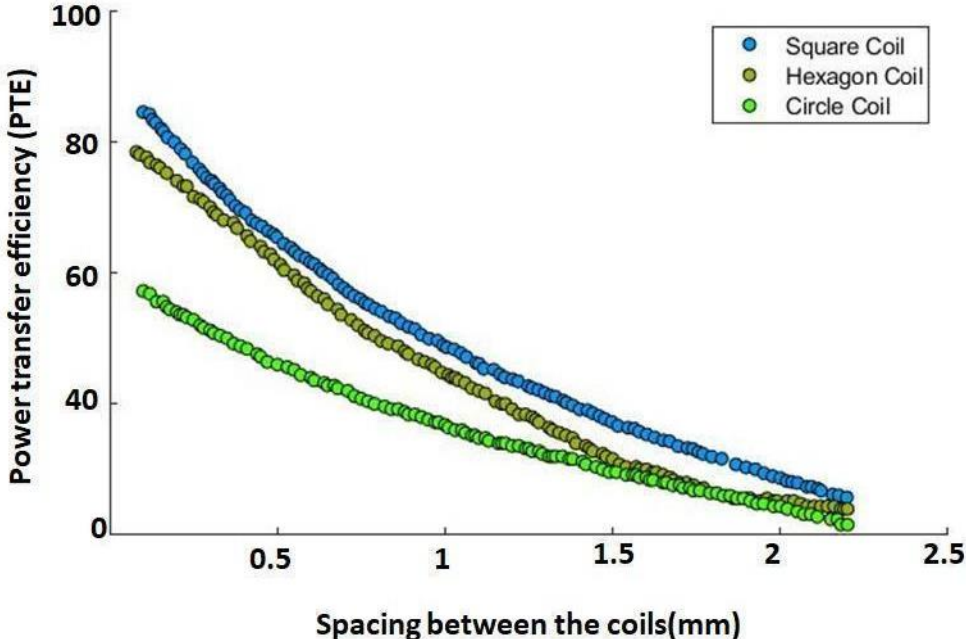


Figure 6.12. Experimental PTE values against the spacing distance.

The PTE values in figure 6.13 are maximised at approximately 10-16 MHz in circular, square and hexagon coils. It can be seen that the squared coil configuration has provided the highest level of Power transfer efficiency (PTE) compared to the hexagonal and circular designs. As the frequency value increases, the generated power transfer efficiency (PTE) obtained from all designs converges and this means the improvement in PTE is very small at higher frequencies.

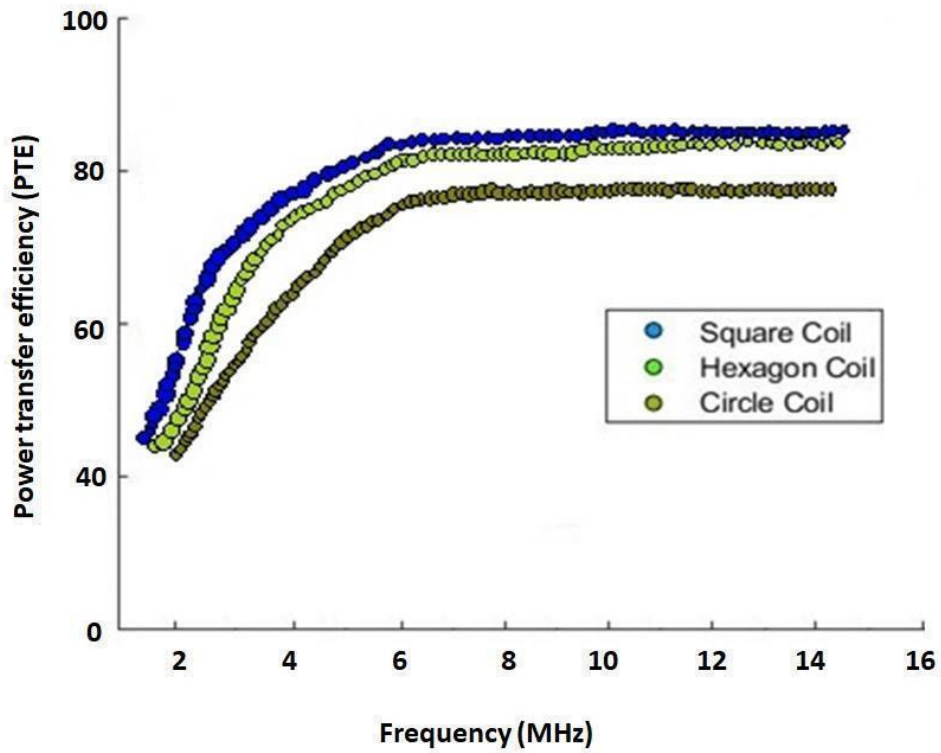


Figure 6.13. PTE values against the Frequency.

Figure 6.14 It can be seen that the load receive power of the three coils increase first and then decrease as the distance between the receiving and transmitting coils becomes bigger, the load receive power reaches its peak when the distance between coupling coils reach a certain value, this means that at larger spacing values, the PDL becomes less dependent on the coil configuration.

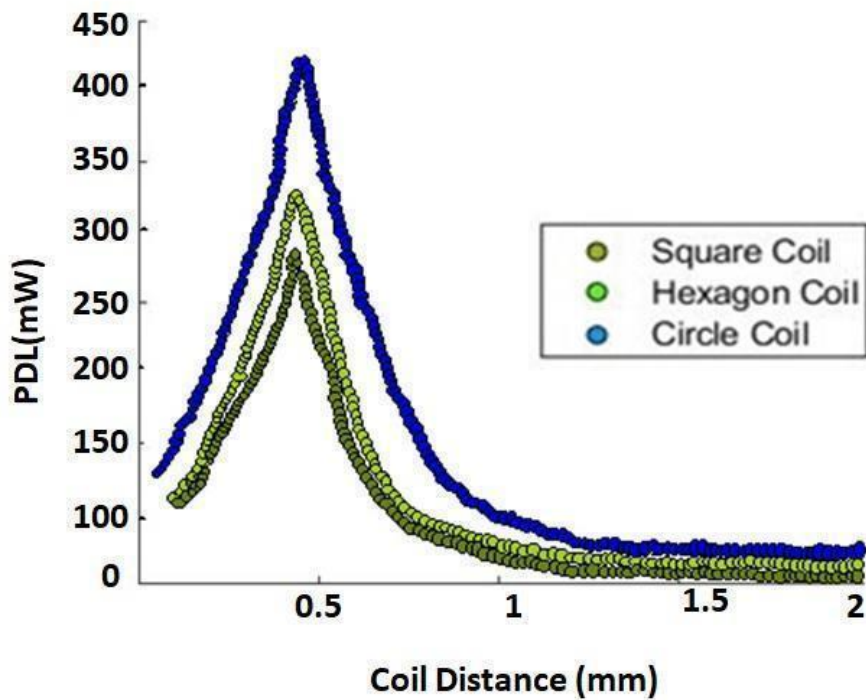


Figure 6.14. PDL values against the spacing distance.

The obtained results in Figure 6.15 shows the variation of the series inductance as a against the frequency for all the different realised integrated coils, it can be seen that the highest inductance recorded for the square coils was 2700 μ H with a lowest value of 1100 μ H. On the other hand, the hexagonal coil design provided a lower maximum flux value when compared to the square coil design. The maximum value for the hexagonal design was around 1900 μ H at 10MHz. The flux values were lowest for the circular design with a maximum of 1200 μ H. The largest inductance value for the square coil, followed by the hexagon and circle coil. Lowest measurement range is for a circle coil which is approximately 600 μ H and the largest measurement range is for square and hexagon coils and is approximately equal to 2700 mm and 1900 μ H respectively.

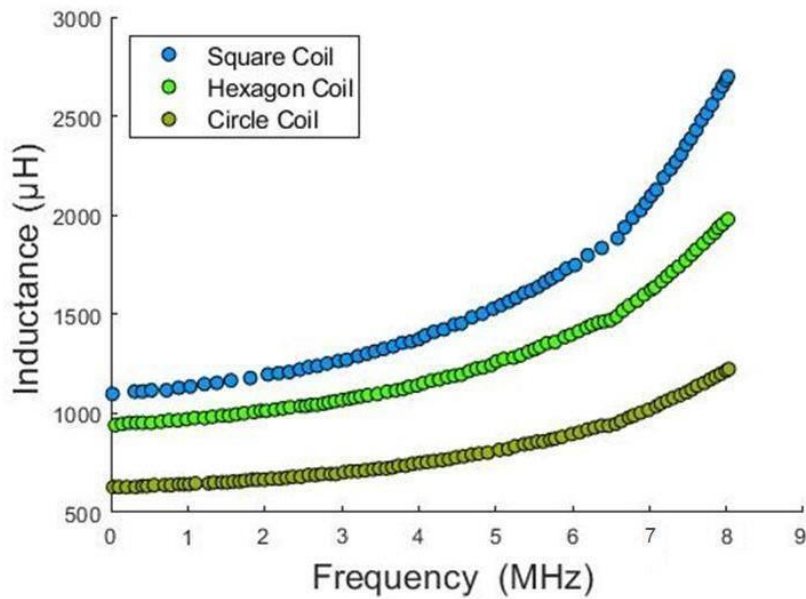


Figure 6.15. Frequency values against the inductance.

Overall, the square coil design provided the highest inductance and power transfer efficiency followed by the hexagonal and then the circular geometry. This was also the case while changing the spacing distance between the coils, moreover it can be seen that for any given spacing value, the squared coil configuration has provided the highest level of inductance compared to the hexagonal and circular designs. Furthermore, it can be seen that the larger the spacing the lower the generated power transfer efficiency (PTE) and this applies to all design configurations. As the spacing value increases, the generated power transfer efficiency (PTE) obtained from all designs converges.

6.11 Conclusions

Wireless charging technology becomes widespread especially for consumer electronics, mobile, and portable devices. The work that presented in this chapter is related to the wireless charging techniques, containing planar type inductors. The geometric and electrical dimensioning of these inductors is an important step that requires taking into account many electrical and geometrical parameters. The conductive spirals of all three coils were made on a PCB of a low cost which makes it applicable to a large number of applications. Three shapes of coils were designed and experimented to calculate the inductance and the power transfer efficiency (PTW) over various spacing distances and frequency. The obtained results showed that the inductance decreases with the frequency and this was found to apply to all inductors. The maximum value of inductance was obtained from the square topology whereas the minimum value was measured in the circle topology. This is due to the geometrical specifications of each topology. It has been observed that the power transfer efficiency (PTE) decreases with increasing the coils spacing distance and the frequency. Comparing the performance of the three shapes, the square coil geometry has shown the best performance. Generally, the experimental measurements concluded that the square mutual inductor in comparison with the circular and hexagonal can transfer the energy better. As the square structure covers a larger area rather than other structures. However, other structures are also useful depending on the PCB shape.

6.12 Summary

The novelty of this chapter was the application of a newly developed model to constrain the uncertain parameters while simulating others to keep the original shape. Fully planar WPT of circular, square and Hexagon are made on FR4 circuit boards and experimented. The significance of these designs is to achieve maximum PTE values with high PDL. This is fabricated to determine the accuracy of power transfer efficiency PTE, PDL and the inductance values over various spacing distances and frequency. It is desirable to achieve the highest possible inductance and quality factor for the targeted 10 MHz application considering the level of specific absorption rate (SAR) in the human body. This chapter was presenting a study of the three shapes of coils were designed, and experimented to calculate the inductance and the power transfer efficiency (PTW) over various spacing distances and frequency. The obtained results showed that the inductance decreases with the frequency and this was found to apply to all inductors. The maximum value of inductance was obtained from the square topology.

CHAPTER 7

DISCUSSION, CONCLUSIONS AND FUTURE WORK

This chapter summarises the contributions and conclusions of this project. In addition to suggestions for further research.

7.1 Discussion

This project discussed the performance, modelling and application of a planar electromagnetic coil. The main four common topics that have been shared amongst all design studies are the involvement of composite materials, the multi-core of planar coil, the application of uncertainty models to simulate the uncertain parameters in the structure and three shapes of coils designed to calculate the maximum power transfer efficiency (PTW) over various spacing distances and frequency and inductance. Due to the small size profiles and their non-contact nature, planar coils are widely used due to their simple and basic design. The uncertain parameters have been identified and simulated using ANSYS that has been run utilising a newly developed MATLAB code. This code has made it possible to run thousands of trials without the need to manually input the various parameters for each run. This has facilitated the process of obtaining all the probable solutions within the defined range of properties. The optimum and robust design properties were then determined. The thesis discusses the experimentation and the finite element modelling (FEM) performed for developing the design of planar coils and used in wireless chargers. In addition, the thesis investigated the performance of various topologies of planar sensors when they are used in wireless chargers. The ANSYS Maxwell FEM package has been used to analyse the models while varying the topologies of the coils. For this purpose, different models in

FEM were constructed and then tested with topologies such as circular, square and hexagon coil configurations. The described methodology is considered an effective way for obtaining maximum PTE with a certain distance on planar coils with better performance. The explored designs are, namely: (1) Optimization of Planar Coil Using Multi-core (chapter 3), (2) planar coil with an Orthogonal Flux Guide(chapter 4), (3) Using the Variable geometry in a Planar Inductor for an Optimised Performance by using the robust design method(chapter 5), (4) Design and Integration of Planar Inductances on wireless charger(chapter 6). In chapter 3 which was the first case study, the aim was to present the behaviour of a newly developed planar coil, built from a Mu-metal, via simulation. The structure consists of an excitation coil, sensing coils and three ferromagnetic cores located on the top, middle and bottom sections of the coil in order to concentrate the field using the iterative optimisation technique. Magnetic materials have characteristics which allows them to influence the magnetic field in its environment. Chapter 4 which presents the optimal geometry and material selection for the planar with an Orthogonal Flux Guide. The study demonstrates the optimising of the materials and geometry of the coil that provides savings in terms of material usage as well as the employed electric current to produce an equivalent magnetic field. Chapter 5 which presents the variable geometry in a planar inductor to obtain the optimised performance. The study has provided the optimum and robust design parameters in terms of different topologies such as circular, square and hexagon coil configurations then been tested and choose the best topology based on performance. The originality of the work is evident through the randomisation of the parameters using the developed MATLAB code and the optimisation of the joint performance under defined conditions. Chapter 6 which presents the development of the planar coil applications. Three shapes of coils are designed and experimented in

order to calculate the inductance and the maximum power transfer efficiency (PTW) over various spacing distances and frequencies.

7.2 Conclusions

In conclusion, this Research shows the investigation and the performance of various topologies of planar sensors when they are used in wireless chargers. For this purpose, different models in the FEM and ANSYS Maxwell FEM package have been used to analyse the models while varying the topologies of the coils were constructed and then tested with topologies such as circular, square and hexagon coil configurations. The described methodology is an effective way for obtaining maximum PTE with a certain distance on planar coils. The proposed multi-core optimisation of Planar Coil studied the schematic of the micro planar structure realised for the triple cores planar. To concentrate the field using the iterative optimisation technique, better performances can be obtained by using magnetic top and bottom shields. In addition to that magnetic field will be easily passed through the material (i.e., the upper and lower cores), it will wrap around the coils instead of going further away from the coil and this will retain the magnetic field to stay altogether within the top and bottom cores. Furthermore, the benefit of having the top and bottom cores is that the magnetic flux can not pollute the environment. Lastly, the main advantage of the multiple cores is that the coils will intensify the field within the sensor which means that less current is consumed in order to obtain the desired results (chapter 3). The multi core planar coil has a novel planar, which has an ability to concentrate and guide the field in a highly efficient manner by employing orthogonally cylindrical ferromagnetic tube and set of ferromagnetic cubes in order to deflect and emit the field in the desired path (chapter 4). The planar coil was improved by determining the Optimal Geometry in Planar inductor Using Robust Design Method. A novel of using the Meta-model-based design

optimisation to develop the electromagnetic sensors by analysing the behaviour of different planar coils topologies: circular, square and hexagon coils for the application such as wireless charger, tracking and location identification, etc. for the smart cities by using Meta-model-based design optimisation (chapter 5). Finally the newly developed model was utilised in the application of the smart city such as wireless charging systems, to constrain the uncertain parameters while simulating others to keep the original shape. Fully planar WPT of circular, square and Hexagon were made on FR4 circuit boards and experimented. The significance of these designs is to achieve maximum PTE values with high PDL. This fabricated to determine the accuracy of power transfer efficiency PTE, PDL and the inductance values over various spacing distances and frequency. It is desirable to achieve the highest possible inductance and quality factor for the targeted 10 MHz application considering the level of specific absorption rate (SAR) in the human body (chapter 6).

7.3 Further work

The novel MATLAB code can further be developed in the future to link with other software tools as well as with industrial equipment to analyse live data from machines. Such industrial data created by industrial equipment might hold more potential values to reduce costs in maintenance and to increase the quality of products. The work can be extended to include more design aspects such as the uncertainty in environmental

conditions on the behaviour of structures. In addition to including other engineering applications in the smart city. The four employed designed and techniques can be compared against existing techniques of uncertainty quantification using chosen case studies which was beyond the scope of the current project. Finally the utilised techniques and newly developed planar coil in the current work can open a new era of research between the various departments and engineering applications both in academia and industry.

References

- [1] Ripka P, "Magnetic Sensors and magnetometers", Artech House Boston, London 2001. 376-379.
- [2] Vop'alensky M, Ripka P, Platil A, "Precise magnetic sensors", Sensors and Actuators 2003. (106):pp. 38 -42.
- [3] Ripka P., "New direction in fluxgate sensors", Journal of Magnetism and Magnetic Materials 2000.pp. 215-216.
- [4] David C, Marina D M, Lucas P, Claudio A. Small fluxgate magnetometers: Development and future trends in Spain. Sensors 2010.(10):pp.1859–1870.
- [5] Cambel V, Karapetrov G, Novosad V, Bartolome E., Gregusova D., Fedor J., Kudela R, Šoltys J, "Novel Hall sensors developed for magnetic field imaging systems," Journal of Magnetism and Magnetic Materials 2007. (316): pp. 232- 235.
- [6] Kejik P, Reymond S, Popovic R. S., "Circular Hall transducer for angular position sensing," Transducers '07 & Eurosensors XXI conference, Lyon, France, Digest of technical papers 2007.(2):pp. 2593-2596.
- [7] Ilg M, Chang B. C, Hepner D, Thompson A, "A microcontroller solution for AMR magnetic sensing in flying munitions systems," IEEE International Conference on Mechatronics 2005.pp. 84-89.
- [8] Baibich M. N, Broto J. M, Fert A, Nguyen Van Dau F, Petroff F, Eitenne P, Creuzet G, Friederich A, Chazelas J, "Giant Magnetoresistance of (001)Fe/(001)Cr Magnetic Superlattices," Physical Review Letters 1988 (61): pp. 2472-247.
- [9] Panina L. V, Mohri K., Bushida K., Noda M., "Giant magneto-impedance and magneto-inductive effects in amorphous alloys," J. App. Phys 1994.(76): pp. 6198-6203.
- [10] Koch H., "Mature SQUID-systems and their application", IEEE Trans. Appl. Supercond 1997. 7 (2):pp.3738–3743.
- [11] Seitz T, "Fluxgate sensor in planar microtechnology," Sensors and Actuators A 1989. (22):pp.799-802.
- [12] Ripka P, Primdahl F, Nielsen O.V, Petersen J R, Ranta A "A.C. magnetic-field measurement using the fluxgate", Sensors and Actuators 1995.pp. 307-311.
- [13] Vopàlensky M, Ripka P, Platil A, "Precise magnetic sensors", Sensors and Actuators 2003.pp. 38 – 42.

- [14] Hall E H, "On a new action of the magnet on electric current," American Journal of Mathematics.1879.pp. 287-292.
- [15] Castagnetti R, "Integrated Magnetotransistors in Bipolar and CMOS technology", Ph.D. thesis of the Physical Electronics Laboratory ETH, Zurich.1994.
- [16] Gopel W, Hesse J, Zemel J N, "SENSORS: A Comprehensive Survey", Magnetic Sensors" 1989.
- [17] Mohri K, Uchiyama T, Panina LV, "Recent advances of micromagnetic sensors and sensing application", Sensors and Actuators 1997. (1).
- [18] O'Handley R C, "Modern Magnetic Materials, Principles and Applications,", John Wiley and Sons 2000.
- [19] Cheng D K, "Fundamentals of Engineering Electromagnetics,", Addison Wesley Publishing Co. 1993.
- [20] Tumanski S. Handbook of Magnetic Measurements. CRC Press; 2011.pp:66-87.
- [21] Garret M W, "Axially symmetric systems for generating and measuring magnetic fields", J. Appl. Phys. 1951.(22):pp.1091–1107.
- [22] Franzen W,"Generation of uniform magnetic fields by means of air-core coils", Rev. Sci. Instrum. 1962.(33):pp. 933–938.
- [23] Freiser M J, "A survey of magneto optic effects", IEEE Trans. Magn. 1968.(4):pp.152–161.
- [24] [24] Bott M H P, "The Interior of the Earth", Elsevier Science 1971.pp125-126.
- [25] Farthing W H, Foltz W C, "Rubidium vapor magnetometer for near earth orbiting spacecraft", Rev. Sci. Instrum 1967.(38):pp.1023–1030.
- [26] Evans M E , Heller F , "Environmental Magnetism", Academic Press 2003.pp.26 28.
- [27] Kadzilko-Hofmohl M, "Earth's magnetism, in Encyclopedia for Modern Physics" 1983.pp.128-129.
- [28] Elsasser W M, "Hydromagnetic dynamo theory", Rev. Modern Phys. 1956.(28):pp.135–163.
- [29] Caruso M J, "Application of magnetic sensors for low cost compass systems", Honeywell Application Note 1996.

- [30] Frandsen A M A , Holzer R E , Smith E J, "OGO searchcoil magnetometer experiment", IEEE Trans. 1969.(7):pp. 61–74.
- [31] Slocum R E , Reilly F N, "Low field helium magnetometer for space applications", IEEE Trans. 1963.(10):pp.165–171.
- [32] Ness N F, Behannon K W, Lepping R P, Schatten K H, "Use of two magnetometers for magnetic measurements on the spacecraft", J. Geophys. Res. 1971. (76):pp.3564–3573.
- [33] Smith E J, Connor B V, Foster G T, " Measuring of the magnetic field of Jupiter and the outer solar system", IEEE Trans. Magn. 1975.(11):pp. 962–980.
- [34] Smith E J, Sonett C P, "Extraterrestrial magnetic fields: Achievements and opportunities", IEEE Trans. 1976.(14):pp. 154–171.
- [35] Staton D J ,Ma Y P , Sepulveda N G, Wikswo J P , "High resolution magnetic mapping using a squid magnetometer array", IEEE Trans. Magn. 1991.(27):pp.3237–3240.
- [36] Smekalova T N, Voss O, Smekalov S L,"Magnetic Surveying in Archeology" 2008.pp.128-129.
- [37] Sabaka J, Olsen N, Langel L A, "Acomprehensive model of the near-Earth magnetic field", Nasa Report 2000.
- [38] Campbell W H, "Introduction to Geomagnetic Fields", Cambridge University Press 2003.
- [39] Butler R F , "Paleomagnetism: Magnetic Domains to Geologic Terranes", University of Arizona, Tucson, AZ, Electronic Edition. 1998.
- [40] Breiner S, "Applications Manual for Portable Magnetometers", Geometrics Application Note. 1999.
- [41] FromWeymouth J W , Geological surveying of archeological sites, in Archeological Geology, G. Rapp (Ed.), Yale University Press, New Haven and London, 1985.
- [42] Dodd C V, Computer modeling for eddy current testing, in Research Techniques in Nondestructive Testing, Academic Press, New York. 1977.
- [43] De Sa A, "A spinner magnetometer", J. Sci. Instrum. 1963.(40):pp.162–165.
- [44]Chiron G, Laj C, Pocachard J, "A high sensitivity portable spinner magnetometer", J. Phys. E 1981. (14):pp. 977–980.

- [45] Foster J H, "A paleomagnetic spinner magnetometer using a fluxgate gradiometer", *Earth Planet. Sci. Lett.* 1966. (1):pp.463–466.
- [46] Caruso M J, "Applications of magnetoresistive sensors in navigation systems", Honeywell Application Note, 1995.
- [47] Hummervoll R, Totland O, "An automatic spinner magnetometer for rock specimens", *J. Phys. E* 1980.(13):pp. 931–935.
- [48] Wellhausen H, "Elektronischer Kompass, *Elektronik*" 1989. (8):pp. 85–89.
- [49] Amundson M, *The role of compassing in telematics, Analysis USA Focus*, 2003.
- [50] Caruso M J, Withanawasam L S, "Vehicle detection and compass applications using AMR magnetic sensors", Honeywell Application Note, 1999.
- [51] ICNIRP, *Guidelines for Limiting Exposure to Time Varying Electric, Magnetic and Electromagnetic Fields*, 1999.
- [52] Mathai A, Song D, Gim Y, Wellstood F C, "Onedimensional magnetic flux microscope based on the DC superconducting quantum interference device", *Appl. Phys. Lett.* , 1992.(61):pp.598–600.
- [53] Kwiatkowski W, Tumanski S, "Application of the thin film permalloy magnetoresistive sensors in electrical measurements", *IEEE Trans. Magn.* 1984.(20):pp. 966–968.
- [54] Wolff J, Heuer T, Gao H., Weinmann M, Voit S, Hartmann U, *Parking monitor system based on magnetic field sensors, IEEE Intelligent Transportation Systems Conference, Toronto 2006*.pp. 1275–1279.
- [55] Uchiyama T, Mohri K, Itho H, Nakashima K, Ohuchi J, Sudo Y, "Car traffic monitoring system using MI sensor built-in disk set on the road", *IEEE Trans. Magn.* 2000.(36):pp. 3670–3672.
- [56] Kirtley J R , "SQUID microscopy for fundamental studies", *Phys. C* 2002. (368):pp.55–65.
- [57] Kirtley J R , Wikswo J P , "Scanning SQUID microscopy", *Ann. Rev. Mater. Sci.* 1999.(29):pp.117–148.
- [58] Howells G D et al., "Scanning Hall probe microscopy of ferromagnetic structures", *J. Magn. Magn. Mater.* 1999.(196):pp.917–919.
- [59] Koch H, "SQUID Magnetocardiography: Status and perspectives", *IEEE Trans.* 2001.(11):pp.49–59.

- [60] Kuperman V, "Magnetic Resonance Imaging", Academic Press, San Diego, 2000.
- [61] Yamamoto S Y , Vier D C , Schultz S , "High resolution contact recording and diagnostics with a raster-scanned MR head", IEEE Trans. Magn. 1996.(32):pp. 3410–3412.
- [62] Yamamoto S Y, Schultz S, "Scanning magnetoresistance microscopy: Imaging with a MR head", J. Appl. Phys. 1997.(81):pp. 4696–4698.
- [63] Guy C, Ffytche D, "An Introduction to the Principles of Medical Imaging", Imperial College Press, 2005.
- [21] Hoshino K, Sano M, Narumi S, Fuyama M, "Magnetic properties and thermal stability of electroplated NiFeCr and NiFeMo films with high resistivity," IEEE Transactions on Magnetics 1999. (35):pp. 3433 – 3435.
- [22] James E. Lenz, "A Review of Magnetic Sensors", Proceeding of the IEEE 1990. (6): pp. 973-989.
- [23] Liu X, Evans P, Zangari G, "Electrodeposited Co-Fe and Co-Fe-Ni alloy films for magnetic recording write heads" IEEE Transactions on Magnetics 2000. (5): pp. 3479-3481.
- [24] Föhse M, Kohlmeier T, Gatzel H , "Thin-film technologies to fabricate a linear microactuator," Sensors and Actuators A: Physical 2001. pp. 145-149.
- [25] Popovic R S, Flanagan J A, Besse P A, "The future of magnetic sensors", Sensors and Actuators 1996. (56):pp. 39-55.
- [26] Flynn D, Toon A, Allen L, Dhariwal R, Desmulliez M P Y, "Characterization of core materials for microscale magnetic components operating in the megahertz frequency range," IEEE Transactions on Magnetics 2007. (7):pp. 3171-3180.
- [27] Mahdia A E, Panina L, Mapps D, "Some new horizons in magnetic sensing: high-T_c SQUIDs, GMR and GMI materials", Sensors and Actuators 2003.(105):pp. 271–285.
- [28] Ripka P, Vopalensky M, Platil A, Doscherd M, Lenssene K.-M.H., Hauser H, "AMR magnetometer", Journal of Magnetism and Magnetic Materials 2003.pp. 254–255.
- [29] Panina L V, Mohri K, "Magneto-impedance effect in amorphous wire", Appl. Phys. 1994. (1189).
- [30] Velazquez J, Vazquez M, Chen D X., Hernando A, "Giant magnetoimpedance in non-magnetostrictive amorphous wires", Phys. Rev 1994.(16737).

- [31] Ripka P, Primdahl F, Nielsen O V, Petersen J R, Ranta A "A.C. magnetic-field measurement using the fluxgate", Sensors and Actuators 1995.pp. 307-311.
- [32] Ripka P, Butta M, Malatek M, Atalay S, Atalay F E, "Characterization of magnetic wires for fluxgate cores," Transducers '07 & Eurosensors XXI conference, Lyon, France, Digest of technical papers 2008. (2):pp.2369-2372.
- [33] Ripka P, Kubik J, Duffy M, Hurley W G and O'Reilly S, "Current Sensor in PCB Technology", IEEE Sensors Journal 2005.
- [34] Vinal A W, "Considerations for applying solid state sensors to high density magnetic disc recording", IEEE Tans. Magn. 1984.(681)
- [35] Mohri K, "Review of recent advances in the field of amorphous metal sensors and transducers," IEEE Transactions on Magnetics 1984.(20):pp.397-401.
- [36] Ripka P, Kaspar P, "Portable fluxgate magnetometer", Sensors and Actuators 1998.(68):pp. 286-289.
- [37] Engelter A, "A fluxgate magnetometer with a metallic glass core," IEEE Transactions on Magnetics 1986. (22):pp. 299-300.
- [38] Garcia D, Mufioz J L, Kurlyandskaya G, Vazquez M, Ali M and Gibbs M R J "Magnetic Domains and Transverse Induced Anisotropy in Magnetically Soft CoFeB Amorphous Thin Films" IEEE Trans. Magn 1998. (4):pp.1153-1155.
- [39] Gersherson M, "High temperature superconductive flux gate magnetometer" IEEE Transactions on Magnetics.1991.(27): pp. 3055-3057.
- [40] Ando B, Baglio S, Bulsara R, Sacco V, "Residence times difference fluxgate magnetometers," IEEE Sensors Journal 2005.(5):pp. 895-904.
- [41] Krongelb S, Romankiw L T, Tornello J A, "Electrochemical process for advanced package fabrication," IBM Journal of Research and Development: Electrochemical Microfabrication 1998.(42):pp. 575-586.
- [42] Seitz T, "Fluxgate sensor in planar microtechnology," Sensors and Actuators A: Physical 1989.(22):pp.799-802.
- [43] Grüger H, Gottfried R, "Performance and applications of a two axes fluxgate magnetic field sensor fabricated by a CMOS process", Sensors and Actuators 2001.pp. 61-64.
- [44] Hwan S, Park J H, Sung Y K, "Theoretical analysis on the automotive electronic compass sensor", TENCON '95 IEEE Region 10 International Conference on Microelectronics 1995.pp. 379 - 382

- [45] Gordon D I, "Recent Advances in Fluxgate Magnetometry", IEEE Trans. Magn. 1972.(1).
- [46] Drljaca P M, Vincent F, Kejik P, Popovic R S, "Advanced process of the magnetic core integration for the micro fluxgate magnetometer," Sensors and Actuators A: Physical 2006.(129):pp.58-61.
- [47] Baschiroto A, Dallago E, Malcovati P, Marchesi M, Venchi G "Fluxgate magnetic sensor in PCB technology", Proceeding of Instrumentation and Measurement Technology Conference 2004(2):pp. 808-812.
- [48] Baibich M N, Broto J M, Fert A, Nguyen F, Petroff F, Eitenne P, Creuzet G, Friederich A, Chazelas J, "Giant Magnetoresistance of (001)Fe/(001)Cr Magnetic Superlattices," Physical Review Letters 1988.(61):pp. 2472-2475.
- [49] Mohri K, Kohsawa T, Kawashima K, Yoshida H, Panina L V, "Magnetoinductive effect (MI effect) in amorphous wires," IEEE Trans. on Magnetics 1992.(28):pp. 3150-3152.
- [50] Ripka P, Platil A, Kaspar P, Tipek A, Malatek M, Kraus L, "Permalloy GMI Sensor," Journal of Magnetism and Magnetic Materials 2003.pp. 633-635.
- [51]Choi S O, Kawahito S, Matsumoto Y, Ishida M, Tadokoro Y, "An integrated micro fluxgate magnetic sensor," Sensors and Actuators 1996. (55):pp.121-126.
- [52] Kawahito S, Sasaki Y, Sato H, Nakamura T, Tadokoro Y, "A fluxgate magnetic sensor with micro-solenoids and electroplated permalloy cores," Sensors and Actuators 1994.(43):pp. 128-134.
- [53] Baschiroto, A, Dallago E, Malcovati P, Marchesi M, Venchi G, "Design and characterization of a family of Fluxgate magnetic sensors in PCB technology", presented paper at the conference AISEM 2004.
- [54] Gise P, Yarbrough R, "An electrodeposited cylindrical magnetometer sensor," IEEE Transactions on Magnetics 1975.(11):pp. 1403-1405.
- [55] Gise P, Yarbrough R, "An improved cylindrical magnetometer sensor," IEEE Transactions on Magnetics 1977. (13):pp. 1104-1106.
- [56] Chiesi L, Flanagan J A, Janossy B, Popovic R S, "Integrated planar fluxgate sensor with an amorphous core," Eurosensors XI proceedings 1997.(3):pp.1607-1610.
- [57] Kejik P, Chiesi L, Janossy B, Popovic R S, "A new compact 2D planar fluxgate sensor with amorphous metal core," Sensors and Actuators 2000.(81):pp.180-183.

- [58] Ripka P, Li X P, Fan J, "Orthogonal fluxgate effect in electroplated wires," IEEE Sensors Conference, Irvine CA, USA, Technical Digest 2005, pp. 69-72.
- [59] Ripka P, Butta M, Malatek M, Atalay S, Atalay F E, "Characterization of magnetic wires for fluxgate cores," Transducers '07 & Eurosensors XXI conference 2007.(2):pp. 2369-2372.
- [60] Beach R S, Smith N, Platt C L, "Magneto-impedance effect in NiFe plated wire," Appl. Phys 1996, pp. 2753-2755.
- [61] Drljaca P M, Kejik P, Vincent F, Popovic R S, "Low noise CMOS microfluxgate magnetometer," Transducers'03 conference. 2003.(1):pp. 304-307.
- [62] Tipek A, Ripka P, O'Donnell T, Kubik J, "PCB technology used in Fluxgate sensor construction", Sensors and Actuators 2004.(115):pp. 286-292.
- [63] Kaluza F, Grulger A, Grulger H, "New and future applications of fluxgate sensors", Sensors and Actuators 2003.(106): pp.48-51.
- [64] Ripka P, Kawahito S, Choi S O, Tipek A, Ishida M, "Micro-fluxgate sensor with closed core," Sensors and Actuators 2001.(91):pp. 65-69.
- [65] Ripka P "Race-track fluxgate with adjustable feedthrough", Sensors and Actuators 2000.(85):pp. 227-231.
- [66] Garcia D, Mufioz J L, Kurlyandskaya G, Vazquez M, Ali M and Gibbs M R J "Induced anisotropy, magnetic domain structure and magnetoimpedance effect in CoFeB amorphous thin films", J. Magn 1999.(191):pp.399-401.
- [67] Ripka P, Butta M, Malatek M, Atalay S, Atalay F E, "Characterization of magnetic wires for fluxgate cores," Transducers '07 & Eurosensors XXI conference, Lyon, France, Digest of technical papers 2007.(2):pp. 2369-2372.
- [68] Marshall S V, "An Analytic Model for the Fluxgate Magnetometer", IEEE Trans. Magn. 1967.(3):pp.134-138.
- [69] Primdahl F, "The Fluxgate Mechanism, Part I: The Gating Curves of Parallel and Orthogonal Fluxgates", IEEE Trans. Magn. 1970.(2):387-389.
- [70] Burgher G R, "The Theoretical Output of a Ring Core Fluxgate Sensor", IEEE Trans. Magn. 1972. (4):pp.456-458.
- [71] P. M. Drljaca, "Integrated Fluxgate Compass for Portable Applications, Hartung-Gorre. 2004, pp.322-324.
- [72] Ripka P, "Advances in fluxgate sensors," Sensors and Actuators A: Physically 2003.(106):pp. 8-14.

- [73] Choi S O, Kawahito S, Matsumoto Y, Ispida M, Tadokoro Y “An integrated micro fluxgate magnetic sensor”, Sensors and Actuators 1996.(55):pp.121-126.
- [74] Chiesi L, Kejik P, Janossy B, Popovic R S “CMOS planar 2D micro-fluxgate sensor”, Sensors and Actuators 2000.(82):pp. 174-180.
- [75] P M Drljača, P. Kejik, F. Vincent and R.S. Popovic “Low noise CMOS micro-fluxgate magnetometer”, The 12th International Conference on Solid State Sensors, Actuators and Microsystems, Boston 2003.
- [76] Drljača P M, Ripka P, Vincent F, Piguet D, Gueissaz F, Popovic R S “Single core fully integrated CMOS micro-fluxgate magnetometer”, Sensors and Actuators 2004.(110):pp. 236-241.
- [77] Ripka P, Primdahl F “Tuned current-output fluxgate”, Sensors and Actuators 2000.(82):pp.161-166.
- [78] Kaluza F, Grüger A, Grüger H “New and future applications of fluxgate sensors”, Sensors and Actuators 2003.pp. 48-51.
- [79] Primdahl F, “Comments on “The Theoretical Output of a Ring Core Fluxgate Sensor”, IEEE Trans. Magn. 1973.(4):pp.366-369.
- [80] Hirai, T.-W. Kim, A. Kawamura,IEEE Trans. PowerElectron.15, 21 (2000).
- [81] Nicola Tesla, “The transmission of electrical energy without wires”, Electrical World and Engineer, March 1905. <http://www.tfcbooks.com/tesla/1904-03-05.htm>, (acc. Dec. 08).
- [82] Karalis A ,Joannopoulos J D, Soljačić M ,Ann Phys,10.1016/j.aop.2007.04.017 (2007).
- [83] H. J. Visser, and R. J. Vullers, “RF energy harvesting and transport for wireless sensor network applications: Principles and requirements,” in Proceedings of the IEEE, vol. 101, no. 6, pp. 1410-1423, June 2013.
- [84] Guo Y, Zhu CB, Song K, et al. Magnetic resonant wireless power transmission technology based on planar core. J Harbin Inst Tech 2014; 46(5): 23–27.
- [85] ANSYS Maxwell Capabilities; [Accessed 30 April 2016]; Available from: <http://www.ansys.com/en-GB/products/electronics/ansys-maxwell/maxwell-capabilities>
- [86] Marshall S V, “An Analytic Model for the Fluxgate Magnetometer”, IEEE Trans. Magn.1967.(3):287-289.

- [87] Ripka P, "New directions in fluxgate sensors," *Journal of Magnetism and Magnetic Materials* 2000.(215):pp.735-739.
- [88] Dolabdjian C, Saez S, Toledo A R , Robbes D "Signal-to-noise improvement of bio-magnetic signals using a flux-gate probe and real time signal processing". *Rev. Sci. Instrum* 1998.(69):pp. 3678–3680.
- [89] Tseng J Z, Wu C C, Dai C L "Modeling and manufacturing of a micromachined magnetic sensor using the CMOS process without any post-process". *Sensors* 2014. (14):pp. 6722–6733.[90] Ripka P "Advances in fluxgate sensors. *Sens. Actuators Phys.* 2003.(106):pp. 8–14.
- [91] Shimada J, Itoh K, Yamaguchi S, Nishikawa A, Miyazaki F, "Magnetic Navigation System for Thoracoscopic Surgery of the Pig Lung Partial Resection with Transbronchial Marking". *Int. Congr. Ser.* 2005.(1281):pp.752–755.
- [92] Munschy M, Boulanger D, Ulrich P, Bouiflane M. "Magnetic mapping for the detection and characterization of UXO: Use of multi-sensor fluxgate 3-axis magnetometers and methods of interpretation". *J. Appl. Geophys.* 2007.(61):pp.168–183.
- [93] Kawahito S, Maier C, Schneider M, Zimmermann M, Baltés H, "A 2-D CMOS microfluxgate sensor system for digital detection of weak magnetic field," *IEEE J. Solid- State Circuits* 1999.(34): pp. 1843–1851.
- [94] Ripka P, Butta M, Malatek M, Atalay S, Atalay F E, "Characterisation of Magnetic Wires for Fluxgate Cores," *TRANSDUCERS, International Solid-State Sensors, Actuators and Microsystems Conference, Lyon 2007*.pp. 2369 – 2372.
- [95] Kawahito S, Cerman A, Aramaki K, Tadokoro Y, "A weak magnetic field measurement system using micro-fluxgate sensors and delta-sigma interface," *IEEE Trans. Instrum. Meas.*2003.(52): pp. 103–110.
- [96] BAČIĆ Ž, and JOGUN, T. MAJIĆ, I., (2018). *Integrated Sensor Systems for Smart Cities*. Croatia: Hamster.
- [97] Alharbi N, and Soh, B., (2019). *Roles and Challenges of Network Sensors in Smart Cities*. IOP Conference Series: Earth and Environmental Science. 332, 1-9.
- [98] Anjomshoaa A, Duarte, F. Rennings, D. Matarazzo, T, J. deSouza, P. and Ratti, C., (2018). *City Scanner: Building and Scheduling a Mobile Sensing Platform for Smart City Services*. Institute of Electrical and Electronic Engineers (IEEE).
- [99] Kumar S., A. Deshpande, S. S. Ho, J. S. Ku, and S. E. Sarma, "Urban street lighting infrastructure monitoring using a mobile sensor platform," *IEEE Sensors J.*, vol. 16, no. 12, pp. 4981–4994, Jun. 2016.

- [100] Li C M , B Liu, Qin R F, and Yang N, “An urban mobile monitoring system integrating remote sensing and environmental sensors,” in Proc. Int. Conf. Design Manuf. Mechatronics Design (ICDMM), World Sci., 2016, pp. 510–519.
- [101] Maricq M = M, Podsiadlik D H, and Chase R E, “Examination of the size-resolved and transient nature of motor vehicle particle emissions,” Environ. Sci. Technol., vol. 33, no. 10, pp. 1618–1626, 1999.
- [102] Mead et al M I , “The use of electrochemical sensors for monitoring urban air quality in low-cost, high-density networks,” Atmos. Environ., vol. 70, pp. 186–203, May 2013.
- [103] Mednis A, Strazdins G, Liepins M, Gordjusins A, and Selavo L, “RoadMic: Road surface monitoring using vehicular sensor networks with microphones,” in Proc. NDT, Prague, Czech Republic: Springer, 2010, pp. 417–429.
- [104] Mohan P, Padmanabhan V N, and Ramjee R, “Nericell: Rich monitoring of road and traffic conditions using mobile smartphones,” in Proc. 6th ACM Conf. Embedded Netw. Sensor Syst., 2008, pp. 323–336.
- [105] S R, “The evolution of connected vehicle technology: From smart drivers to smart cars to . . . self-driving cars,” J. Inst. Transp. Eng., vol. 83, no. 7, p. 22, 2013.
- [106] Measuring the Temperature of the Sky and Clouds, NASA, Washington, DC, USA, May 2018. [Online]. Available: https://myasadata.larc.nasa.gov/science_projects/measuring-the-temperature-of-the-sky-and-clouds/.
- [107] Pendor M S S, Renge M. A. S., and Inzalkar S., “A survey on state of the art and future developments of measurement applications on smartphones.” Int. J. Sci. Eng. Res., vol. 4, no. 12, pp. 41–47, 2013.
- [108] Phan L N, “Automated rapid thermal imaging systems technology,” Ph.D. dissertation, Dept. Mech. Eng., Massachusetts Inst. Technol., Cambridge, MA, USA, 2012.
- [109] Saponara S and Neri B, “Radar sensor signal acquisition and 3D FFT processing for smart mobility surveillance systems,” in Proc. IEEE Sensors Appl. Symp. (SAS), Catania, Italy, 2016, pp. 1–6.
- [110] Goldfine, N J Magnetometers for improved materials characterization in aerospace applications. Mater. Eval. 1993, 51, 396–405.
- [111] Anjomshoaa A; Duarte F; Rennings D; Matarazzo TJ; deSouza P.; Ratti, C. City Scanner: Building and Scheduling a MobileSensing Platform for Smart City Services. IEEE Internet Things J. 2018, 5, 4567–4579.

[112] Bi Y ; Govindaraju M R; Jiles D C The dependence of magnetic properties on fatigue in A533B nuclear pressure vessel steels. *IEEE Trans. Magn.* 1997, 33, 3928–3930.

[113] Shi Y; Jiles D Fem Analysis of the Influence of Fatigue Crack on Magnetic Properties of Steel. In *Proceedings of the 1998 IEEE International Magnetism Conference (INTERMAG)*, San Francisco, CA, USA, 6–9 January 1998; pp. 51–51.

[114] Bi Y; Jiles D C Dependence of Magnetic Properties on Crack Size in Steels. *IEEE Trans. Magn.* 1998, 34, 2021–2023.

[115] Varsier N ; Plets D ; Corre Y; Vermeeren G.; Joseph W.; Aerts S.; Martens L.; Wiart J. A novel method to assess human population exposure induced by a wireless cellular network. *Bioelectromagnetics* 2015, 36, 451–463.

[116] Jow U ; Ghovanloo M Design and Optimization of Printed Spiral Coils for Efficient Transcutaneous Inductive Power Transmission. *IEEE Trans. Biomed. Circuits Syst.* 2007, 1, 139–202.

[117] Siris V A; Tragos E Z ; Petroulakis N.E. Experiences with a metropolitan multiradio wireless mesh network: Design, performance, and application. *IEEE Commun. Mag.* 2012, 50, 128–136.

[118] Diez L ; de Lope .R.; Agüer R ; Corre Y.; Stéphan J.; Siradel M.B.; Aerts S; Vermeeren G; Martens L.; Joseph W. Optimal dosimeter deployment into a smart city IoT platform for wideband EMF exposure assessment. In *Proceedings of the 2015 European Conference on Networks and Communications (EuCNC)*, Paris, France, 29 June–2 July 2015; pp. 528–532.

[119] Hull B; Bychkovsky V; Zhang Y; Chen K; Goraczko M; Miu A; Shih E; Balakrishnan H.; Madden S. Cartel: A distributed mobile sensor computing system. In *Proceedings of the 4th International Conference on Embedded Networked Sensor Systems*, Boulder, CO, USA, 31 October–3 November 2006; pp. 125–138.

[120] Van Le D; Tham C K.; Zhu Y Quality of information (QoI)—Aware cooperative sensing in vehicular sensor networks. In *Proceedings of the 2017 IEEE International Conference on Pervasive Computing and Communications Workshops (PerCom Workshops)*, Kona, HI, USA, 13–17 March 2017; pp. 369–374.

[121] Primdahl F. The fluxgate mechanism, part I: The gating curves of parallel and orthogonal fluxgates. *IEEE Trans. Magn.* 1970, 6, 376–383.

[122] Campolo C; Iera A; Molinaro A; Paratore S Y; Ruggeri G SMaRTCaR: An integrated smartphone-based platform to support traffic management applications. In *Proceedings of the 2012 First International Workshop on Vehicular Traffic Management for Smart Cities (VTM)*, Dublin, Ireland, 20–20 November 2012; pp. 1–6.

- [123] Mukhopadhyay S C; Woolley J.D.M.; Gupta G S Inspectiion off Saxophone Reeds Employing a Novell Planar Electromagnetic Sensing Technique. In Proceedings of the 2005 IEEE Instrumentation and Measurement Technology Conference Proceedings, Ottawa, ON, Canada, 16–19 May 2005; Volume 1, pp. 209–213.
- [124] Jolani F; Yu Y; Chen Z A Planar Magnetically Coupled Resonant Wireless Power Transfer System Using Printed Spiral Coils. *IEEE Antennas Wirel. Propag. Lett.* 2014, 13, 1648–1651.
- [125] Mukhopadhyay S; Gooneratne C A Novel Planar-Type Biosensorfor Noninvasive Meat Inspection. *IEEE Sens. J.* 2007, 7, 1340–1346.
- [126] Mukhopadhyay S C ; Gooneratne C P; Gupta G.S.; Demidenko S N A low-cost sensing system for quality monitoring of dairy products. *IEEE Trans. Instrum. Meas.* 2006, 55, 1331–1338.
- [127] Mukhopadhyay S; Yamada S.; Iwahara M. Inspection of electroplated materials-performance comparison with planar meander and mesh type magnetic sensor. *Int. J. Appl. Electromagn. Mech.* 2002, 15, 323–329.
- [128] Mukhopadhyay S C. Quality inspection of electroplated materials using planar type micro-magnetic sensors with post-pro- cessing from neural network model. *IEE Proc.-Sci. Meas. Technol.* 2002, 149, 165–171.
- [129] Gooneratne C; Mukhopadhyay SC ; Purchas R.; Gupta G.S. Interaction of planar electromagnetic sensors with pork belly cuts. In Proceedings of the 1st International Conference on Sensing Technology, Palmerston North, New Zealand, 21–23 November 2005.
- [130] Mukhopadhyay S C. A novel planar mesh type micro-electromagnetic sensor: Part II–estimation of system properties. *IEEE Sens. J.* 2004, 4, 308–312.
- [131] Mamishev A ; Sundara-Rajan K.; Yang F.; Du Y.; Zahn M. Interdigital sensors and transducers. *Proc. IEEE* 2004, 92, 808–845.
- [132] Fratticcioli E.; Dionigi M.; Sorrentino R. A planar resonant sensor for the complex permittivity characterization of materials. In Proceedings of the 2002 IEEE MTT-S International Microwave Symposium Digest (Cat. No.02CH37278), Seattle, WA, USA, 2–7 June 2002; pp. 647–649.
- [133] Toda K; Komatsu Y; Oguni S; Hashiguchi S.; Sanemesa I. Planar gas sensor combined with interdigitated array electrodes. *Anal. Sci.* 1999, 15, 87–89.
- [134] Timmer B H.; Sparreboom W.; Olthuis W; Bergveld P; van den Berg A. Planar interdigitated conductivity sensors for low electrolyte concentrations. In Proceedings

Semiconductor Sensor and Actuator Technology, SeSens, Veldhoven; STW: Utrecht, The Netherlands, 2001; pp. 878–883.

[135] Yoon S ; Sim J.K.; Cho Y.H. On-chip flexible multi-layer sensors for Human stress monitoring. In Proceedings of IEEE SEN- SORS 2014, Valencia, Spain, 2–5 November 2014; pp. 851–854.

[136] Gramacy R B ; Lee H.K.H. Gaussian Processes and Limiting Linear Models. *Comput. Stat. Data Anal.* 2008, 53, 123–136.

[137] Paciorek C J Nonstationary Gaussian Processes for Regression and Spatial Modelling. Ph.D. Thesis, Carnegie Mellon University, Pittsburgh, PA, USA, 2003.

[138] Sakata A ; Ashida F; Zako M. Structural optimization using kriging approximation. *Comput. Meth. Appl. Mech. Eng.* 2003, 192, 923–939.

[139] Chady T; Enokizono M; Sikora R. Neural network models of eddy current multi-frequency systems for nondestructive test- ing. *IEEE Trans. Magn.* 2000, 36, 1724–1727.

[140] Chady T; Enokizono M; Sikora R; Todaka T; Tsuchida Y. Natural crack recognition using inverse neural model and multi- frequency eddy current method. *IEEE Trans. Magn.* 2001, 37, 2797–2799.

[141] Alexander F.; András S.; Andy K. *Engineering Design Via Surrogate Modelling*; University Southampton: Southampton, UK, 2008; ISBN 9780470770795, 0470770791.

[142] Joseph V R ; Hung Y; Sudjianto A. Blind kriging: A new method for developing metamodels. *ASME J. Mech. Des.* 2008, 130, 031102:1–031102:8.

[143] Razavi S ; Tolson B A ; Burn D H Review of surrogate modeling in water resources. *Water Resour. Res.* 2012, 48, W07401. doi:10.1029/2011WR011527.

[144] Jack P C K *Kriging: Methods and Applications*; Tilburg University: Tilburg, The Netherlands, 2017.

[145] Tesla N. Apparatus for transmitting electrical energy. Patent No. 1119732, USA, 1914.

[146] Fernandez J M ; Borrás J A , U.S. patent 6,184,651 (2001).

[147] World Health Organization, “Electromagnetic fields and public health”, Fact Sheet No. 304, May 2006.

[148] A. Esser H.-C. Skudelny, *IEEE Trans. Ind. Appl.* 27, 872(1991).

- [149] Hirai, Kim T W ,Kawamura A ,IEEE Trans. PowerElectron.15, 21 (2000).
- [150] Kurs A, Karalis A, Moffatt R, et al. Wireless power transfer via strongly coupled magnetic resonances. Science 2007; 317: 83–86.
- [151] Fu, WZ, Zhang B, Qiu DY, et al. Maximum efficiency analysis and design of self-resonance coupling coils for wireless power transmission system. Proc CSEE 2009; 29(18): 21–29.